

Tissue Competition: Interplay of Mechanics, Interfaces, and Evolution

Inaugural-Dissertation

zur

Erlangung des Doktorgrades
der Mathematisch-Naturwissenschaftlichen Fakultät
der Universität zu Köln
vorgelegt von

Tobias Büscher
aus Nordhorn

2020

Berichterstatter: PD Dr. Jens Elgeti
(Gutachter): Prof. Dr. Joachim Krug

Tag der mündlichen Prüfung: 15.07.2020

Dedicated to Juliette and Janek

Why believe in others

We have to be idealists in a way, because then
we wind up as the true, the real realists. [...]
If we take man as he is, we make him worse,
but if we take man as he should be,
we make him capable of becoming what he can be.
So, if you don't recognize a young man's
will to meaning, man's search for meaning,
you make him worse, you make him dull,
you make him frustrated, you still add
and contribute to his frustration.
While, if you presuppose in this man, [...]
there must be a spark of search for meaning.
Let's recognize this! Let's presuppose it!
And then you will elicit it from him,
and you will make him become
what he in principle is capable of becoming.
Viktor Frankl, 1972

Kurzzusammenfassung

Wettbewerb zwischen Geweben tritt häufig in lebenden Systemen auf. Gut untersuchte Beispiele sind der Wettbewerb zwischen verschiedenen Klonen während der Entwicklung in der Flügelscheibe der *Drosophila* und Krebs, wo der Tumor mit dem umliegenden Wirtsgewebe konkurriert. Der Wettbewerb ist durch verschiedenste biochemische und physikalische Faktoren beeinflusst, einschließlich Konzentrationen von Nährstoffen und anderen Chemikalien, Zell-Zell-Kommunikation und geometrischen Einschränkungen.

In dieser Dissertation untersuchen wir rein mechanisch regulierten Wettbewerb zwischen verschiedenen Geweben, mit Krebs als biologischem Beispiel im Kopf. Dabei fokussieren wir uns auf die Rolle der Grenzfläche und der Wechselwirkung zwischen verschiedenen Zellpopulationen, einschließlich evolutionärer Aspekte. Für mechanisch regulierten Wettbewerb wurde vorgeschlagen, dass das Ergebnis allein vom homeostatischen Druck bestimmt wird - dem Druck an dem sich Zellteilungen und Zellapoptose ausgleichen. Das Gewebe mit dem höheren homeostatischen Druck gewinnt gegen das Schwächere. Demzufolge besteht die Tumorentwicklung aus aufeinander folgenden Runden der Übernahme des Gewebes durch eine Zellpopulation mit einem höheren homeostatischen Druck. Experimente mit wachsenden Gewebesphäroiden zeigen jedoch, dass Oberflächeneffekte eine dominante Rolle im Gewebewachstum spielen können. Zellen teilen sich bevorzugt an der Oberfläche und vollziehen Apoptose im Kern. Es stellt sich heraus, dass ähnliche Effekte eine Rolle im Wettbewerb zwischen Zellpopulationen spielen und die Evolution des Gewebes ändern.

Um die Mechanik des Gewebewettbewerbs zu untersuchen benutzen wir ein teilchenbasiertes Simulationsmodell, in welchem eine Zelle durch zwei Teilchen dargestellt wird, welche sich mit einer aktiven Wachstumskraft abstoßen. Zellen teilen sich, wenn der Abstand zwischen den beiden Teilchen einen bestimmten Schwellenwert erreicht, während Zelltod zufällig mit einer bestimmten Rate erfolgt. Zellen wechselwirken miteinander wie weiche, klebrige Kugeln und ein "dissipative particle dynamics" Thermostat berücksichtigt Energiedissipation und zufällige Fluktuationen.

Wir untersuchen zuerst die Rolle der Adhäsion zwischen verschiedenen Geweben, indem wir einen Extremfall betrachten: verschwindende Adhäsion zwischen Zellen verschiedener Gewebe ("cross-adhesion"). Die resultierende starke Grenzflächenspannung

führt zu einer Trennung der konkurrierenden Gewebe. In der Nähe der Grenzfläche ist die Teilungsrate beider Gewebe stark erhöht. Die erhöhte Zahl an Teilungen erzeugt einen Fluss von Zellen von der Grenzfläche ins Volumen, ähnlich zu wachsenden Gewebesphäroiden. Um den Zustrom an Zellen von der Grenzfläche zu kompensieren ist der Systemdruck immer größer als der individuelle homeostatische Druck beider Gewebe; im Mittel sterben im Volumen mehr Zellen als sich teilen. Dies resultiert in einer stabilen Koexistenz beider Gewebe mit einer Vielfalt verschiedener Strukturen, selbst bei ungleichem homeostatischem Druck.

Als Nächstes untersuchen wir die evolutionäre Entwicklung eines Gewebes unter dem Einfluss von Mutationen, welche die mechanischen Eigenschaften einer Zelle verändern. Für unabhängige Mutationen entwickelt sich das Gewebe in Richtung von Populationen mit niedriger interner Adhäsion und hoher Wachstumskraft, was beides den homeostatischen Druck erhöht. Motiviert von den Resultaten des vorherigen Kapitels und biologischer Evidenz führen wir eine Kopplung zwischen den beiden Parametern ein, so dass eine höhere Wachstumskraft eine höhere interne Adhäsion bedingt. Interessanterweise kann dies zu einer divergierenden evolutionären Entwicklung führen, während der sich das Gewebe in Richtung einer sehr heterogenen Verteilung an Populationen entwickelt. Das Gewebe besteht dann aus Zellen mit sehr unterschiedlichen Eigenschaften, die in einem dynamischen Zustand koexistieren. Überraschenderweise kann dieser Zustand von der Zellpopulation mit dem niedrigsten homeostatischem Druck dominiert werden. Der Wettbewerb zwischen nur zwei Zellpopulationen und ein passendes phänomenologisches Modell liefern eine qualitative Erklärung dieser Resultate. Des Weiteren zeigen wir, dass die Rate mit der Mutationen erfolgen nur eine untergeordnete Rolle im Wettbewerb spielt und lediglich die evolutionäre Zeitskala beeinflusst.

Drittens studieren wir Wettbewerb auf einem Substrat, wobei wir uns auf die Stabilität der Grenzfläche fokussieren. Zellen wechselwirken mit dem Substrat durch Reibung, was eine endliche Abfalllänge mechanischer Spannungen bedingt. Aufgrund von Diffusion ist die Grenzfläche zwischen zwei identischen Geweben instabil. Jedoch sind schon kleine Unterschiede zwischen den konkurrierenden Geweben ausreichend für eine stabile, fast flache Grenzfläche, welche sich mit konstanter Geschwindigkeit fortbewegt. Eine reduzierte Apoptoserate bedingt eine erhöhte Gewebeviskosität. Bei einer höheren Viskosität des Gewebes mit dem niedrigeren homeostatischen Druck entsteht eine Fingerinstabilität, welche an das viskose Fingern der Saffman-Taylor-Instabilität erinnert. Außer durch homeostatischen Druck kann der Wettbewerb auch von kollektiver Motilität eines Gewebes in Richtung des anderen Gewebes getrieben werden. Kleine Motilitätskräfte genügen für eine Fortbewegung mit stabiler Grenzfläche. Jenseits einer kritischen Stärke

der Motilität bilden sich jedoch Ausbuchtungen des beweglichen Gewebes in das Nichtbewegliche mit wohldefinierter Wellenlänge. Das resultierende, beinahe sinusförmige Muster der Grenzfläche ist zeitlich erstaunlich stabil, im Gegensatz zur zuvor diskutierten, sehr dynamischen Fingerinstabilität.

Zusammengefasst führt das Zusammenspiel von Mechanik, evolutionären Kräften und Wechselwirkungen zwischen Zellen verschiedener Gewebe zu interessanten Grenzflächenphänomenen. Diese reichen von stabiler Koexistenz zwischen zwei oder mehreren Zellpopulationen in einer Vielfalt von Strukturen bis zu einer instabilen Front während der Fortbewegung auf einem Substrat.

Abstract

Competitions between tissues occur frequently in living systems. Well-studied examples are the competition between different clones during development in the *Drosophila* wing disc and cancer, in which the tumor competes with the surrounding host tissue. The competition is affected by various biochemical and physical factors, including concentrations of nutrients and other chemicals, cell-cell communication, and geometrical constraints.

In this thesis, we study the competition between different tissues regulated solely by the mechanical interactions between cells, with cancer as the biological example in mind. In particular, we focus on the role of the interface and the interactions between different cell populations including evolutionary aspects. For mechanically-regulated competition, it has been proposed that the outcome is solely determined by the homeostatic pressure, the pressure at which division and apoptosis balance. The tissue with the higher homeostatic pressure outcompetes the weaker one. Accordingly, tumorigenesis consists of subsequent rounds of takeover of the tissue by a cell population with a higher homeostatic pressure. However, experiments on growing tissue spheroids reveal that surface effects can play a dominant role in tissue growth. Cells divide preferentially at the surface and undergo apoptosis in the bulk. It turns out that similar interfacial effects play a role in the competition between cell populations and alter the evolution of a tissue.

To explore the mechanics of tissue competition we employ a particle-based simulation model, in which a cell is represented by two particles which repel each other via an active growth force. Cells divide when the distance between the two particles reaches a certain threshold, while cell death occurs randomly at a constant rate. Cells interact with each other like soft sticky spheres and a dissipative particle dynamics thermostat accounts for energy dissipation and random fluctuations.

First, we study the role of the adhesion between different tissues by looking at an extreme case: vanishing cross-adhesion strength. The resulting strong interfacial tension leads to segregation of the competing tissues. In a small region near the interface, the division rate of both tissues is enhanced. The enhanced division leads to a flux of cells from the interface towards the bulk, similar to growing tissue spheroids. To compensate for the influx of cells from the interface, the system pressure is always larger than each

individual homeostatic pressure and both tissues undergo net apoptosis in the bulk. This results in stable coexistence between the two tissues in a variety of different structures, even for a difference in homeostatic pressure.

Next, we study the evolution of a tissue under the influence of mutations which change the mechanical properties of a cell. For independent mutations, the tissue evolves towards populations with low internal adhesion and high growth-force strength, which both increase its homeostatic pressure. Motivated by the results from the previous chapter and biological evidence, we impose a coupling between the two parameters, such that a higher growth force comes at the cost of a higher adhesion strength. Interestingly, this can result in a diverging evolution in which the tissue evolves towards a very heterogeneous distribution of populations. The compartment is then occupied by cells with very different properties, coexisting in a highly dynamic state. Surprisingly, this state can be dominated by the cell population with the lowest homeostatic pressure. Competitions between two cell populations alone and a phenomenological model provide a qualitative explanation of these results. We further reveal that the rate at which mutations occur plays a minor role in the competition and only affects the evolutionary time scale.

Third, we study competition on a substrate, in which we focus on the stability of the interface between the competing tissues. Cells interact with the substrate via friction, resulting in a finite stress-decay length. The interface between two identical tissues is unstable due to diffusion. Already small differences between the competing tissues suffice to arrive at a stable, almost flat interface which propagates at constant velocity. A reduced apoptosis rate results in an increased tissue viscosity. For larger viscosity of the tissue with the lower homeostatic pressure, a fingering instability emerges, reminiscent of Saffman-Taylor viscous fingering. Besides homeostatic pressure, the competition can also be driven by collective motility of one tissue directed towards the other. Small motility forces suffice to result in propagation with a stable interface. However, above a critical motility strength, protrusions of the motile tissue into the non-motile one form at a well-defined wavelength. The resulting almost sinusoidal interface pattern is remarkably stable over time, contrary to the highly dynamic fingering instability discussed before.

In summary, the interplay between mechanics, evolutionary forces, and cross-interactions gives rise to interesting interfacial phenomena. This includes stable coexistence between two or many cell populations in a variety of structures and an unstable front during propagation on a substrate.

Contents

Kurzzusammenfassung	v
Abstract	ix
1 Introduction	1
1.1 From condensed to soft, from soft to active, from active to growing matter	1
1.2 Mechanical aspects of cells and tissues	2
1.3 Physics of cancer	6
1.4 Continuum mechanics of tissue growth and competition	8
1.5 Computational modeling approaches	14
1.6 Structure of the thesis	19
2 Mechanics of tissue competition: interfaces stabilize coexistence	31
2.1 Abstract	31
2.2 Introduction	31
2.3 Model	32
2.4 Results	35
2.5 Conclusions	42
2.6 Acknowledgements	43
2.7 Supplementary Informations: Mechanics of tissue competition: interfaces stabilize coexistence	49
3 Tissue evolution: mechanical interplay of adhesion, pressure, and hetero- geneity	53
3.1 Abstract	53
3.2 Introduction	53
3.3 Simulation model	55
3.4 Results	57
3.5 Discussion	65
3.6 Acknowledgements	66

3.7	Supplementary Informations: Tissue evolution: mechanical interplay of adhesion, pressure, and heterogeneity	71
4	Instability and fingering of interfaces in growing tissue	79
4.1	Abstract	79
4.2	Introduction	79
4.3	Simulation model	81
4.4	Results	85
4.5	Discussion	93
4.6	Acknowledgements	94
4.7	Supplementary Informations: Instability and fingering of interfaces in growing tissue	98
5	Summary and outlook	101
5.1	Summary	101
5.2	Outlook	106
	Acknowledgements	115
	Declaration of individual contributions	117
	Erklärung der Selbstständigkeit	119
	Lebenslauf	121

Nomenclature

β_T	isothermal compressibility
Γ	interfacial tension
γ_b	background dissipation coefficient
γ_c	intracell dissipation coefficient
γ_t	intercell dissipation coefficient
Δk_s	surface/interface growth enhancement
ΔP_H	homeostatic pressure difference
$\Delta \sigma_H$	homeostatic stress difference
Δt	time step
κ	pressure response coefficient
ϕ	cell number fraction
ρ	cell density
$\sigma_{\alpha\beta}$	stress tensor
σ_H	homeostatic stress
τ	tradeoff parameter
ξ	substrate friction
A	area
a	thickness of surface/interface growth region
f_0	repulsive cell-cell potential coefficient
f_1	attractive cell-cell potential coefficient
f_c	cross-adhesion strength
\mathbf{F}_i	force on particle i
f_m	motility-force strength
G	growth-force strength
k	growth rate
k_a	apoptosis rate
k_b	bulk growth rate
$k_B T$	noise intensity

k_d	division rate
k_{div}	division rate altered division mechanism
k_m	mutation rate
L_α	system size in α -direction
m	mass
N	total number of cells
P	pressure
\mathbf{p}	unit vector between the two cell particles
P_H	homeostatic pressure
P_i	imposed pressure
p_m	mutation probability
q	wave vector
R_{pp}	pair potential interaction range
r_0	cellular expansion pressure constant
r_{ct}	cell division distance threshold
r'_{ct}	reduced cell division distance threshold
r_d	new cell particle initial distance
\mathbf{r}_i	position of particle i
s	distance to interface
t	time
t_P	relaxation time constant
\mathbf{v}	velocity field
V	volume
\mathbf{v}_i	velocity of particle i
v_{int}	interface velocity
w	interface width
w_{sat}	interface saturation width
$x/y/z$	Cartesian coordinates

Abbreviations

CA	cellular automaton
CBM	center-based model
CPM	Cellular Potts model
DAH	differential adhesion hypothesis
ECM	extracellular matrix
EMT	epithelial-mesenchymal transition
HBEC	human bronchial epithelial cells
MDCK	Madin-Darby Canine Kidney
PDE	partial differential equation
VM	vertex-based model

1 Introduction

1.1 From condensed to soft, from soft to active, from active to growing matter

The study of matter itself is one of the oldest studies mankind has carried out throughout its history. The question what constitutes matter at the smallest scale dates back to ancient Greece. However, the answer to this question, that all matter is made up of atoms, has only been proven at the beginning of the twentieth century. Since then, technological advance has greatly broadened our understanding how macroscopic properties of a material arise from the atomistic scale, which is what defines the field of *condensed* matter.

As fundamental as the question of what constitutes matter is the question of what holds these constituents together. Of the (up to the current day) four known fundamental interactions, only the electromagnetic force is important for the answer to this question (at least above the scale of single atoms, besides some astronomical objects). This force binds atoms together and mediates interactions between molecules and is thus responsible not only for the electric and magnetic, but also the mechanical properties of a material. The strength of the bonds formed by these interactions varies over many orders of magnitude, which constitutes different subfields of condensed matter. It is the softness of the underlying interactions which gives the field of *soft* matter its name. The strength of the relevant interactions, e.g. hydrogen bonds or van-der-Waals interactions, is on the order of the thermal energy in the system and thermal fluctuations thus play an important role in soft matter. Classical examples of soft matter are colloidal suspensions, polymer networks, and liquid crystals.

These classical soft matter systems can be studied in and out of thermodynamic equilibrium. Biology provides us with a particular type of non-equilibrium soft matter systems. What distinguishes these systems from classical non-equilibrium systems, such as earth's atmosphere or the stirring of a cup of coffee, is that the forces which drive the system out of equilibrium are generated by the constituents of the system itself. The non-equilibrium character is thus an inherent property of these systems, as they

are constantly driven away from equilibrium. Examples of such systems can be found at strikingly different lengths scales, ranging from the cytoskeletal network inside a cell over bacterial colonies to schools of fish. Together with synthetic and simplified model systems, such as self-propelled colloids or active Brownian particles, these systems comprise the field of *active* matter.

Cells and multicellular tissues form a special kind of soft, active matter. Not only do cells consume energy, generate stresses and move through their environment, but they also grow, divide, and die and thus generate new material, which distinguishes multicellular tissues from most other active matter systems and defines the name *growing* matter. Another example of growing matter are bacterial colonies, in which growth typically takes place on a shorter time scale. The self-renewing character of multicellular tissues is one of the main, but by far not the only reason why they are an interesting system to be studied not only from a biological, but also from a physical point of view. Already the simplest arising questions, e.g. how tissues maintain a finite size, how different tissues develop into well-defined, segregated compartments, or how mechanics feeds back onto growth, bear surprisingly rich and complex answers.

1.2 Mechanical aspects of cells and tissues

An early example of modern statistical and thermodynamical principles applied to multicellular systems is the differential adhesion hypothesis (DAH). The DAH originates from the work of Townes and Holtfreter from the fifties, who found that cells from different germ layers rearrange from a mixture into the developmentally correct positions [1]. Building up on this, Steinberg proposed that multicellular tissues can be treated as immiscible liquids. Accordingly, cell sorting is governed by differences in the adhesiveness (or, respectively, surface tensions) of different cell types and minimization of the free energy in the system [2]. In vitro experiments have confirmed several predictions of the DAH, e.g. tissue surface tension being proportional to the number of adhesion molecules [3, 4]. However, a simple order of magnitude comparison between the energy associated with tissue surface tension ($\approx 10^{-3} \text{ J/m}^2$), for example measured by parallel-plate compression, and the adhesion energy per unit area ($\approx 10^{-7} \text{ J/m}^2$), obtained via force measurement during membrane separation, shows that the DAH does not capture the whole picture [5, 6, 7, 8, 9]. More recent experiments indicate that tissue surface tension is dominated by mechanical polarization of cells at the outer tissue boundary, increasing the cortical tension along this boundary relative to internal cell-cell junctions [10, 11]. The scaling of tissue surface tension with the number of adhesion

molecules can be explained by their additional function as signaling molecules [12]. These results show that cells are able to actively change their mechanical properties in response to external signals, in this case by changing the actomyosin contractility locally [13].

Cell response to external signals also works in the opposite direction, i.e. cells are able to change their biochemical properties as a reaction to a mechanical signal, a mechanism termed mechanotransduction. One way for cells to convert mechanical stimulus into a chemical signal are mechanosensitive membrane channels, which open or close in response to tension in the membrane [14, 15].

Mechanosensing is involved in signaling processes connected to various different cell behaviors such as cell division, differentiation, or programmed cell death (apoptosis) [16, 17]. It has been shown that the application of cyclic mechanical strain to the underlying substrate of vascular smooth muscle cells leads to an increase in cell number compared to unstrained cells, with the largest increase occurring at zones of maximal strain [18, 19]. The observed delay between the onset of strain and increased DNA production (as a determinant for cell growth) hints at the conclusion that strain does not directly activate growth receptors, but leads to the production and secretion of growth factors, induced by interactions between matrix proteins coated on the substrate and integrins. Similar results have been obtained for other cell types such as embryonic chick heart cells, pulmonary endothelial cells, or epithelial cells [20, 21, 22]. In a somewhat different experimental approach, mechanical strain has also been shown to increase proliferation in the *Drosophila* wing disc [23]. Experiments focusing on the opposite direction, i.e. studying growth under mechanical compression, have mostly been carried out for growing tissue spheroids. Stress is exerted either indirectly by putting the spheroids into an elastic medium, which is compressed due to growth and thus exerts a solid stress back onto the spheroid, or directly by an osmotic pressure [24, 25, 26, 27]. The growth rate has consistently been found to decrease with growing compressional stress.

Interestingly, mechanical compression does not only reduce the proliferation rate, but has also been shown to increase the apoptosis rate. Thus, both effects have to be distinguished in experiments on the effects of stress onto growth [28, 29, 30]. For osmotic stress, proliferation is already significantly decreased for stresses as small as 500 Pa [29, 30], while apoptosis is only affected at way higher stresses, of the order of 1 MPa [31, 32]. These findings hint at the idea that different mechanisms are behind the effect of osmotic stress on proliferation and apoptosis. Indeed, osmotic stress enhances the activity of the MAPK pathway, which is connected to the regulation of apoptosis [33, 34, 35, 36]. The effect of mechanical compression on growth, on the other hand, can be explained by purely mechanical arguments, which do not invoke complex biochemical pathways: the

growing tissue spheroid needs to deform its environment in order to grow, leading to a pressure exerted back onto the spheroid, which stalls growth when the spheroid can not overcome this pressure anymore. The growth of tissue spheroids is discussed in more detail in section 1.4.1.

The ability of cells to sense the mechanical properties of their environment also plays an important role in cell migration [37]. Cell migration is crucial in biological processes such as wound healing, immune response, or development, but can also have severe consequences in tumor progression when cancer cells metastasize [38]. In order for cells to move in a directed fashion, they need to be able to react to some cue in their environment. This cue can be a chemical, e.g. morphogens or nutrients, which is termed chemotaxis. However, the cue can also be of physical origin, for instance fluidic shear stress [39]. A particularly interesting form of mechanically-guided cell migration is durotaxis, in which cells migrate according to gradients in rigidity, i.e. cells are able to sense the mechanical properties of their environment and react to it accordingly [40, 41]. Cells form focal adhesions, large protein complexes which connect the actin cytoskeleton (a dynamic network of filaments inside the cell) with the extracellular matrix (ECM) or the underlying substrate. Focal adhesions are crucial in the understanding of cell migration, as they anchor the cell to the substrate, exert pulling forces to it, and act to sense mechanical forces [42, 43]. These signals are transmitted to the interior of the cell, where they ultimately result in changes of the cytoskeleton, i.e. its contractility, as a response [44]. The rigidity sensing seems to be achieved by fluctuations in the pulling forces exerted by the focal adhesions to the ECM [45].

Cell migration also takes place at the tissue level, where it gives rise to collective phenomena. Collective cell migration is studied by different experimental approaches under the use of in vitro and in vivo model systems, reflecting its importance in various distinct biological processes. One of the best studied in vitro systems, in combination with modern experimental techniques such as traction force microscopy, are confluent cell monolayers during migration into empty regions on a substrate [46, 47, 48]. This model allows for the tracement of individual cells and the local measurement of stresses at subcellular resolution, which gives quantitative insight into the physical mechanisms at play. For example, in a radially expanding colony of epithelial Madin-Darby Canine Kidney (MDCK) cells, it has been shown that traction forces driving the migration are not generated by leader cells at the front alone, but also by cells in the bulk many rows behind the front. The colony as a whole is under tension, with tension being strongest at the center [33]. However, leader cells can give rise to a fingering instability, even for the same cell type, in wound healing assays, in which cell monolayers are grown to confluency

before removing a barrier, upon which cells start to migrate into the free space [47, 50]. These experiments reveal further that, upon wound creation, the average cell velocity rapidly increases both at the front and in the bulk, with long-range correlations in the velocity field. These correlations are less pronounced for more independently moving fibroblast-like NRK cells, which do not form strong cell-cell adhesions, in contrast to MDCK cells.

Let us close this section with a discussion on the question under which conditions the underlying assumption of the DAH, namely that tissues behave like a liquid, is actually valid. Intuitively, one might actually expect an elastic characterization of multicellular tissues. This gives rise to various further questions: What is the appropriate rheological model for multicellular tissues? On which time scales do tissues show viscous behavior? How do cell division and apoptosis affect tissue rheology?

In order to measure macroscopic material properties of multicellular tissues, such as viscosity, surface tension, or the elastic modulus, the length scale at consideration in an experimental setup has to be sufficiently larger than the size of a single cell. Additionally, the time scale at which these quantities are measured strongly affects the results, as the time it takes to form saturated adhesive bonds between cells can be of the order of an hour, e.g. due to bond strengthening after initial adhesion [51, 52]. For example, in studies on the aggregation of cells in sheared suspension, the development of slowly forming adhesive bonds is prevented, as cells are only in contact for about a second [53], which might yield misleading results. The time it takes for adhesive bonds to rupture and reform sets the time scale above which tissues can be expected to show liquid-like behavior. At shorter times (order of seconds to minutes), tissues have commonly been found to show an elastic response to an applied mechanical force. Thus, tissues can be best described as viscoelastic materials [54, 55]. The existence of a yield stress and the corresponding rheological models have been discussed, but the former, if existent, appears to be rather small, such that stresses which arise from surface tension can overcome it [56, 57, 58]. The viscoelastic character of multicellular tissues has motivated different experimental setups to determine the corresponding macroscopic material properties. This includes aggregate centrifugation, parallel-plate compression, detachment experiments, and micropipette aspiration, all of which track the deformation of a tissue aggregate in response to an external force over time [54, 55, 59, 60]. The viscoelastic properties are then obtained by fitting a certain rheological model to the measured deformations.

At the time scale of growth, division and apoptosis locally relax stress and, at the same time, remodel the tissue, which gives rise to a diffusive motion of cells. The presence of

diffusion corresponds to a liquid-like behavior, even when the tissue is otherwise considered as an elastic solid, i.e. no other mechanisms of stress relaxation are present [61]. Additionally, proliferation gradients, for instance observed in experiments on the growth of tissue spheroids (see section 1.4.1 for a detailed discussion), yield convective flows [62]. Hence, as long as cells divide and die, tissues can be characterized as liquids on long timescales.

All of the experiments underlying the discussion on tissue rheology so far were performed on three-dimensional tissue aggregates without geometrical constraints, for which a viscoelastic model appears to be the appropriate description. In two dimensions, however, a limitation of the available space can give rise to interesting phenomena for confluent cell monolayers. In experiments on MDCK cells, once confluency is reached, the average velocity drops, while collective motility patterns arise [47]. With increasing cell density (as cells continue to proliferate after reaching confluency), the length scale of these collective motility patterns grows, while the average velocity further decreases. Below a critical density ρ_g the monolayer is best described as a fluid, while it undergoes a glass transition to a more solid-like state when approaching ρ_g . In a similar study on human bronchial epithelial cells (HBEC), the authors found that the glass transition (also termed jamming transition) is not necessarily driven by increasing cell density alone. Adhesive bonds mature over time and thus increasing cell-cell and cell-substrate adhesion affect the transition as well [63]. Hence, it has been suggested that the phase space for the jamming transition is spanned by cell density, adhesion, and motility, in analogy to classical jammed materials such as foams, for which the phase diagram is spanned by temperature, density, and mechanical load [64, 65].

In this section, we have gained an overview of the mechanics of multicellular tissues and individual cells as their constituents, described the material properties of tissues, and discussed how mechanics affect cell processes such as growth, division, and migration. In the next section, we take a closer look at cancer cells and tumors and discuss different fields of cancer research in which physical methods have shown to be useful.

1.3 Physics of cancer

The contribution of physics to the field of cancer research has grown quite extensively over the past decades. The questions addressed by physicists cover a broad range of scales, ranging from the level of single cancer cells to that of the whole host tissue. Additionally, physical knowledge is essential for certain treatments, such as radiation therapy. Furthermore, methods of statistical physics are employed when studying com-

plex signaling networks or the evolutionary nature of cancer.

At the cellular level, several studies address the question whether cancer cells have altered mechanical properties in comparison to healthy cells [66], as this opens up the possibility to diagnose cancer by measuring these properties of a sample of cells. A second field where the mechanics of cancer cells play an important role is their migration through the tumor microenvironment, especially during the metastatic process.

Over various different cancer types, cancer cells have commonly been found to have a lower elastic modulus than their healthy counterparts and are thus softer and more deformable [67, 68, 69]. This softening is associated to a reduction of actin polymers in the cytoskeleton, and thus a less dense network of actin filaments, whose structure determines the mechanical properties of a cell to a large degree [70, 71, 72]. It is tempting to assume that a larger deformability is beneficial for cancer cells in the metastatic process, during which cancer cells often have to migrate through a dense network of ECM fibers, which poses a steric hindrance. Indeed, a larger deformability has been shown to be correlated with higher invasiveness [73, 74]. In cancer diagnosis, the larger deformability of cancer cells has successfully been used to distinguish malignant from healthy cells, e.g. in oral squamous cell carcinomas [75, 76].

Deformability is not the only mechanical property of cancer cells which affects their migration during the metastatic process. Another property which is believed to be crucial for cancer cell migration is their ability to generate strong traction forces. For migration on a substrate, it has indeed been shown that metastatic cells are able to generate higher forces than non-metastatic cells. These results are consistent over various different cell lines, varying substrate stiffness, and collagen density [77]. However, when turning to migration in a three-dimensional matrix, it has been found that it is the directionality of traction forces and not their strength alone which correlates with higher invasiveness [78].

More recently, it has been recognized that the properties of the tumor microenvironment, especially the ECM, are as important as those of the migrating cancer cells themselves [79]. The ECM consists of several macromolecules, e.g. collagen, which form a complex network and provide structural support to tissues. As for cell migration on a two-dimensional substrate, the stiffness of the ECM similarly affects cell migration in three dimensions, e.g. the migration speed and direction [80, 81]. Additionally, the structure of the ECM network becomes important. Cancer cells migrate along collagen fibers and thus alignment of these fibers leads to more persistent migration, which correlates with higher invasiveness [82, 83]. On the other hand, migration becomes effectively stalled when the average pore size of the collagen network is of the order of the size of the cell nucleus [84, 85]. However, cancer cells can overcome such restric-

tions by secretion of matrix-degrading proteins and are thus able to actively remodel the ECM network [86, 87]. Lastly, increased ECM stiffness has been shown to be involved in phenotypical changes in cells towards more malignant phenotypes, e.g. inducing the epithelial-mesenchymal transition (EMT) [88, 89]. During the EMT cells change from a non-motile, epithelial to an invasive, mesenchymal phenotype. The transition is accompanied by a loss of cell-cell adhesion and cell polarity.

An apparent contradiction arises when comparing the mechanical properties of single cancer cells to the properties of the whole tumor. As discussed before, cancer cells are typically softer than their healthy counterparts, while tumors, however, are found to be stiffer than the surrounding host tissue. Indeed, tumors are often detected via palpation as a rigid mass. This contradiction can be resolved by looking at the composition of tumors, which do not consist of cancer cells alone. The enhanced rigidity is attributed to an increase in ECM density, which stiffens the tumor as a whole [90, 91]. These observations are used in more sophisticated cancer diagnosis than simple palpation. Magnetic resonance elastography yields local stiffness maps of tumors and the surrounding host tissue at high resolution in a non-invasive way [92]. More recently, tomoelastography has been developed, which allows to measure the complex shear modulus as an indicator of the fluidity of a tissue. For the liver, it has been shown that malignant lesions can be distinguished from benign ones by their higher fluidity [93].

So far, we put a focus on experimental research of cells and tissues in general and cancer in particular. Another major contribution which physics can provide to cancer research is based on theoretical analysis and numerical calculations. Theoretical approaches aim at extraction of general physical laws which underlie the experimental observations. Computational modeling can span the bridge between the two worlds, as it provides a possibility to test experimental hypotheses and theoretical predictions in a clean and reproducible fashion.

1.4 Continuum mechanics of tissue growth and competition

The study of tissue growth from a theoretical perspective can be very broadly distinguished into two categories: (i) continuum-mechanics descriptions, which focus on the behavior at the mesoscopic scale and do not take single cell properties into account explicitly, and (ii) discrete models, which account at least for some of the mechanical properties of a single cell. We will discuss the latter in section 1.5 and focus on continuum-mechanics descriptions in this section.

1.4.1 Tissue growth

In order to introduce growth into continuum mechanics, the probably simplest way is the addition of a source term to the continuity equation

$$\partial_t \rho + \nabla(\rho \mathbf{v}) = k\rho, \quad (1.4.1)$$

with cell density ρ , velocity field \mathbf{v} , time t , and net growth rate $k = k_d - k_a$, the difference between division rate k_d and apoptosis rate k_a . In order to introduce a coupling between mechanics and growth, the growth rate k can be made dependent on the local mechanical environment. Equation (1.4.1) obviously violates mass conservation, as one expects for growing matter. In order to restore mass conservation, a two- or multi-component description needs to be employed [94]. Equation (1.4.1) is then recovered in the limit of large permeation lengths.

Allowing for a spatially varying growth rate k in equation (1.4.1), without further assumptions about the origin of these variations, suffices to arrive at already quite complex behavior. This can be motivated by in vitro experiments on growing tissue spheroids, which reveal an enhanced growth rate at the spheroids surface, while the bulk growth rate may be negative [29, 30, 62, 95] (see figure 1.1(a)). Biochemistry explains this observation with the higher concentration of nutrients at the surface due to limited diffusion into the core, while mechanics point out a different explanation: in order to grow, a cells needs to increase its volume and thus deform its surrounding, i.e. it imposes a strain dipole. At the surface of the spheroid, a part of the necessary strain field is cut away, which in turn favors proliferation locally.

The enhanced surface growth rate and the spherical symmetry motivate a two-rate growth model of the form

$$k(r) = \begin{cases} k_b & \text{for } r < R - a \\ k_b + \Delta k_s & \text{for } r > R - a \end{cases}, \quad (1.4.2)$$

with radial distance r , spheroid size R , bulk growth rate k_b , and surface growth rate enhancement Δk_s within a small region of width $a \ll R$ (see figure 1.1(b) for a sketch). Integration of equation (1.4.2) over space yields a differential equation for the spheroid volume V , given by

$$\partial_t V = k_b V + a \Delta k_s (36\pi)^{1/3} V^{2/3}, \quad (1.4.3)$$

assuming constant density ρ and neglecting terms $\mathcal{O}(a^2)$. For $k_b < 0$ and $k_b + \Delta k_s > 0$, i.e. a negative bulk and a positive surface growth rate, equation (1.4.3) has a steady

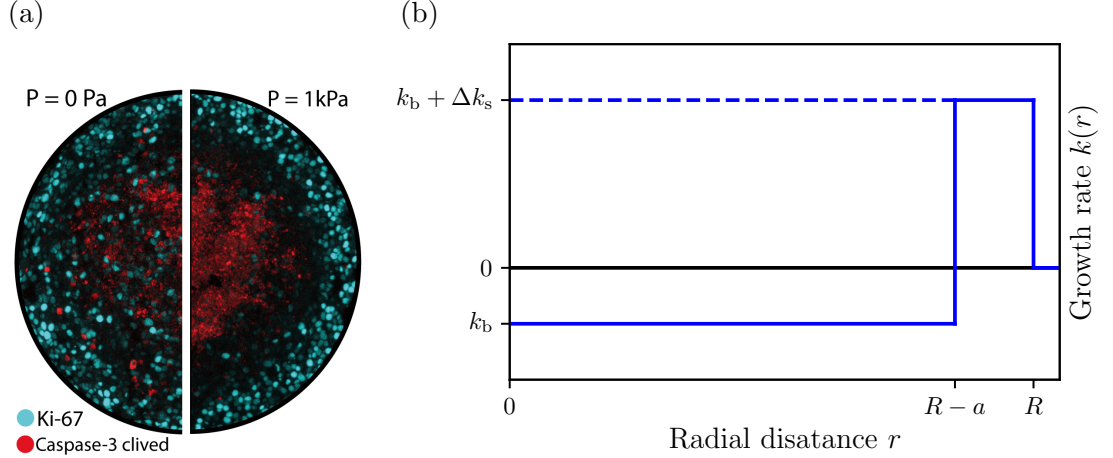


Figure 1.1: Cryosection and two-rate growth model sketch. (a) Tissue spheroid cryosection, with (right) and without (left) external pressure. "Cryosections and immunofluorescence of the spheroids are used to label the cell divisions [antibody against Ki-67 in light gray (cyan)] and apoptosis [antibody against cleaved Caspase-3 in dark gray (red)]. (Left) Half section of a spheroid grown in a normal medium for 4 days. (Right) Half section of a spheroid grown with a stress of 1 kPa for 4 days." Taken with permission from [29]. (b) Sketch of the two-rate growth model motivated by the experimental results displayed in (a).

state solution for the radius $R_{ss} = -3a\Delta k_s/k_b$. The steady state is sustained by a flow of cells from the proliferative rim towards the apoptotic core of the spheroid. This flow of cells can actually be "visualized" by tracer particles inserted into surface cells [96]. The analytic solution to equation (1.4.3) is given by (with $V(0) = 1$)

$$V(t) = \left[\left(1 + \frac{(36\pi)^{1/3} a \Delta k_s}{k_b} \right) \exp(k_b t/3) - \frac{(36\pi)^{1/3} a \Delta k_s}{k_b} \right]^3. \quad (1.4.4)$$

In [30], the growth of tumor spheroids has been studied under varying compressional stress by adding a polymer of high molecular weight to the growth medium. The polymer is not able to diffuse into the spheroid and thus causes an osmotic pressure. Equation 1.4.4 has been fitted with very good agreement to the obtained growth curves (see figure 1.2(a)), which allows the extraction of numerical values for k_b and Δk_s (see figure 1.2(b)). While the surface growth rate enhancement is basically independent of the external pressure, the bulk growth rate decreases in a linear fashion.

The idea that the growth rate of a tissue depends on the external pressure has been formulated in the concept of *homeostatic pressure* [97]. This concept can be understood as follows. A growing tissue increases its volume, which, by simple thermodynamic

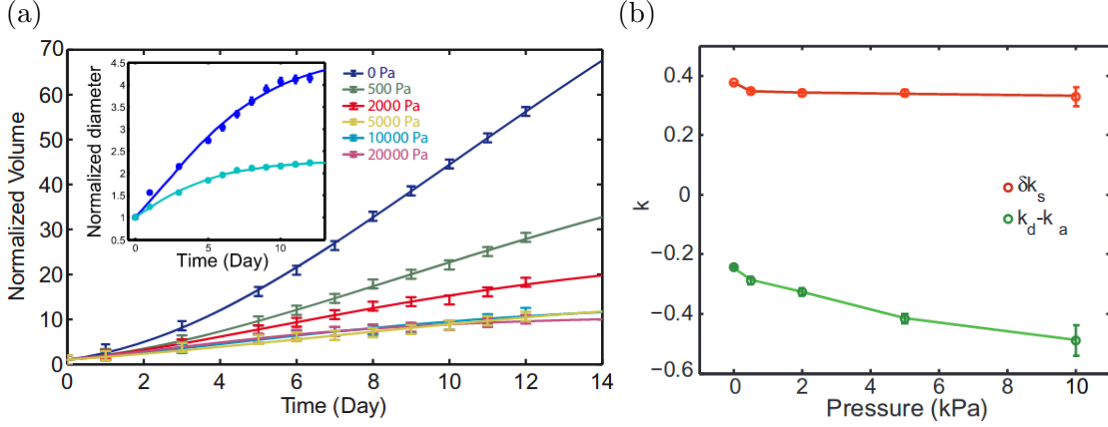


Figure 1.2: Growth dependence on pressure. (a) Normalized tissue spheroid volume V as a function of time t in experiments for different external pressures. Solid lines represent fits to equation (1.4.4). The inset shows the normalized spheroid diameter for two exemplary pressure values. (b) Values for surface growth rate enhancement (red) and bulk growth rate (green) obtained by the fits in (a) as a function of pressure. Both taken with permission from [30].

arguments, is connected to a pressure which the tissue exerts onto its surrounding. Figure 1.3(a) depicts a gedankenexperiment, in which the tissue grows inside a chamber which provides a constant biochemical environment. One side of this chamber is a movable piston, which is connected to a spring. As the tissue grows, it will start to compress the spring, which exerts a pressure back onto the tissue, until it reaches a steady state at which the tissue and the spring pressure balance each other. At this state the division rate equals the apoptosis rate and thus the total growth rate vanishes on average. This state is termed the *homeostatic* state and thus the pressure at this state defines the homeostatic pressure P_H . The homeostatic state is stable because any perturbation drives the system back to this state: further growth compresses the spring and the resulting excess pressure causes net apoptosis of the tissue, until the system reaches the homeostatic state again. This motivates the expansion of the growth rate to linear order in terms of the difference of the external pressure P to the homeostatic pressure

$$k = \kappa(P_H - P) + \mathcal{O}((P_H - P)^2), \quad (1.4.5)$$

with the pressure response coefficient κ . In the growth experiments displayed in figure 1.2, the bulk growth rate is negative for a vanishing external pressure. This indicates that the homeostatic pressure is actually negative. A linear extrapolation to the homeostatic state, i.e. a vanishing growth rate, estimates a homeostatic pressure of about

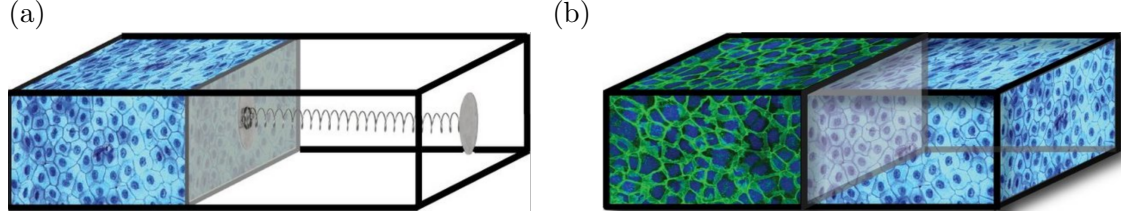


Figure 1.3: Gedankenexperiment homeostatic pressure and tissue competition. (a) A growing tissue in a box with a movable piston connected to a spring on one side. The growing tissue exerts a pressure onto its surrounding and compresses the spring until the tissue pressure balances the spring pressure. (b) Spring in (a) replaced by a second tissue, leading to a pressure-driven competition between the two. With permission from Markus Basan.

-5 kPa [98]. In order to arrive at a steady state spheroid size in the two-rate growth model, a negative homeostatic pressure is necessary for zero external pressure. This can be seen by plugging equation (1.4.5) into the expression for the steady state spheroid size R_{ss} , which yields $R_{ss} = -3a\Delta k_s/(\kappa P_H)$.

1.4.2 Tissue competition

The concept of homeostatic pressure has originally been proposed in order to explain the competition for space between two different tissues, e.g. tumor and host [97]. Figure 1.3(b) extends the discussed gedankenexperiment by replacing the spring by a second tissue (termed tissue B), which has a higher homeostatic pressure $P_H^B > P_H^A$ than the original tissue A. If we assume incompressibility, the total cell number N_{tot} is conserved, i.e.

$$\partial_t N_{tot} = k_A N_A + k_B N_B = 0. \quad (1.4.6)$$

Plugging equation (1.4.5) into equation (1.4.6) under the assumption of an identical pressure response coefficient κ for both tissues yields the pressure

$$P = P_H^A \phi + P_H^B (1 - \phi), \quad (1.4.7)$$

with the fraction $\phi = N_A/N_{tot}$ of cells of tissue A. Thus, the system pressure balances between the two homeostatic pressures. According to equation (1.4.5), tissue B will start to grow at the expense of tissue A and finally take over the compartment. Inserting equation (1.4.7) into equation (1.4.5) yields

$$\partial_t \phi = \kappa \Delta P_H \phi (1 - \phi) \quad (1.4.8)$$

for the dynamics, with the difference in homeostatic pressure $\Delta P_H = P_H^B - P_H^A$ between the two tissues. Hence, the takeover of the compartment by tissue B occurs in a logistic fashion and the outcome of this tissue competition is solely determined by the homeostatic pressures of the competing tissues.

In a circular or spherical geometry, an additional Laplace pressure due to interfacial tension may act on the tumor. The Laplace pressure causes a critical radius, which the tumor needs to overcome in order to grow further [97]. This provides a tentative explanation for metastatic inefficiency, i.e. the relatively small amount of metastatic cells that actually manage to grow to a secondary tumor of macroscopic size in comparison to the number of cells which detach from the primary tumor [99]. Metastases usually start to grow from a single or very few cells. As division and apoptosis are at least to some extent stochastic processes, the metastasis might be able to grow above the critical size threshold by chance. This chance, however, may be very small depending on the strength of interfacial tension.

The homeostatic pressure concept has since then been employed to study interface propagation between two competing tissues [100, 101, 102]. In [100], a generalized Fisher-Kolmogorov equation is derived (originally proposed to describe the expansion of an advantageous allele in a population [103]), which takes into account diffusion and convection. Accordingly, they find two regimes of interface propagation, a diffusive regime and one in which convective fluxes due to tissue growth dominate. In a circular geometry, diffusion leads to a broadening of the interface, which reduces the additional Laplace pressure and thus helps the invading tissue to overcome the critical radius, even if its initial radius is smaller than it.

The broadening of an interface due to diffusion raises the question whether the interface between two competing tissues is stable and which mechanisms determine its stability. Obviously, the interface between two identical tissues will grow indefinitely just by diffusion alone. Interfacial tension as in the DAH favors a well-defined, sharp interface. Reference [101] shows that interfacial tension can also be active due to anisotropic cell growth. They find that a difference in homeostatic pressure suffices to arrive at a stable propagating interface between two otherwise identical tissues. Reference [102] employs a linear stability analysis of interface propagation on a substrate. Three possible instabilities are found which could arise due to a difference in homeostatic pressure or cell motility between the competing tissues. We will explore the competition on a substrate and the stability of the interface by numerical means in chapter 4.

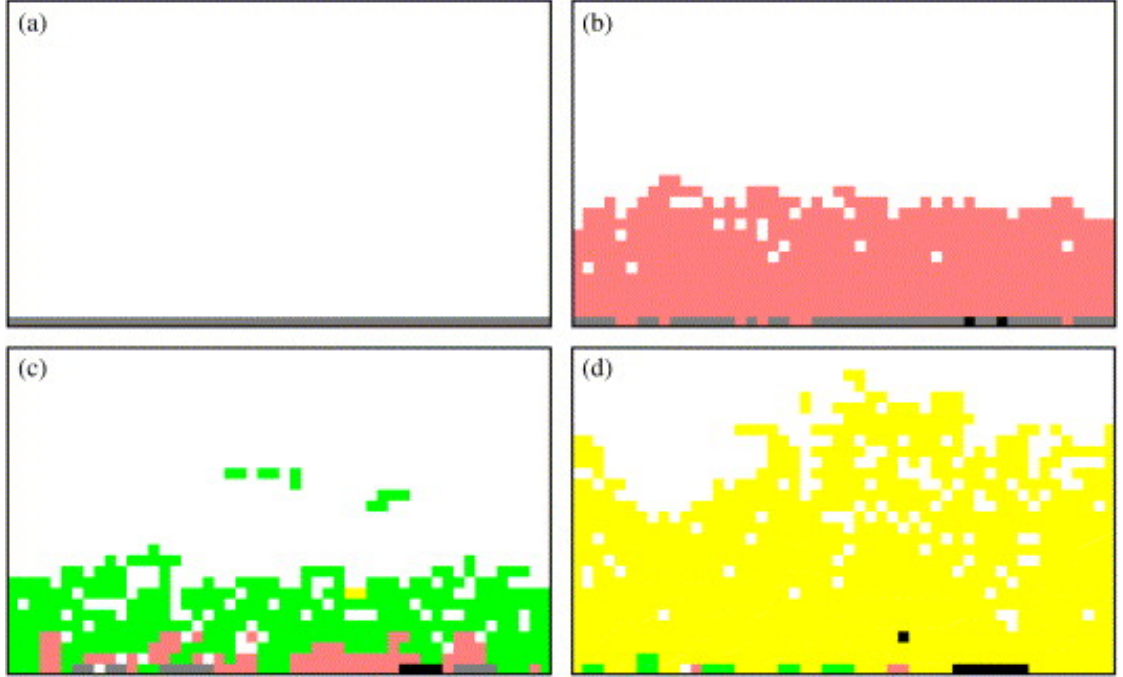


Figure 1.4: Evolutionary adaptation in cellular automaton model. Temporal evolution of a cellular automaton model with multiple cell phenotypes. Transport and conversion of nutrients and chemicals are taken into account by a reaction-diffusion model. Colors depict epithelial (gray), hyperplastic (pink), glycolytic (green), and glycolytic-acid-resistant (yellow) cells. Other phenotypes are depicted in black. (a) Initial condition of a single-layered epithelium connected to the basement membrane. (b)-(d) display the system after 100, 200, and 300 generations, respectively. Taken with permission from [104].

1.5 Computational modeling approaches

With growing computational power and increasing interest in the mechanics of multicellular tissues, a variety of computational models have been developed, based on different simulation techniques. The major complexity in the development of a cell-based model lies in the broad range of length and time scales which are present in tissue growth and tumorigenesis. Intracellular processes occur on the scale of nanometers and seconds, while tumors grow over years at the scale of the whole organ. For this reason, most models focus on a specific step during tumorigenesis, e.g. the formation of blood vessels during vascularisation of a tumor or the migration of cells through the ECM during the metastatic process. We will discuss different simulation techniques and describe certain models in more detail, with a special focus on cancer and tumorigenesis.

Broadly, cell-based models can be distinguished into lattice-based and off-lattice mod-

els. Most lattice-based models are cellular automata adapted to model tissue growth (CA). CA can be further distinguished by whether a single lattice site holds at most one or more than one cell. We limit our discussion here to the former. According to a set of rules, at each time step cells can remain at their lattice site, migrate to a neighboring one, undergo apoptosis, or divide. The rules typically consist of transition probabilities which depend on the current state of the lattice site and that of its local environment. CA models are thus solved by Monte-Carlo methods. The state of a lattice site can further contain information about the local concentrations of fields of nutrients and other chemicals, which in turn affect the transition probabilities. The dynamics of these fields are governed by partial differential equations (PDE), e.g. a reaction-diffusion model, which are solved numerically on the lattice. Such CA are hybrids between discrete and continuum models and have for example been employed to study tumor growth under oxygen limitation (hypoxia). Figure 1.6 displays snapshots at different times of the model of [104, 105]. In there, a constant oxygen level is imposed at the basement membrane (lower boundary). One cell might become hyperplastic due to a mutation or epigenetic changes. Hyperplastic cells are highly proliferative and start to grow away from the basement membrane, which induces hypoxic regions due to limited diffusion of oxygen from the basement membrane. In these regions, an evolutionary selection of those cells which can adopt their metabolism and switch to anaerobic glycolysis takes place. This change in metabolism causes an acidic environment due to production of hydrogen ions and thus another selection of those cells which are immune to this environment. These results show how evolutionary forces shape a more malignant phenotype of cancer cells, as glycolytic-acid-resistant cells create an environment toxic to other cells, but not harmful to themselves. Inclusion of a static microvessel network into the model allows for transport of the hydrogen ions away from their production site, which minimizes the advantage of cancer cells in comparison to normal cells [106].

One of the limitations of CA is that the shape of a cell is fixed by the lattice structure. Cellular Potts Model (CPM) account for varying cell shapes by using multiple lattice sites to represent a single cell. CPM use an energy functional, which allows to represent biological and physical behavior, e.g. cell-cell adhesion or a target cell volume, directly in the model. Cell growth can be implemented by changing the target volume of a cell in response to its environment, e.g. the local nutrient concentration. CPM are solved by Monte-Carlo methods under use of the Metropolis algorithm and allow for explicit representation of the microenvironment, e.g. ECM or vasculature. Cells can remodel the microenvironment and interact with it, e.g. migrate along ECM fibers or induce formation of new blood vessels [108, 109]. Reference [107] employs a CPM to study

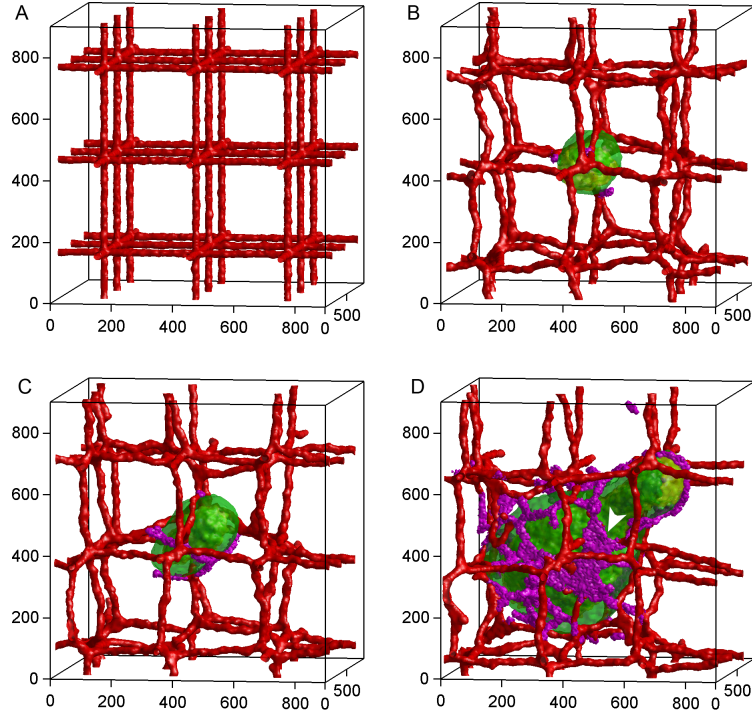


Figure 1.5: Cellular Potts Model with angiogenesis. Initial growth of a tumor and onset of angiogenesis in a Cellular Potts Model. The tumor starts to grow and deform the vasculature. Oxygen is the only nutrient in the system. Hypoxic cells secrete angiogenesis promoting factors, which attract endothelial cells. Different cell types are normal cancer cells (green), hypoxic cancer cells (yellow), vascular endothelial cells (red), and neovascular endothelial cells (purple). (a) Initial condition with a pre-existing vasculature and a single tumor cell. (b)-(d) display the system after 15, 30, and 75 days, respectively. Taken from [107].

the initial growth of an avascular tumor and the following onset of angiogenesis (see figure 1.5 for snapshots displaying the temporal evolution). Oxygen is the only nutrient in the system, assuming that other nutrients are not growth limiting and cancer cells do not change their metabolism. Only a single cancer cell type exists, which, however, can become hypoxic or necrotic depending on the supply with oxygen. Initially, the tumor starts to grow from a single cell in a pre-existing vascular network. The avascular tumor first grows exponentially, but saturates at a finite size once a lack of oxygen limits further growth. At the surface of the tumor, oxygen levels are still sufficient to sustain proliferation, while the core becomes necrotic (compare two-rate growth model in section 1.4.1). Hypoxic cells produce angiogenesis promoting factors, which attracts endothelial cells via chemotaxis and induces the formation of new blood vessels. This

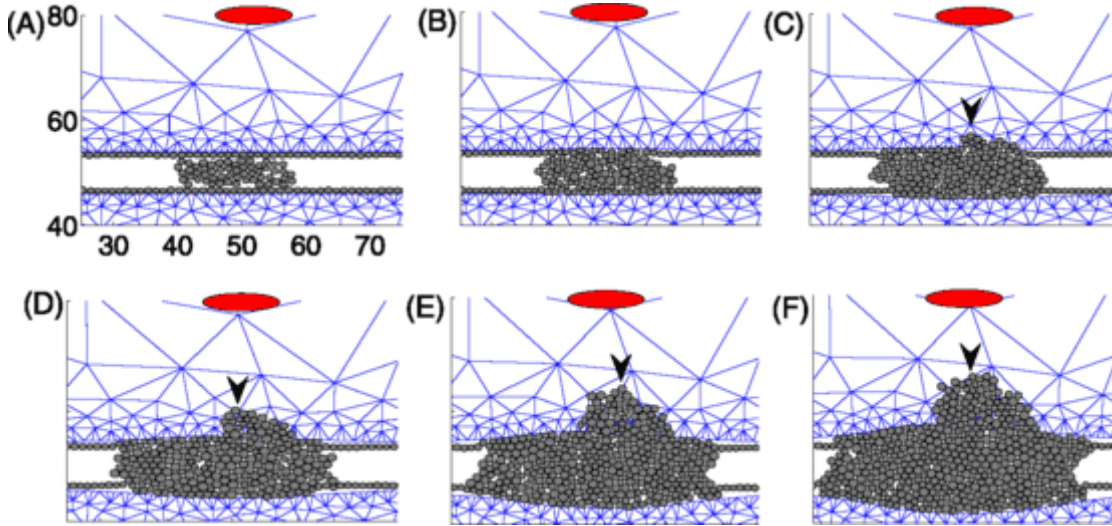


Figure 1.6: Tumor invasion in center-based model. Temporal evolution of the invasion of a tumor through the basement membrane into the stroma in a center-based model. Tumor cells (gray circles) invade the stroma (blue mesh) through the basal membrane in reaction to signaling molecules secreted by the stromal fibroblasts (red ellipse). Taken with permission from [110].

neovasculture then promotes further growth of the tumor.

Lattice-based models have an intrinsic lower length scale given by the size of a lattice site, while the lattice itself can give rise to artifacts, e.g. reflection of its structure in the shape of a large cell colony [111]. Such artifacts can be overcome by abandoning the discretization of space, the basis which all off-lattice models have in common. Off-lattice models can be further distinguished into models focusing on cell volume and those which focus on cell boundaries. Among the former are center-based models (CBM), in which cells are represented by one or very few centers of spheres or other simple objects. Most CBM are force-based and integrate Newton's equations of motion in order to evolve the system in time, while, however, Monte-Carlo methods are employed as well [112, 113]. The former has the advantages of a well-defined time scale and direct representation of physical laws. Force-based models consist of interactions between different cells, usually accounting for an excluded cell volume and cell-cell adhesion, and between cells and the environment, e.g. friction with the underlying substrate. Other forces regard the motility of cells, usually modeled by an active, propulsive force, and their growth, e.g. by increasing the volume of a cell over time. Reference [110] employs a CBM to study the interactions between a tumor and the surrounding stroma, including the initial steps of invasion. The stroma is modeled as a viscoelastic continuum which contains fibroblasts

at low density, while the ECM is given by a density field. Fibroblasts and migratory tumor cells secrete different proteinases. The fibroblast-secreted proteinase activates migration in tumor cells above a given threshold concentration, while tumor-associated proteinase degrades the basal membrane and the ECM. Once the first cells have become invasive, a positive feedback loop is created, as degradation of the basement membrane exposes more cells to fibroblast-secreted proteinase, causing more tumor cells to become migratory and more degradation, finally leading to collective invasion of tumor cells into the stroma.

Among the models which focus on the boundaries rather than the volume of cells are vertex-based models (VM). Cells are described as polygons (polyhedra in 3D) whose edges form the boundary to neighboring cells. Hence, VM are employed to study tightly packed, confluent tissues with negligible space between cells. The mechanics of cells and the interactions between different cells consist of a preferred cell area (volume in 3D) and cell perimeter (area in 3D), resulting in line tensions along cell edges. Line tensions consist of two competing terms, contractility of the actomyosin cortex, which acts to reduce the edge length, and the opposing cell-cell adhesion. Cell division and apoptosis can be included by insertion and removal of edges and vertices from the network. Epithelial tissues are the common example when VM are employed. Epithelial cells show a polarization between their apical and basal surface, which can be accounted for in 3D by different tensions along apical and basal edges. Reference [114] shows how such an imbalance can affect cancer morphogenesis in tubular ducts. Motivated by the experimentally observed loss of apical-basal polarization in transformed cells, the model has been employed in order to test whether this change suffices to explain the observed tumor morphology. Depending on the radius of the tube, the cancerous lesions expanded outwards for small and inwards for large tube size. The simulations revealed that proliferation of the transformed cells alone always results in outward growth of the lesion, irrespective of the tube radius, while inward expansion is only possible for additional loss of polarization.

In this section, we have seen how different models can be used to study very distinct stages and aspects of tumor growth, ranging from initial growth of cancerous lesions to invasion into the stroma. With the advance in experimental techniques, which nowadays allow for measurements of forces at the single-cell level and tumor growth in vivo, as well as the growth of available computational power, simulations of agent-based models provide a great tool to test experimental hypotheses and span the bridge between experiments and theoretical modeling, as we have seen in the paragraph on VM.

For the rest of this thesis we employ a center-based model of growing tissues, which

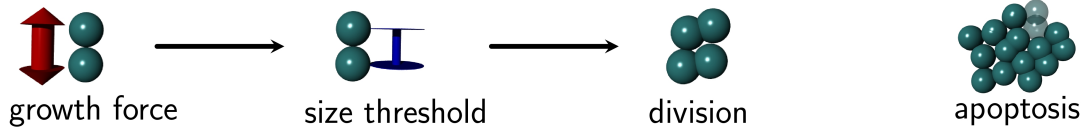


Figure 1.7: Growth mechanism of the simulation model used in this thesis. Sketch of the mechanisms regarding growth of the center-based model used in this thesis. A cell is constituted by two particles, which repel each other via an active growth force. When the distance reaches a certain size threshold, the cell divides and two new particles are placed close to the particles of the mother cell, which then constitute the two daughter cells. Cells are removed at a constant rate from the simulation box in order to model apoptosis.

we adapt in each chapter in order to study different aspects of tissue competition, while the basics of the model stay the same throughout the thesis. Figure 1.7 displays a sketch of the growth mechanism used in this model. Briefly, a cell is represented by two point particles which interact via a repulsive growth force. Cells divide when the distance between the two particles reaches a certain size threshold, while apoptosis is modeled by removing cells randomly at a constant rate. Cells interact via a volume-exclusion force on short distances and a constant adhesive force on intermediate distances and thus behave like soft sticky spheres. Additionally, a dissipative particle dynamics thermostat accounts for energy dissipation and random fluctuations. This model has first been developed to study the rheology of growing tissues and test the predictions regarding the competition for space between different tissues made by the homeostatic pressure concept [61, 115]. It has since then been employed to study different systems of collectively growing cells, ranging from wound healing assays over growing tissue spheroids to bacterial colonies under nutrient limitations in microfluidic devices [29, 116, 117].

1.6 Structure of the thesis

As we have seen in the previous sections, multicellular tissues are an example of active, growing matter. We have discussed several experimental results, which show how mechanics influence the behavior of single cells and tissues, as well as how growing tissues can be studied theoretically under the use of continuum mechanics and computationally by simulations of cell-based models. Furthermore, we looked at cancer as an example of tissue competition for space, how this competition is affected by mechanics, and discussed the contributions of physics to cancer research, as for instance in cancer diagnosis. In this thesis, we study the mechanically-regulated competition for space between tissues with different mechanical properties, with a focus on the role of the interface between

different tissues and the evolutionary nature of tumorigenesis.

In chapter 2 we study three-dimensional bulk competition between tumor and host and focus on the cross-adhesion between them. A strongly reduced cross-adhesion leads to segregation of the competing tissues and an enhanced growth rate at the interface between them. This growth enhancement leads to stable coexistence between host and tumor in a variety of different structures, even when the two differ in their respective homeostatic pressures. In chapter 3 we focus on the evolutionary aspect of tumorigenesis by introducing a mutation rate with which cells change their mechanical properties. In the simplest case, the tissue evolves to a strongly-growing, low-adhesive phenotype. Motivated by biological evidence, we couple mutations changing growth and adhesion strength by introducing a tradeoff between the two. In a certain parameter range we find highly dynamic coexistence between multiple cell populations with distinct mechanical properties. We switch from three- to two-dimensional tissue competition in chapter 4 in order to study the stability of the interface between the competing tissues. We find that a small motility force of one tissue suffices to stabilize the interface between two otherwise identical tissues, while larger motility forces cause a finite-wavelength instability of the interface. A different instability arises above a critical difference in homeostatic stress between the two tissues when the weaker tissue has a higher viscosity than the stronger tissue, while the interface is remarkably stable otherwise. The final chapter contains a summarizing discussion of this thesis and gives an outlook on possible future studies.

Bibliography chapter 1

- [1] P. L. Townes and J. Holtfreter (1955), “Directed movements and selective adhesion of embryonic amphibian cells”, *J. Exp. Zool.*, **128**(1), 53–120.
- [2] M. S. Steinberg (1963), “Reconstruction of tissues by dissociated cells”, *Science*, **141**(3579), 401–408.
- [3] D. Duguay, R. A. Foty, and M. S. Steinberg (2003), “Cadherin-mediated cell adhesion and tissue segregation: qualitative and quantitative determinants”, *Dev. Biol.*, **253**(2), 309–323.
- [4] R. A. Foty and M. S. Steinberg (2005), “The differential adhesion hypothesis: a direct evaluation”, *Dev. Biol.*, **278**(1), 255–263.
- [5] J. D. Amack and M. L. Manning (2012), “Knowing the boundaries: extending the differential adhesion hypothesis in embryonic cell sorting”, *Science*, **338**(6104), 212–215.
- [6] A. Prakasam, V. Maruthamuthu, and D. E. Leckband (2006), “Similarities between heterophilic and homophilic cadherin adhesion”, *Proc. Natl. Acad. Sci. U.S.A.*, **103**(42), 15434–15439.
- [7] J. Youssef, A. K. Nurse, L. Freund, and J. R. Morgan (2011), “Quantification of the forces driving self-assembly of three-dimensional microtissues”, *Proc. Natl. Acad. Sci. U.S.A.*, **108**(17), 6993–6998.
- [8] A. Mgharbel, H. Delanoë-Ayari, and J.-P. Rieu (2009), “Measuring accurately liquid and tissue surface tension with a compression plate tensiometer”, *HFSP J.*, **3**(3), 213–221.
- [9] A. K. Harris (1976), “Is cell sorting caused by differences in the work of intercellular adhesion? A critique of the Steinberg hypothesis”, *J. Theor. Biol.*, **61**(2), 267–285.
- [10] V. Maruthamuthu, B. Sabass, U. S. Schwarz, and M. L. Gardel (2011), “Cell-ECM traction force modulates endogenous tension at cell–cell contacts”, *Proc. Natl. Acad. Sci. U.S.A.*, **108**(12), 4708–4713.
- [11] A. F. Mertz, et al. (2012), “Scaling of traction forces with the size of cohesive cell colonies”, *Phys. Rev. Lett.*, **108**(19), 198101.

- [12] S. Yamada and W. J. Nelson (2007), “Localized zones of Rho and Rac activities drive initiation and expansion of epithelial cell–cell adhesion”, *J. Cell Biol.*, **178**(3), 517–527.
- [13] M. Krieg, et al. (2008), “Tensile forces govern germ-layer organization in zebrafish”, *Nat. Cell Biol.*, **10**(4), 429.
- [14] A. W. Orr, B. P. Helmke, B. R. Blackman, and M. A. Schwartz (2006), “Mechanisms of mechanotransduction”, *Dev. Cell*, **10**(1), 11–20.
- [15] B. Martinac (2004), “Mechanosensitive ion channels: molecules of mechanotransduction”, *J. Cell Sci.*, **117**(12), 2449–2460.
- [16] L. LeGoff and T. Lecuit (2015), “Mechanical forces and growth in animal tissues”, *Cold Spring Harb. Perspect. Biol.*, **8**(3), a019232.
- [17] D. Eder, C. Aegerter, and K. Basler (2017), “Forces controlling organ growth and size”, *Mech. Dev.*, **144**, 53–61.
- [18] E. Wilson, Q. Mai, K. Sudhir, R. H. Weiss, and H. E. Ives (1993), “Mechanical strain induces growth of vascular smooth muscle cells via autocrine action of PDGF”, *J. Cell Biol.*, **123**(3), 741–747.
- [19] E. Wilson, K. Sudhir, and H. E. Ives (1995), “Mechanical strain of rat vascular smooth muscle cells is sensed by specific extracellular matrix/integrin interactions”, *J. Clin. Invest.*, **96**(5), 2364–2372.
- [20] C. E. Miller, K. J. Donlon, L. Toia, C. L. Wong, and P. R. Chess (2000), “Cyclic strain induces proliferation of cultured embryonic heart cells”, *In Vitro Cell. Dev. Biol. Anim.*, **36**(10), 633–639.
- [21] K. Nishimura, et al. (2006), “Role of AKT in cyclic strain-induced endothelial cell proliferation and survival”, *Am. J. Physiol., Cell Physiol.*, **290**(3), C812–C821.
- [22] P. R. Chess, L. Toia, and J. N. Finkelstein (2000), “Mechanical strain-induced proliferation and signaling in pulmonary epithelial H441 cells”, *Am. J. Physiol. Lung Cell Mol. Physiol.*, **279**(1), L43–L51.
- [23] T. Schluck, U. Nienhaus, T. Aegerter-Wilmsen, and C. M. Aegerter (2013), “Mechanical control of organ size in the development of the drosophila wing disc”, *PLoS ONE*, **8**(10), e76171.

- [24] G. Cheng, J. Tse, R. K. Jain, and L. L. Munn (2009), “Micro-environmental mechanical stress controls tumor spheroid size and morphology by suppressing proliferation and inducing apoptosis in cancer cells”, *PLoS ONE*, **4**(2), e4632.
- [25] K. Alessandri, et al. (2013), “Cellular capsules as a tool for multicellular spheroid production and for investigating the mechanics of tumor progression in vitro”, *Proc. Natl. Acad. Sci. U.S.A.*, **110**(37), 14843–14848.
- [26] G. Helmlinger, P. A. Netti, H. C. Lichtenbeld, R. J. Melder, and R. K. Jain (1997), “Solid stress inhibits the growth of multicellular tumor spheroids”, *Nat. Biotechnol.*, **15**(8), 778–783.
- [27] A. Taloni, et al. (2014), “Mechanical properties of growing melanocytic nevi and the progression to melanoma”, *PLoS ONE*, **9**(4), e94229.
- [28] G. Cheng, J. Tse, R. K. Jain, and L. L. Munn (2009), “Micro-environmental mechanical stress controls tumor spheroid size and morphology by suppressing proliferation and inducing apoptosis in cancer cells”, *PLoS ONE*, **4**(2), e4632.
- [29] F. Montel, et al. (2011), “Stress clamp experiments on multicellular tumor spheroids”, *Phys. Rev. Lett.*, **107**(18), 188102.
- [30] F. Montel, et al. (2012), “Isotropic stress reduces cell proliferation in tumor spheroids”, *New J. Phys.*, **14**(5), 055008.
- [31] B. Racz, et al. (2007), “Hyperosmotic stress-induced apoptotic signaling pathways in chondrocytes”, *Bone*, **40**(6), 1536–1543.
- [32] N. I. Dmitrieva, L. F. Michea, G. M. Rocha, and M. B. Burg (2001), “Cell cycle delay and apoptosis in response to osmotic stress”, *Comp. Biochem. Physiol., Part A Mol. Integr. Physiol.*, **130**(3), 411–420.
- [33] K. J. Cowan and K. B. Storey (2003), “Mitogen-activated protein kinases: new signaling pathways functioning in cellular responses to environmental stress”, *J. Exp. Biol.*, **206**(7), 1107–1115.
- [34] Y. Xie, et al. (2007), “Using hyperosmolar stress to measure biologic and stress-activated protein kinase responses in preimplantation embryos”, *Mol. Hum. Reprod.*, **13**(7), 473–481.
- [35] M.-B. Nielsen, S. T. Christensen, and E. K. Hoffmann (2008), “Effects of osmotic stress on the activity of MAPKs and PDGFR- β -mediated signal transduction in NIH-3T3 fibroblasts”, *Am. J. Physiol., Cell Physiol.*, **294**(4), C1046–C1055.

- [36] D. Kong, et al. (2013), “Static mechanical stress induces apoptosis in rat endplate chondrocytes through MAPK and mitochondria-dependent caspase activation signaling pathways”, *PloS ONE*, **8**(7), e69403.
- [37] G. Charras and E. Sahai (2014), “Physical influences of the extracellular environment on cell migration”, *Nat. Rev. Mol. Cell Biol.*, **15**(12), 813.
- [38] P. Friedl and D. Gilmour (2009), “Collective cell migration in morphogenesis, regeneration and cancer”, *Nat. Rev. Mol. Cell Biol.*, **10**(7), 445–457.
- [39] S. Li, et al. (2002), “The role of the dynamics of focal adhesion kinase in the mechanotaxis of endothelial cells”, *Proc. Natl. Acad. Sci. U.S.A.*, **99**(6), 3546–3551.
- [40] C.-M. Lo, H.-B. Wang, M. Dembo, and Y.-l. Wang (2000), “Cell movement is guided by the rigidity of the substrate”, *Biophys. J.*, **79**(1), 144–152.
- [41] B. C. Isenberg, P. A. DiMilla, M. Walker, S. Kim, and J. Y. Wong (2009), “Vascular smooth muscle cell durotaxis depends on substrate stiffness gradient strength”, *Biophys. J.*, **97**(5), 1313–1322.
- [42] K. A. Beningo, M. Dembo, I. Kaverina, J. V. Small, and Y.-l. Wang (2001), “Nascent focal adhesions are responsible for the generation of strong propulsive forces in migrating fibroblasts”, *J. Cell Biol.*, **153**(4), 881–888.
- [43] M. L. Gardel, et al. (2008), “Traction stress in focal adhesions correlates biphasically with actin retrograde flow speed”, *J. Cell Biol.*, **183**(6), 999–1005.
- [44] D. Riveline, et al. (2001), “Focal contacts as mechanosensors: externally applied local mechanical force induces growth of focal contacts by an mDia1-dependent and ROCK-independent mechanism”, *J. Cell Biol.*, **153**(6), 1175–1186.
- [45] S. V. Plotnikov, A. M. Pasapera, B. Sabass, and C. M. Waterman (2012), “Force fluctuations within focal adhesions mediate ECM-rigidity sensing to guide directed cell migration”, *Cell*, **151**(7), 1513–1527.
- [46] C. D. Nobes and A. Hall (1999), “Rho GTPases control polarity, protrusion, and adhesion during cell movement”, *J. Cell Biol.*, **144**(6), 1235–1244.
- [47] T. E. Angelini, et al. (2011), “Glass-like dynamics of collective cell migration”, *Proc. Natl. Acad. Sci. U.S.A.*, **108**(12), 4714–4719.

- [48] M. Poujade, et al. (2007), “Collective migration of an epithelial monolayer in response to a model wound”, *Proc. Natl. Acad. Sci. U.S.A.*, **104**(41), 15988–15993.
- [49] X. Trepat, et al. (2009), “Physical forces during collective cell migration”, *Nat. Phys.*, **5**(6), 426–430.
- [50] L. Petitjean, et al. (2010), “Velocity fields in a collectively migrating epithelium”, *Biophys. J.*, **98**(9), 1790–1800.
- [51] C. L. Adams, W. J. Nelson, and S. J. Smith (1996), “Quantitative analysis of cadherin-catenin-actin reorganization during development of cell-cell adhesion”, *J. Cell Biol.*, **135**(6), 1899–1911.
- [52] B. Angres, A. Barth, and W. J. Nelson (1996), “Mechanism for transition from initial to stable cell-cell adhesion: kinetic analysis of E-cadherin-mediated adhesion using a quantitative adhesion assay”, *J. Cell Biol.*, **134**(2), 549–557.
- [53] A. Nose, A. Nagafuchi, and M. Takeichi (1988), “Expressed recombinant cadherins mediate cell sorting in model systems”, *Cell*, **54**(7), 993–1001.
- [54] G. Forgacs, R. A. Foty, Y. Shafrir, and M. S. Steinberg (1998), “Viscoelastic properties of living embryonic tissues: a quantitative study”, *Biophys. J.*, **74**(5), 2227–2234.
- [55] K. Guevorkian, M.-J. Colbert, M. Durth, S. Dufour, and F. Brochard-Wyart (2010), “Aspiration of biological viscoelastic drops”, *Phys. Rev. Lett.*, **104**(21), 218101.
- [56] L. Preziosi, D. Ambrosi, and C. Verdier (2010), “An elasto-visco-plastic model of cell aggregates”, *J. Theor. Biol.*, **262**(1), 35–47.
- [57] K. Jakab, et al. (2008), “Relating cell and tissue mechanics: implications and applications”, *Dev. Dyn.*, **237**(9), 2438–2449.
- [58] D. Gonzalez-Rodriguez, K. Guevorkian, S. Douezan, and F. Brochard-Wyart (2012), “Soft matter models of developing tissues and tumors”, *Science*, **338**(6109), 910–917.
- [59] D. Gonzalez-Rodriguez, et al. (2013), “Detachment and fracture of cellular aggregates”, *Soft Matter*, **9**(7), 2282–2290.

- [60] A. Kalantarian, et al. (2009), “Axisymmetric drop shape analysis for estimating the surface tension of cell aggregates by centrifugation”, *Biophys. J.*, **96**(4), 1606–1616.
- [61] J. Ranft, et al. (2010), “Fluidization of tissues by cell division and apoptosis”, *Proc. Natl. Acad. Sci. U.S.A.*, **107**(49), 20863–20868.
- [62] M. Delarue, et al. (2013), “Mechanical control of cell flow in multicellular spheroids”, *Phys. Rev. Lett.*, **110**(13), 138103.
- [63] S. Garcia, et al. (2015), “Physics of active jamming during collective cellular motion in a monolayer”, *Proc. Natl. Acad. Sci. U.S.A.*, **112**(50), 15314–15319.
- [64] A. J. Liu and S. R. Nagel (1998), “Nonlinear dynamics: Jamming is not just cool any more”, *Nature*, **396**(6706), 21.
- [65] M. Sadati, N. T. Qazvini, R. Krishnan, C. Y. Park, and J. J. Fredberg (2013), “Collective migration and cell jamming”, *Differentiation*, **86**(3), 121–125.
- [66] S. Suresh (2007), “Biomechanics and biophysics of cancer cells”, *Acta Biomater.*, **3**(4), 413–438.
- [67] M. Lekka, et al. (1999), “Elasticity of normal and cancerous human bladder cells studied by scanning force microscopy”, *Eur. Biophys. J.*, **28**(4), 312–316.
- [68] S. E. Cross, Y.-S. Jin, J. Rao, and J. K. Gimzewski (2007), “Nanomechanical analysis of cells from cancer patients”, *Nat. Nanotechnol.*, **2**(12), 780–783.
- [69] J. Guck, et al. (2005), “Optical deformability as an inherent cell marker for testing malignant transformation and metastatic competence”, *Biophys. J.*, **88**(5), 3689–3698.
- [70] H. Kubitschke, et al. (2017), “Actin and microtubule networks contribute differently to cell response for small and large strains”, *New J. Phys.*, **19**(9), 093003.
- [71] A. Hall (2009), “The cytoskeleton and cancer”, *Cancer Metastasis Rev.*, **28**(1-2), 5–14.
- [72] Y. M. Efremov, et al. (2014), “Mechanical properties of fibroblasts depend on level of cancer transformation”, *Biochim. Biophys. Acta Mol. Cell Res.*, **1843**(5), 1013–1019.

- [73] V. Swaminathan, et al. (2011), “Mechanical stiffness grades metastatic potential in patient tumor cells and in cancer cell lines”, *Cancer Res.*, **71**(15), 5075–5080.
- [74] W. Xu, et al. (2012), “Cell stiffness is a biomarker of the metastatic potential of ovarian cancer cells”, *PloS ONE*, **7**(10), e46609.
- [75] T. W. Remmerbach, et al. (2009), “Oral cancer diagnosis by mechanical phenotyping”, *Cancer Res.*, **69**(5), 1728–1732.
- [76] F. Meinhövel, et al. (2018), “Changing cell mechanics - a precondition for malignant transformation of oral squamous carcinoma cells”, *Converg. Sci. Phys. Oncol.*, **4**(3), 034001.
- [77] C. M. Kraning-Rush, J. P. Califano, and C. A. Reinhart-King (2012), “Cellular traction stresses increase with increasing metastatic potential”, *PloS ONE*, **7**(2).
- [78] T. M. Koch, S. Münster, N. Bonakdar, J. P. Butler, and B. Fabry (2012), “3D traction forces in cancer cell invasion”, *PloS ONE*, **7**(3), e33476.
- [79] F. Spill, D. S. Reynolds, R. D. Kamm, and M. H. Zaman (2016), “Impact of the physical microenvironment on tumor progression and metastasis”, *Curr. Opin. Biotechnol.*, **40**, 41–48.
- [80] M. H. Zaman, et al. (2006), “Migration of tumor cells in 3D matrices is governed by matrix stiffness along with cell-matrix adhesion and proteolysis”, *Proc. Natl. Acad. Sci. U.S.A.*, **103**(29), 10889–10894.
- [81] S. P. Singh, M. P. Schwartz, J. Y. Lee, B. D. Fairbanks, and K. S. Anseth (2014), “A peptide functionalized poly(ethylene glycol)(PEG) hydrogel for investigating the influence of biochemical and biophysical matrix properties on tumor cell migration”, *Biomater. Sci.*, **2**(7), 1024–1034.
- [82] P. P. Provenzano, et al. (2006), “Collagen reorganization at the tumor-stromal interface facilitates local invasion”, *BMC Med.*, **4**(1), 38.
- [83] K. M. Riching, et al. (2014), “3D collagen alignment limits protrusions to enhance breast cancer cell persistence”, *Biophys. J.*, **107**(11), 2546–2558.
- [84] M. Miron-Mendoza, J. Seemann, and F. Grinnell (2010), “The differential regulation of cell motile activity through matrix stiffness and porosity in three dimensional collagen matrices”, *Biomaterials*, **31**(25), 6425–6435.

- [85] S. P. Carey, C. M. Kraning-Rush, R. M. Williams, and C. A. Reinhart-King (2012), “Biophysical control of invasive tumor cell behavior by extracellular matrix microarchitecture”, *Biomaterials*, **33**(16), 4157–4165.
- [86] K. Wolf, et al. (2013), “Physical limits of cell migration: control by ECM space and nuclear deformation and tuning by proteolysis and traction force”, *J. Cell Biol.*, **201**(7), 1069–1084.
- [87] S. I. Fraley, et al. (2015), “Three-dimensional matrix fiber alignment modulates cell migration and MT1-MMP utility by spatially and temporally directing protrusions”, *Sci. Rep.*, **5**(1), 1–13.
- [88] O. Chaudhuri, et al. (2014), “Extracellular matrix stiffness and composition jointly regulate the induction of malignant phenotypes in mammary epithelium”, *Nat. Mater.*, **13**(10), 970–978.
- [89] S. C. Wei, et al. (2015), “Matrix stiffness drives epithelial–mesenchymal transition and tumour metastasis through a TWIST1–G3BP2 mechanotransduction pathway”, *Nat. Cell Biol.*, **17**(5), 678–688.
- [90] M. Paszek, et al. (2005), “Tensional homeostasis and the malignant phenotype”, *Cancer Cell*, **8**(3), 241–254.
- [91] C. Frantz, K. M. Stewart, and V. M. Weaver (2010), “The extracellular matrix at a glance”, *J. Cell Sci.*, **123**(24), 4195–4200.
- [92] R. Sinkus, et al. (2005), “Viscoelastic shear properties of in vivo breast lesions measured by mr elastography”, *Magn. Reson. Imaging*, **23**(2), 159–165.
- [93] M. Shahryari, et al. (2019), “Tomoelastography distinguishes noninvasively between benign and malignant liver lesions”, *Cancer Res.*, **79**(22), 5704–5710.
- [94] J. Ranft, J. Prost, F. Jülicher, and J.-F. Joanny (2012), “Tissue dynamics with permeation”, *Eur. Phys. J. E*, **35**(6), 46.
- [95] M. Delarue, et al. (2014), “Compressive stress inhibits proliferation in tumor spheroids through a volume limitation”, *Biophys. J.*, **107**(8), 1821–1828.
- [96] M. Delarue, et al. (2013), “Mechanical control of cell flow in multicellular spheroids”, *Phys. Rev. Lett.*, **110**(13), 138103.

- [97] M. Basan, T. Risler, J.-F. Joanny, X. Sastre-Garau, and J. Prost (2009), “Homeostatic competition drives tumor growth and metastasis nucleation”, *HFSP J.*, **3**(4), 265–272.
- [98] N. Podewitz, M. Delarue, and J. Elgeti (2015), “Tissue homeostasis: A tensile state”, *Europhys. Lett.*, **109**(5), 58005.
- [99] R. A. Weinberg (2007), *The biology of cancer*. New York: Garland Science.
- [100] J. Ranft, M. Aliee, J. Prost, F. Jülicher, and J.-F. Joanny (2014), “Mechanically driven interface propagation in biological tissues”, *New J. Phys.*, **16**(3), 035002.
- [101] N. Podewitz, F. Jülicher, G. Gompper, and J. Elgeti (2016), “Interface dynamics of competing tissues”, *New J. Phys.*, **18**(8), 083020.
- [102] J. J. Williamson and G. Salbreux (2018), “Stability and roughness of interfaces in mechanically regulated tissues”, *Phys. Rev. Lett.*, **121**(23), 238102.
- [103] R. A. Fisher (1937), “The wave of advance of advantageous genes”, *Ann. Eugen.*, **7**(4), 355–369.
- [104] K. Smallbone, R. A. Gatenby, R. J. Gillies, P. K. Maini, and D. J. Gavaghan (2007), “Metabolic changes during carcinogenesis: potential impact on invasiveness”, *J. Theor. Biol.*, **244**(4), 703–713.
- [105] R. Gatenby, et al. (2007), “Cellular adaptations to hypoxia and acidosis during somatic evolution of breast cancer”, *Br. J. Cancer*, **97**(5), 646–653.
- [106] A. A. Patel, E. T. Gawlinski, S. K. Lemieux, and R. A. Gatenby (2001), “A cellular automaton model of early tumor growth and invasion: the effects of native tissue vascularity and increased anaerobic tumor metabolism”, *J. Theor. Biol.*, **213**(3), 315–331.
- [107] A. Shirinifard, et al. (2009), “3D multi-cell simulation of tumor growth and angiogenesis”, *PloS ONE*, **4**(10), e7190.
- [108] A. L. Bauer, T. L. Jackson, and Y. Jiang (2007), “A cell-based model exhibiting branching and anastomosis during tumor-induced angiogenesis”, *Biophys. J.*, **92**(9), 3105–3121.
- [109] M. Scianna, L. Preziosi, and K. Wolf (2013), “A cellular potts model simulating cell migration on and in matrix environments”, *Math. Biosci. Eng.*, **10**(1), 235–261.

- [110] Y. Kim and H. G. Othmer (2013), “A hybrid model of tumor–stromal interactions in breast cancer”, *Bull. Math. Biol.*, **75**(8), 1304–1350.
- [111] P. Van Liedekerke, M. M. Palm, N. Jagiella, and D. Drasdo (2015), “Simulating tissue mechanics with agent-based models: concepts, perspectives and some novel results”, *Comp. Part. Mech.*, **2**(4), 401–444.
- [112] D. Drasdo, R. Kree, and J. McCaskill (1995), “Monte carlo approach to tissue-cell populations”, *Phys. Rev. E*, **52**(6), 6635.
- [113] D. Drasdo and S. Höhme (2005), “A single-cell-based model of tumor growth in vitro: monolayers and spheroids”, *Phys. Biol.*, **2**(3), 133–147.
- [114] H. A. Messal, et al. (2019), “Tissue curvature and apicobasal mechanical tension imbalance instruct cancer morphogenesis”, *Nature*, **566**(7742), 126–130.
- [115] M. Basan, J. Prost, J.-F. Joanny, and J. Elgeti (2011), “Dissipative particle dynamics simulations for biological tissues: rheology and competition”, *Phys. Biol.*, **8**(2), 026014.
- [116] M. Basan, J. Elgeti, E. Hannezo, W.-J. Rappel, and H. Levine (2013), “Alignment of cellular motility forces with tissue flow as a mechanism for efficient wound healing”, *Proc. Natl. Acad. Sci. U.S.A.*, **110**(7), 2452–2459.
- [117] R. Hornung, et al. (2018), “Quantitative modelling of nutrient-limited growth of bacterial colonies in microfluidic cultivation”, *J. R. Soc. Interface*, **15**(139), 20170713.

2 Mechanics of tissue competition: interfaces stabilize coexistence

2.1 Abstract

Mechanical forces influence the dynamics of growing tissues. Computer simulations are employed to study the importance of interfacial effects in tissue competition. It was speculated previously that mechanical pressure determines the competition, where the determining quantity is the homeostatic pressure - the pressure where division and apoptosis balance; the tissue with the higher homeostatic pressure overwhelms the other. In contrast, we find that a weaker tissue can persist in stable coexistence with a stronger tissue, if adhesion between them is small enough. An analytic continuum description can quantitatively describe the underlying mechanism and reproduce the resulting pressures and cell-number fractions. Furthermore, simulations reveal a variety of coexisting structures, ranging from spherical inclusions to a bicontinuous state.

2.2 Introduction

Mechanical forces influence the growth of cells and tissues in several ways, via mechanotransduction [1] or mechanical feedback as regulator of growth and shape [2, 3]. This occurs in systems ranging from plants adapting their growth patterns to mechanical loads [4, 5], all the way to tumors responding in their growth to the pressure of the embedding medium [6, 7, 8]. Cells have been shown to differentiate according to substrate stiffness [9], and divide according to mechanical stress and strain [10, 11, 12, 13, 14, 15, 16]. Spheroids of many cells, grown in elastic gels [17, 18, 19] or shells [20, 21], or even in suspension with osmotic stress [22, 23, 24, 25], show strong dependence of growth on the properties of the embedding medium.

Given the evidence of the effect of mechanical stress on growth, it seems clear that mechanics should also influence tissue competition, such as the competition between different mutants in the imaginal wing disk of *Drosophila* [26, 27], or clonal expansion in multistep cancerogenesis [28, 29]. Several theoretical studies support and quantify

this idea for both, competition [2] and size determination [30] in the wing, and tumor growth [8, 31].

A tissue grown in a finite compartment exerts a certain pressure onto its surrounding. When reaching a steady state - the homeostatic state - this is the homeostatic pressure P_H . Under an external pressure P below P_H , the tissue grows; whereas it shrinks if the pressure is above it. This can be formulated as a linear expansion of the bulk growth rate k_b around the homeostatic pressure [31],

$$k_b = \kappa(P_H - P) \quad (2.2.1)$$

with the pressure response factor κ . To study the role of pressure on growth, cell-culture experiments and computer simulations have been developed to explore this effect [22, 23, 24, 32, 33, 34]. While confirming the general picture - that mechanical pressure reduces growth - these experiments and simulations have revealed that tissues preferentially divide at the surface, even to the extent that they die (on average) in the bulk and sustain a finite size only by surface growth. While consideration of nutrient transport may be necessary for quantitative description of certain experiments [35, 36], mechanics alone already results in enhanced surface growth, and matches other experiments [33]. For tissue competition in general, and metastatic inefficiency in particular, it has been argued that metastases need to reach a critical size, below which the Laplace pressure from the interfacial tension exceeds the homeostatic pressure difference, and the metastasis disappears [31].

In this work, we study the role of interfacial effects on mechanical tissue competition by numerical simulations, in particular the effect of the strength of adhesive interactions between different tissues. We find that similar to free surfaces, cells divide preferentially at the low-adhesive interfaces. This interfacial growth in turn can stabilize coexistence of two tissues with different homeostatic pressures. Interfaces in tissue competition have been studied mostly from a theoretical perspective. Besides the above mentioned critical size threshold due to interfacial tension, existing studies focus mainly on the propagation of interfaces driven by a difference in homeostatic pressure [34, 37, 38], while the role of an enhanced interfacial growth rate and of interactions across the interface has not yet been considered.

2.3 Model

Agent-based modelling has been very successful in studying various aspects of tissue growth, such as buckling and stem cell distribution in mammalian skin [39], formation

of vascular networks [40] or wound healing [41]. For tumor growth, existing models focus on different stages of tumor progression, e.g. avascular growth [42], angiogenesis [43], or formation of metastasis [44, 45]. We follow the approach of [32] and model growing and dividing cells by two point-like particles, which repel each other with a growth force

$$\mathbf{F}_{ij}^G = \frac{G}{(r_{ij} + r_0)^2} \hat{\mathbf{r}}_{ij}, \quad (2.3.1)$$

with the growth strength factor G , the distance r_{ij} and unit vector $\hat{\mathbf{r}}_{ij}$ between the two particles and a constant r_0 . \mathbf{F}_{ij}^G is applied during the whole life time of a cell. Cells divide when r_{ij} reaches a certain size threshold r_{ct} . After division, a new particle is placed randomly near each of the particles of the divided cell within a short distance r_d . Apoptosis is modeled by a constant rate of cell removal k_a . Both processes occur instantaneously. Volume exclusion is maintained by a relatively soft repulsive force \mathbf{F}_{ij}^V , while adhesion between cells is modeled by a constant attractive force \mathbf{F}_{ij}^A , given by

$$\mathbf{F}_{ij}^V = f_0 \left(\frac{R_{PP}^5}{r_{ij}^5} - 1 \right) \hat{\mathbf{r}}_{ij} \quad (2.3.2)$$

$$\mathbf{F}_{ij}^A = -f_1 \hat{\mathbf{r}}_{ij}, \quad (2.3.3)$$

with the strength of volume exclusion and adhesion force f_0 and f_1 , respectively. R_{PP} is the cut-off length of pairwise particle interactions. Division threshold r_{ct} , the constant r_0 in equation (4.3.1) as well as R_{PP} are all of the order of the typical cell size. A dissipative particle dynamics (DPD)-type thermostat is employed to account for dissipation of energy and random fluctuations, which mimics the stochasticity of many biological processes, e.g. the dynamic structure of the cytoskeleton or interactions with the extracellular matrix. The thermostat consists of a dissipative force

$$\mathbf{F}_{ij}^D = -\gamma \omega^D(r_{ij}) (\hat{\mathbf{r}}_{ij} \cdot \mathbf{v}_{ij}) \hat{\mathbf{r}}_{ij}, \quad (2.3.4)$$

with the strength γ , a weight function $\omega^D(r_{ij})$ and the relative velocity $\mathbf{v}_{ij} = \mathbf{v}_j - \mathbf{v}_i$, as well as a random force

$$\mathbf{F}_{ij}^R = \sigma \omega^R(r_{ij}) \xi_{ij} \hat{\mathbf{r}}_{ij}, \quad (2.3.5)$$

with strength $\sigma = \sqrt{2k_B T \gamma}$, a Gaussian random variable ξ_{ij} with zero mean and unit variance and a weight function $\omega^R(r_{ij}) = \sqrt{\omega^D(r_{ij})}$. T is an effective temperature which characterizes the strength of the fluctuations. Its value is chosen such that cells do not

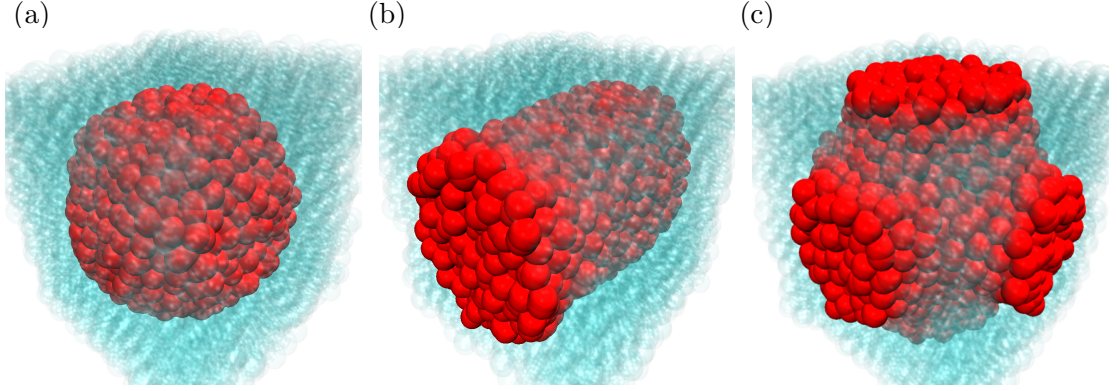


Figure 2.1: Snapshots of various structures of tissue coexistence. Both tissues are identical (reference tissue), interacting via $f_c = 0$. (a) Spherical inclusion. (b) Cylindrical inclusion. (c) Schwarz-P like bicontinuous structure. Other structures observed include flat interfaces, perforated lamellar, combinations (e.g. perforated lamellar together with a spheroid), and inverted (e.g. inverse spheroid) structures.

get stuck in local minima but has no noticeable effect otherwise.

The dynamics of particle i is then determined by

$$m_i \ddot{\mathbf{r}}_i = \mathbf{F}_{ik}^G + \mathbf{F}_{ik}^D + \mathbf{F}_{ik}^R + \sum_{j \neq i, k} (\mathbf{F}_{ij}^A + \mathbf{F}_{ij}^V + \mathbf{F}_{ij}^D + \mathbf{F}_{ij}^R) + \mathbf{F}_i^B, \quad (2.3.6)$$

with mass m_i of particle i , particle k that forms a cell with particle i , and the background dissipation force $\mathbf{F}_i^B = -\gamma_b \mathbf{v}_i$. We integrate the equations of motion with a self-consistent velocity-Verlet algorithm. Note that the division rate k_d is not fixed, but is obtained from the simulations and depends on the other model parameters.

This model results in pressure-dependent growth, in reasonable agreement with experiments [22, 23, 24, 32, 33, 34]. For two competing tissues A and B, parameters for each tissue can be set independently. In this work, we only vary the growth strengths G^A and G^B , the self adhesion strengths f_1^{AA} , f_1^{BB} and the cross-adhesion strength $f_1^{AB} := f_c$. We define a reference tissue (see SI for numerical values) and report parameters in terms of this reference tissue, denoted by a dagger, e.g. $G^\dagger = G/G_0$. We measure space in units of the pair potential interaction range R_{pp} , time by the inverse of the apoptosis rate k_a , force in units of G_0/R_{pp}^2 and thus stress by G_0/R_{pp}^4 . Quantities measured in these units are denoted by an asterisk *.

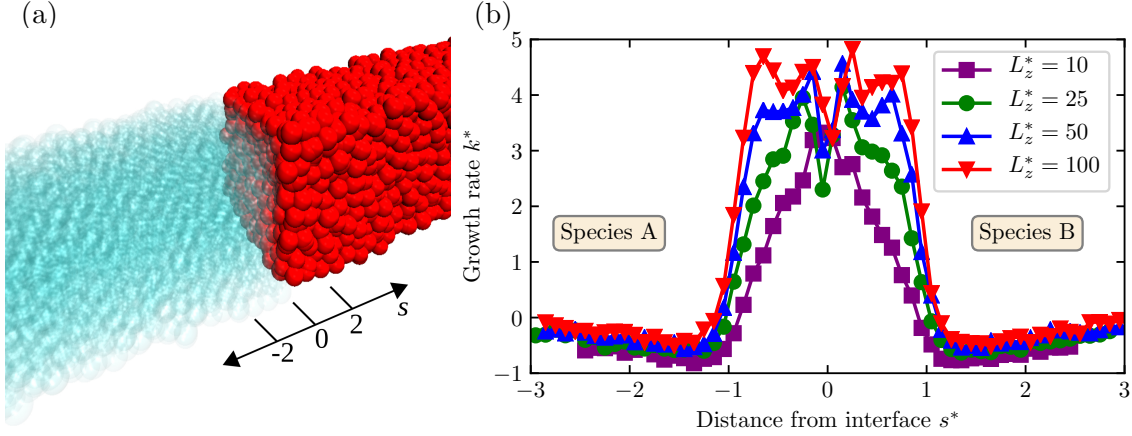


Figure 2.2: Planar interface between two competing tissues. (a) Simulation snapshot. (b) Net growth rate $k^* = (k_d - k_a)/k_a$ as a function of the distance from the interface s^* for the competition between two identical (reference) tissues with $f_c = 0$ for various box lengths L_z^* .

2.4 Results

Very small *cross-adhesion* strengths f_c between cells of different tissues (i.e. $f_c \ll \min(f_1^{AA}, f_1^{BB})$) result in fundamentally different outcomes of the tissue competition than predicted from simply assuming increased surface tension [31]. Instead of one tissue overwhelming the other for different homeostatic pressures or the existence of a critical size threshold explained above, we observe stable coexistence in a variety of segregated structures depending on initial conditions (see figure 2.1). While segregation of the tissues can be expected because of the high interfacial tension ($\gamma^{AB} \gg \gamma^{AA}, \gamma^{BB}$) [46], the stable coexistence comes at a surprise. Even for two identical tissues (i.e the same tissue parameters but dissimilar cells, with cross-adhesion different from self-adhesion) a single A cell in a host of B grows into a stable spheroid occupying about a third of the volume. Similarly, a random 1:2 mixture of stronger A cells in a host of B can result in a stable 3:1 Schwarz-P bicontinuous structure. Movie 1 and 2 in the SI show the temporal evolution during simulations similar to these two scenarios.

2.4.1 Flat interfaces - origin of coexistence

In order to understand the underlying physical mechanism of this behavior, we turn to a simpler geometry of a slab-like tissue arrangement and develop an appropriate analytic model. Cells are confined to a finite (periodic) compartment of size $L_x \times L_y \times L_z$. All

cells in the left half ($z < L_z/2$) are type B cells, all others type A. Due to the periodic boundary conditions, the system contains two interfaces. Large adhesion between cells of the same tissue and no adhesion between cells of different tissues leads to a large interfacial tension, stabilizing the flat interface with nearly vanishing roughness. This allows the measurement of the division rate k_d as a function of the distance to the interface. The growth rate profile (see figure 2.9(b)) reveals that cells divide more in a small region of width a (roughly the cut-off length R_{PP} , with a weak dependence on other model parameters) at the interface. In the bulk of the tissue, the net growth rate is negative due to an elevated pressure. These results motivate a two-rate growth model [22, 23, 24, 32, 33]

$$\partial_t \rho(s) + \nabla \cdot (\rho(s) \mathbf{v}) = k_b \rho(s) + \Delta k_s \Theta(s - a) \rho(s), \quad (2.4.1)$$

where $\rho(s)$ is the cellular density of either tissue, Θ the Heaviside step function, s the distance to the nearest interface and \mathbf{v} the cell-velocity field. The additional growth at the interface is modeled as a growth rate enhancement Δk_s near the interface (less than a away).

Division and apoptosis events locally relax stress and thus lead to a liquefaction of the tissue on long timescales [47, 48, 49]. Indeed, some experiments on tissue rheology suggest liquid behavior on long timescales [50, 51, 52], while some other experiments on *Drosophila* wing discs suggest that not all stress is relaxed by growth [53, 54, 55]. However, our model tissue clearly behaves as a liquid [47]. With the low velocities (cells move a few cell diameters at most during their lifetime) and no external forcing, we can thus assume a constant pressure across the system. Within a sharp-kink approximation with constant density $\rho(s) = \rho_0$ we integrate equation (2.4.1) over space, which gives for the total cell number N_A of tissue A

$$\partial_t N_A = k_b^A N_A + \Delta k_s^A \rho_0 2a L_x L_y, \quad (2.4.2)$$

and similarly for tissue B. We define the cell number fraction $\phi = L_A/L_z = N_A/(N_A + N_B)$ of type A cells, and divide equation (2.4.2) by $(N_A + N_B) = \rho_0 L_x L_y L_z$ and obtain

$$\partial_t \phi = k_b^A \phi + 2a \Delta k_s^A / L_z, \quad (2.4.3)$$

for tissue A, and

$$\partial_t (1 - \phi) = k_b^B (1 - \phi) + 2a \Delta k_s^B / L_z, \quad (2.4.4)$$

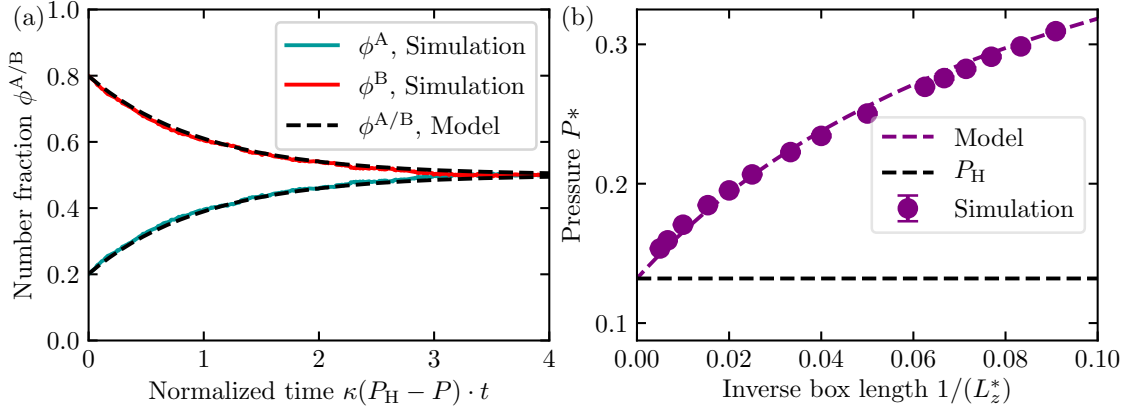


Figure 2.3: (a) Solid cyan and red lines show the time evolution of the cell number fractions $\phi^{A/B}$ in a competition with zero cross-adhesion $f_c = 0$ between two identical (reference) tissues for a box length $L_z^* = 100$. Dashed black lines show equation (2.4.6) for both tissues with parameters fixed by independent simulations. (b) Average pressure measured in competition as in (a) in terms of the inverse box length L_z^* . Dashed purple line shows equation (2.4.5), with parameters as in (a). Errors are determined by block averaging method (see. [56]).

for tissue B. The homogeneous pressure motivates the linear dependence of k_b on $(P_H - P)$ as in equation (2.2.1), and similarly $\Delta k_s \simeq \Delta k_s^0 + \Delta k_s^1 (P_H - P)$.

For simplicity, we first explore two identical tissues. Insertion of the linear pressure dependence of k_b and Δk_s in equation (2.4.3) and (2.4.4) yields the pressure

$$P = P_H + \frac{4a\Delta k_s^0}{(4a\Delta k_s^1 + \kappa L_z)}, \quad (2.4.5)$$

i.e. the additional growth at the interface elevates the pressure above the homeostatic pressure, which in turn causes the negative net growth rate in the bulk. Similarly, from equation (2.4.3) and equation (2.4.4), we obtain

$$\phi(t) = \frac{1}{2} + \left(\phi_0 - \frac{1}{2}\right)e^{-\kappa(P - P_H)t}, \quad (2.4.6)$$

with the initial number fraction ϕ_0 . Thus, the number fractions of two tissues with identical parameters, but no cross-adhesion, will relax exponentially towards $1/2$.

We determine the bulk parameters P_H, κ from bulk simulations as in [33] by using the

virial stress

$$\sigma_{\alpha\beta} = -\frac{1}{V} \left[\sum_i m_i v_\alpha^i v_\beta^i + \sum_{i,j} r_\alpha^{ij} f_\beta^{ij} \right]. \quad (2.4.7)$$

Here, \sum_i sums over all particles, v_α^i is the α component of the velocity of particle i , $\sum_{i,j}$ sums over all interacting pairs of particles, r_α^{ij} is the α component of the distance vector between i and j and f_β^{ij} the β component of the force on particle i due to j . The mean pressure is $P = -1/3\text{Tr}\langle\sigma_{\alpha\beta}\rangle$. The pressure response coefficient κ is obtained as the slope of a linear fit to the growth rates k for different pressures P around the homeostatic pressure P_H . We use a constant-pressure ensemble to impose a pressure P_i [33], where the pressure is imposed by periodic rescaling of the volume of the simulation box by a factor

$$\chi = 1 - \beta_T \frac{\Delta t}{t_P} (P - P_i), \quad (2.4.8)$$

with isothermal compressibility β_T , simulation time step Δt and relaxation time t_P . In order to measure the interface growth coefficients $a\Delta k_s^0, a\Delta k_s^1$ we make use of mirror boundary conditions. Particles closer to the boundary than $R_{PP}/2$ interact with the mirrored image of themselves as they would with a particle of the other tissue. We employ the mirror boundary conditions in z -direction and measure the average pressure for different box lengths L_z . $a\Delta k_s^0, a\Delta k_s^1$ are obtained by fitting equation (2.4.5) to simulation results. As shown in [33], the homeostatic pressure grows approximately linearly with G , and decreases linearly with f_1 . κ is essentially independent of f_1 , but decreases linearly with G . The interface growth coefficient $a\Delta k_s^0$ is only weakly dependent on G , but grows linearly with f_1 , while $a\Delta k_s^1$ does not show a clear dependence on tissue parameters (see figures in SI). With the parameters determined independently, equations (2.4.5) and (2.4.6) reproduce the simulations without further parameter adjustment (see figure 2.3).

2.4.2 Competition with flat interface

Next, we explore the competition between two tissues with different homeostatic pressures with a planar interface. We balance the pressures on both sides of the interface and obtain

$$P = P_H^A + \frac{2a\Delta k_s^{0A}}{(2a\Delta k_s^{1A} + \kappa^A L^A)} = P_H^B + \frac{2a\Delta k_s^{0B}}{(2a\Delta k_s^{1B} + \kappa^B L^B)}, \quad (2.4.9)$$

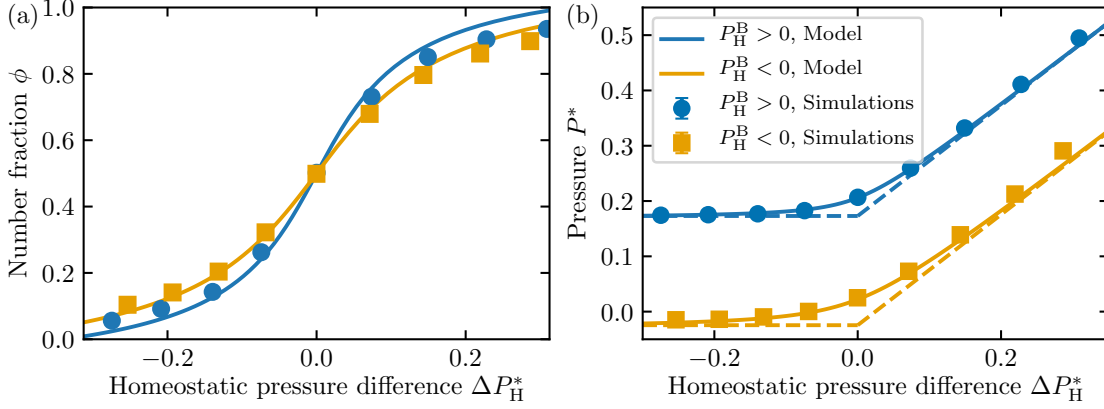


Figure 2.4: (a) Cell number fractions ϕ for various homeostatic pressure differences ΔP_H^* . Tissue B is fixed (as reference tissue (blue bullets) and as one with a higher growth-force strength and a higher cell-cell adhesion coefficient (yellow squares)) and the homeostatic pressure of tissue A is varied. Symbols are simulation results while the solid lines are predictions by the two-rate model according to equation (2.4.10), using the parameters of tissue B. See table S2 in the SI for numerical values of the simulation and model parameters of the two fixed tissues. (b) Average pressure measured during the simulations shown in (a) together with a plot of equation (2.4.9), using the parameter of tissue B. The results are not symmetric around $\Delta P_H = 0$ because tissue B is fixed. Dashed lines are lower bounds from $L^{A,B} < L_z$. Boxsize $L_x^* = L_y^* = 7$; $L_z^* = 40$. Errors are determined by block averaging method.

where L^B and $L^A (= L_z - L^B)$ are the lengths occupied by tissue A and B. Note that the insertion of $L^{A,B} < L_z$ in equation (2.4.9) gives a lower bound for the pressure: The system pressure is always larger than the homeostatic pressure of the stronger tissue, plus a system-size-dependent constant. Indeed, this lower bound describes the pressure rather well. The stronger tissue occupies the larger part of the system, and thus $L^{\text{stronger}} \approx L_z$. Thus, for fixed host tissue B, the pressure is almost constant for $\Delta P_H \equiv P_H^B - P_H^A < 0$, and grows almost linearly for $\Delta P_H > 0$ (see figure 2.4(b)). The weaker tissue supports the higher pressure by decreasing in size, and thus its apoptotic volume, sustained by interface growth. In simulations, tissue B is fixed and the growth-force strength G of tissue A is varied in order to change its homeostatic pressure. Simulations for two different fixed tissues are performed, the reference tissue and one with a higher growth-force strength and a higher cell-cell adhesion coefficient, which results in a negative homeostatic pressure. For the simulated tissues, the parameter κ , Δk_s^0 and Δk_s^1 only show small variations with G (see SI). We therefore assume them to be the same for

both tissues to obtain

$$\phi = \frac{1}{2} + \frac{2a\Delta k_s^0}{\kappa\Delta P_H L_z} \pm \left[\left(\frac{2a\Delta k_s^0}{\kappa\Delta P_H L_z} \right)^2 + \left(\frac{1}{2} + \frac{2a\Delta k_s^1}{\kappa L_z} \right)^2 \right]^{\frac{1}{2}}. \quad (2.4.10)$$

Note that for $\Delta P_H \rightarrow 0$, equation (2.4.10) reproduces $\phi = 1/2$ as expected. Around $\Delta P_H = 0$, ϕ grows linearly with ΔP_H and then slows down (see figure 2.4(a)). For large differences in homeostatic pressure, the model predicts two interfaces less than $2a$ apart, thus violating its assumptions, and consequently fails to predict the simulation results properly. Equations (2.4.9) and (2.4.10) reproduce simulation results well (see figure 2.4) in a broad parameter range. Note that this also holds true for negative homeostatic bulk pressures.

2.4.3 Non-planar interfaces

These results show that indeed the enhanced growth at the interface lies at the heart of tissue coexistence observed in our simulations. However, a flat interface is not the only stable structure for two competing tissues. Depending on initial conditions and parameters, a large range of other structures can be found (see figure 2.1). These different structures result in different interface-to-volume ratios (and possibly other interfacial effects, e.g. due to curvature of the interface), changing the steady-state volume fractions and pressures. We present simulation results for these structures in figure 2.5. Simulations are started from initial conditions morphologically similar to the final structure, but with an initial number fraction different than that at steady state.

Compared to flat interfaces, the number fraction ϕ of tissues in spherical or cylindrical configuration is smaller, with spheroids being smaller than cylinders. Spheroids become unstable with growing homeostatic pressure difference (around $\Delta P_H^* \approx 0.2$). They then transform into cylinders, which again become unstable with further increasing homeostatic pressure difference around $\Delta P_H^* \approx 0.3$ and turn into a slab-like structure, which becomes unstable as well at even larger ΔP_H^* and turns into inverted structures. Vice versa, cylinders turn into spheroids if the difference in homeostatic pressure is very negative ($\Delta P_H^* \approx -0.3$). The number fraction of the bicontinuous phase is roughly the same as for flat interfaces, but the bicontinuous phase is only stable in a small regime ($\Delta P_H^* \approx [-0.15, 0.15]$ for $P_H^B < 0$). For larger ΔP_H , the bicontinuous structure turns into a perforated lamellar phase of the weaker tissue inside the stronger tissue. The stability limits of the individual phases can be estimated in figure 2.5, where data is only shown within the respective stability regime. In general, the number fraction ϕ of all structures

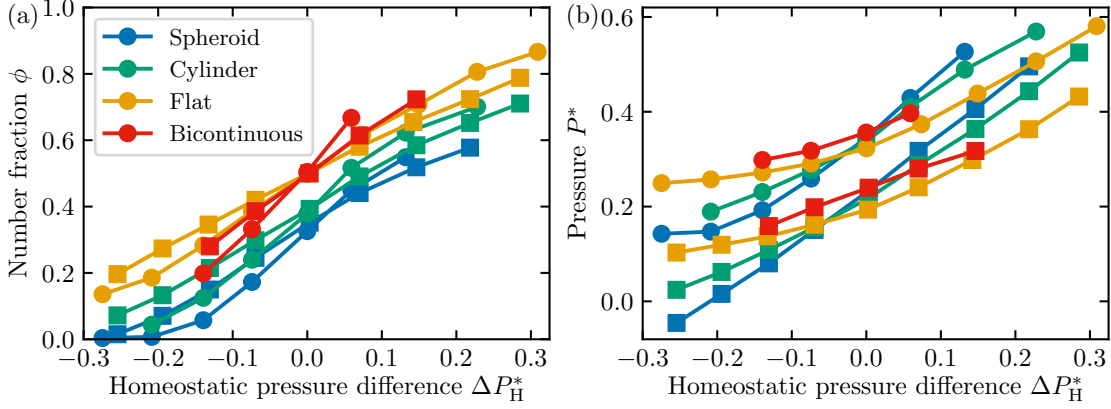


Figure 2.5: Cell number fractions ϕ for different homeostatic pressure differences ΔP_H^* and different structures, as indicated by color. Circles correspond to a positive homeostatic pressure of tissues B and squares to a negative one (same parameters as in figure 2.4, except cubic box size $L^* = 10$). (b) Average pressure measured in the simulations shown in (a). $L_x^* = L_y^* = L_z^* = 10$. Errors are determined by block averaging method.

changes sigmoidally with homeostatic pressure difference.

While all of these structures are very stable over time, the question arises how stable they are when the interfacial effects become smaller. We study this effect numerically, by observing the structures for two identical tissues formed under zero cross-adhesion and continuously increase the cross-adhesion strength f_c to the value of self-adhesion strength (i.e. $f_c = f_1^{AA} = f_1^{BB}$). Figure 2.6 shows that all structures remain almost unchanged up to a cross-adhesion f_c approximately two thirds of the self adhesion f_1 . For higher f_c , only a mixed, sponge-like state remains. Mixing occurs before cross-adhesion strength reaches self-adhesion strength because of the active growth. The total adhesion force $\mathbf{F}_i^{A, \text{tot}} = \sum_j \mathbf{F}_{ij}^A$ on a particle i close to the interface acts perpendicular to the interface towards the tissue species of i . The amplitude of this force decreases linearly towards zero when cross-adhesion strength approaches self-adhesion strength, thus, at some value $f_c < f_1$ the active growth force \mathbf{F}_i^G overcomes the total adhesive force and the interface becomes unstable.

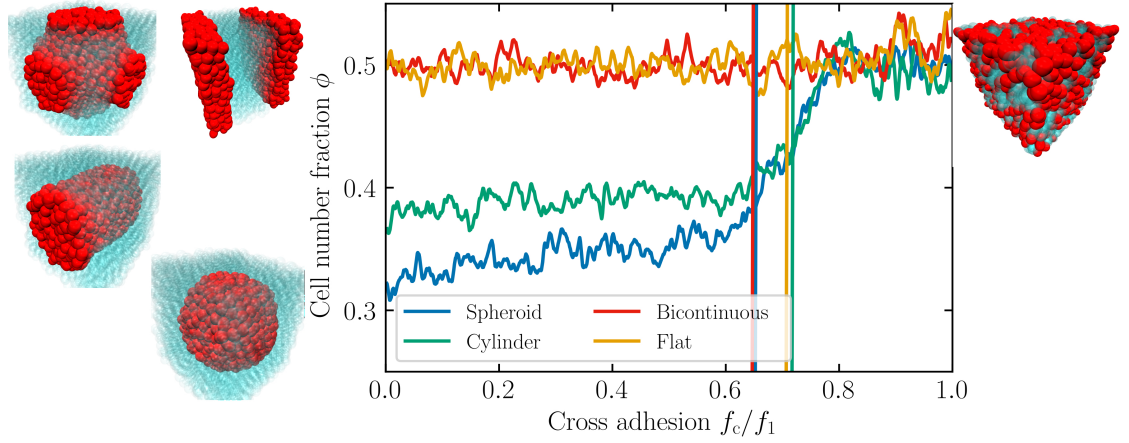


Figure 2.6: Variation of cell number fraction ϕ with time with increasing cross-adhesion $f_c/f_1 = t^*/240$ between two identical (reference) tissues. Simulations are started from spherical (blue) and cylindrical inclusions (green) of tissue A in B as well as from flat interfaces (yellow) and a bicontinuous phase (red). Solid vertical lines are marking transition points after which cells start to detach from the initial structures. Cubic box size $L^* = 10$. Simulation snapshots at the sides show initial and final configurations.

2.5 Conclusions

In summary, the interface between two tissues plays an important role in the competition between them. The enhanced growth at the interface can stabilize coexisting phases even when one tissue has a higher homeostatic pressure. The coexisting phase appears in a variety of different structures, ranging from a spherical inclusion over a flat interface to a bicontinuous structure.

Interesting future directions are interfacial dynamics, roughness, and shapes, as previously explored for tissues on substrates and without additional interfacial growth [34, 37, 38]. Vice versa, it would be interesting to add interfacial growth to tissues growing on substrates.

Finally, our results tentatively suggest an explanation for tumor heterogeneity and the abundance of occult tumors: small symptom-free micro-tumors that are frequently found in the human body [57]. For the thyroid, it might even be 'normal' to find microscopic lesions [58]. Our results provide a possible mechanical explanation how coexistence of different tissues can be stabilized. For example, a mutation might downregulate cadherins - an important cellular adhesion protein - as it often happens in tumors [59]. While this might reduce survival signaling [60], the lack of adhesion could favour our mechanism of coexistence, even for weaker tissue growth.

2.6 Acknowledgements

The authors gratefully acknowledge the computing time granted through JARA-HPC on the supercomputer JURECA [61] at Forschungszentrum Jülich

Bibliography chapter 2

- [1] M. A. Wozniak and C. S. Chen (2009), “Mechanotransduction in development: a growing role for contractility”, *Nat. Rev. Mol. Cell Biol.*, **10**(1), 34–43.
- [2] B. I. Shraiman (2005), “Mechanical feedback as a possible regulator of tissue growth”, *Proc. Natl. Acad. Sci. U.S.A.*, **102**(9), 3318–3323.
- [3] K. D. Irvine and B. I. Shraiman (2017), “Mechanical control of growth: ideas, facts and challenges”, *Development*, **144**(23), 4238–4248.
- [4] M. Jarvis, S. Briggs, and J. Knox (2003), “Intercellular adhesion and cell separation in plants”, *Plant Cell Environ.*, **26**(7), 977.
- [5] E. Coen, R. Kennaway, and C. Whitewoods (2017), “On genes and form”, *Development*, **144**(23), 4203–4213.
- [6] S. Kumar and V. M. Weaver (2009), “Mechanics, malignancy, and metastasis: The force journey of a tumor cell”, *Cancer Metastasis Rev.*, **28**(1), 113.
- [7] D. T. Butcher, T. Alliston, and V. M. Weaver (2009), “A tense situation: forcing tumour progression”, *Nat. Rev. Cancer*, **9**(2), 108–122.
- [8] A. Taloni, M. Ben Amar, S. Zapperi, and C. A. La Porta (2015), “The role of pressure in cancer growth”, *Eur. Phys. J. Plus.*, **130**(11), 224.
- [9] A. J. Engler, S. Sen, H. L. Sweeney, and D. E. Discher (2006), “Matrix elasticity directs stem cell lineage specification”, *Cell*, **126**(4), 677–689.
- [10] C. M. Nelson, et al. (2005), “Emergent patterns of growth controlled by multicellular form and mechanics”, *Proc. Natl. Acad. Sci. U.S.A.*, **102**(33), 11594–11599.
- [11] G. Cheng, J. Tse, R. K. Jain, and L. L. Munn (2009), “Micro-environmental mechanical stress controls tumor spheroid size and morphology by suppressing proliferation and inducing apoptosis in cancer cells”, *PLoS ONE*, **4**(2), e4632.
- [12] J. Fink, et al. (2011), “External forces control mitotic spindle positioning”, *Nat. Cell Biol.*, **13**(7), 771.
- [13] M. Uyttewaal, et al. (2012), “Mechanical stress acts via katanin to amplify differences in growth rate between adjacent cells in arabidopsis”, *Cell*, **149**(2), 439–451.

- [14] S. J. Streichan, C. R. Hoerner, T. Schneidt, D. Holzer, and L. Hufnagel (2014), “Spatial constraints control cell proliferation in tissues”, *Proc. Natl. Acad. Sci. U.S.A.*, **111**(15), 5586–5591.
- [15] L. LeGoff and T. Lecuit (2015), “Mechanical forces and growth in animal tissues”, *Cold Spring Harb. Perspect. Biol.*, **8**(3), a019232.
- [16] D. Eder, C. Aegerter, and K. Basler (2017), “Forces controlling organ growth and size”, *Mech. Dev.*, **144**, 53–61.
- [17] G. Helmlinger, P. A. Netti, H. C. Lichtenbeld, R. J. Melder, and R. K. Jain (1997), “Solid stress inhibits the growth of multicellular tumor spheroids”, *Nat. Biotechnol.*, **15**(8), 778–783.
- [18] V. D. Gordon, et al. (2003), “Measuring the mechanical stress induced by an expanding multicellular tumor system: a case study”, *Exp. Cell Res.*, **289**(1), 58.
- [19] L. J. Kaufman, et al. (2005), “Glioma expansion in collagen I matrices: analyzing collagen concentration-dependent growth and motility patterns”, *Biophys. J.*, **89**(1), 635–650.
- [20] K. Alessandri, et al. (2013), “Cellular capsules as a tool for multicellular spheroid production and for investigating the mechanics of tumor progression in vitro”, *Proc. Natl. Acad. Sci. U.S.A.*, **110**(37), 14843–14848.
- [21] H. Domejean, et al. (2017), “Controlled production of sub-millimeter liquid core hydrogel capsules for parallelized 3D cell culture”, *Lab Chip*, **17**(1), 110.
- [22] F. Montel, et al. (2011), “Stress clamp experiments on multicellular tumor spheroids”, *Phys. Rev. Lett.*, **107**(18), 188102.
- [23] F. Montel, et al. (2012), “Isotropic stress reduces cell proliferation in tumor spheroids”, *New J. Phys.*, **14**(5), 055008.
- [24] M. Delarue, et al. (2013), “Mechanical control of cell flow in multicellular spheroids”, *Phys. Rev. Lett.*, **110**(13), 138103.
- [25] A. Taloni, et al. (2014), “Mechanical properties of growing melanocytic nevi and the progression to melanoma”, *PLoS ONE*, **9**(4), e94229.
- [26] G. Morata and P. Ripoll (1975), “Minutes: Mutants of drosophila autonomously affecting cell division rate”, *Dev. Biol.*, **42**(2), 211–221.

- [27] B. Diaz and E. Moreno (2005), “The competitive nature of cells”, *Exp. Cell Res.*, **306**(2), 317 – 322.
- [28] S. H. Moolgavkar and E. G. Luebeck (2003), “Multistage carcinogenesis and the incidence of human cancer”, *Genes Chromosom. Cancer*, **38**(4), 302–306.
- [29] R. Meza and J. T. Chang (2015), “Multistage carcinogenesis and the incidence of thyroid cancer in the us by sex, race, stage and histology”, *BMC Public Health*, **15**(1), 789.
- [30] L. Hufnagel, A. A. Teleman, H. Rouault, S. M. Cohen, and B. I. Shraiman (2007), “On the mechanism of wing size determination in fly development”, *Proc. Natl. Acad. Sci. U.S.A.*, **104**(10), 3835–3840.
- [31] M. Basan, T. Risler, J.-F. Joanny, X. Sastre-Garau, and J. Prost (2009), “Homeostatic competition drives tumor growth and metastasis nucleation”, *HFSP J.*, **3**(4), 265–272.
- [32] M. Basan, J. Prost, J.-F. Joanny, and J. Elgeti (2011), “Dissipative particle dynamics simulations for biological tissues: rheology and competition”, *Phys. Biol.*, **8**(2), 026014.
- [33] N. Podewitz, M. Delarue, and J. Elgeti (2015), “Tissue homeostasis: A tensile state”, *Europhys. Lett.*, **109**(5), 58005.
- [34] N. Podewitz, F. Jülicher, G. Gompper, and J. Elgeti (2016), “Interface dynamics of competing tissues”, *New J. Phys.*, **18**(8), 083020.
- [35] N. Jagiella, B. Mueller, M. Mueller, I. E. Vignon-Clementel, and D. Drasdo (2016), “Inferring growth control mechanisms in growing multi-cellular spheroids of nslc cells from spatial-temporal image data”, *PLoS Comput. Biol.*, **12**(2), 1.
- [36] R. Hornung, et al. (2018), “Quantitative modelling of nutrient-limited growth of bacterial colonies in microfluidic cultivation”, *J. R. Soc. Interface*, **15**(139), 20170713.
- [37] J. Ranft, M. Aliee, J. Prost, F. Jülicher, and J.-F. Joanny (2014), “Mechanically driven interface propagation in biological tissues”, *New J. Phys.*, **16**(3), 035002.
- [38] J. J. Williamson and G. Salbreux (2018), “Stability and roughness of interfaces in mechanically regulated tissues”, *Phys. Rev. Lett.*, **121**(23), 238102.

- [39] Y. Kobayashi, et al. (2018), “Interplay between epidermal stem cell dynamics and dermal deformation”, *Npj Comput. Mater.*, **4**(1), 45.
- [40] R. F. M. van Oers, E. G. Rens, D. J. LaValley, C. A. Reinhart-King, and R. M. H. Merks (2014), “Mechanical cell-matrix feedback explains pairwise and collective endothelial cell behavior in vitro”, *PLoS Comput. Biol.*, **10**(8), 1–14.
- [41] D. C. Walker, G. Hill, S. M. Wood, R. H. Smallwood, and J. Southgate (2004), “Agent-based computational modeling of wounded epithelial cell monolayers”, *IEEE Trans. NanoBiosci.*, **3**(3), 153–163.
- [42] D. Drasdo and S. Höhme (2005), “A single-cell-based model of tumor growth in vitro: monolayers and spheroids”, *Phys. Biol.*, **2**(3), 133–147.
- [43] M. Welter, K. Barthä, and H. Rieger (2009), “Vascular remodelling of an arterio-venous blood vessel network during solid tumour growth”, *J. Theor. Biol.*, **259**(3), 405–422.
- [44] M. Wynn, P. M Kulesa, and S. Schnell (2012), “Computational modelling of cell chain migration reveals mechanisms that sustain follow-the-leader behaviour”, *J. R. Soc. Interface*, **9**(72), 1576–1588.
- [45] K.-A. Norton and A. S. Popel (2014), “An agent-based model of cancer stem cell initiated avascular tumour growth and metastasis: the effect of seeding frequency and location”, *J. R. Soc. Interface*, **11**(100), 20140640.
- [46] R. Foty and M. S Steinberg (2004), “Cadherin-mediated cell-cell adhesion and tissue segregation in relation to malignancy”, *Int. J. Dev. Biol.*, **48**(5-6), 397–409.
- [47] J. Ranft, et al. (2010), “Fluidization of tissues by cell division and apoptosis”, *Proc. Natl. Acad. Sci. U.S.A.*, **107**(49), 20863–20868.
- [48] N. Khalilgharibi, J. Fouchard, P. Recho, G. Charras, and A. Kabla (2016), “The dynamic mechanical properties of cellularised aggregates”, *Curr. Opin. Cell Biol.*, **42**, 113.
- [49] D. A. Matoz-Fernandez, E. Agoritsas, J.-L. Barrat, E. Bertin, and K. Martens (2017), “Nonlinear Rheology in a Model Biological Tissue”, *Phys. Rev. Lett.*, **118**(15), 158105.
- [50] H. Phillips and M. Steinberg (1978), “Embryonic tissues as elasticoviscous liquids. i. rapid and slow shape changes in centrifuged cell aggregates”, *J. Cell Sci.*, **30**(1), 1–20.

- [51] K. Guevorkian, M.-J. Colbert, M. Durth, S. Dufour, and F. Brochard-Wyart (2010), “Aspiration of biological viscoelastic drops”, *Phys. Rev. Lett.*, **104**(21), 218101.
- [52] D. Gonzalez-Rodriguez, et al. (2013), “Detachment and fracture of cellular aggregates”, *Soft Matter*, **9**(7), 2282–2290.
- [53] L. LeGoff, H. Rouault, and T. Lecuit (2013), “A global pattern of mechanical stress polarizes cell divisions and cell shape in the growing drosophila wing disc”, *Development*, **140**(19), 4051–4059.
- [54] Y. Mao, et al. (2013), “Differential proliferation rates generate patterns of mechanical tension that orient tissue growth”, *EMBO J.*, **32**(21), 2790–2803.
- [55] Y. Pan, I. Heemskerk, C. Ibar, B. I. Shraiman, and K. D. Irvine (2016), “Differential growth triggers mechanical feedback that elevates Hippo signaling”, *Proc. Natl. Acad. Sci. U.S.A.*, **113**(45), E6974–E6983.
- [56] M. P. Allen and D. J. Tildesley (1989), *Computer simulation of liquids*. Oxford: Clarendon Press.
- [57] M. J. Bissell and W. C. Hines (2011), “Why don’t we get more cancer? A proposed role of the microenvironment in restraining cancer progression”, *Nat. Med.*, **17**(3), 320–329.
- [58] H. R. Harach, K. O. Franssila, and V. M. Wasenius (1985), “Occult papillary carcinoma of the thyroid. A ”normal” finding in finland. A systematic autopsy study”, *Cancer*, **56**(3), 531–538.
- [59] R. A. Weinberg (2007), *The biology of cancer*. New York: Garland Science.
- [60] B. Alberts, et al. (1994), *Molecular Biology of the Cell*, 3rd edition. New York: Garland Science.
- [61] Jülich Supercomputing Centre (2018), “JURECA: Modular supercomputer at Jülich Supercomputing Centre”, *J. Large-Scale Res. Facil.*, **4**(A132).

2.7 Supplementary Informations: Mechanics of tissue competition: interfaces stabilize coexistence

We define a set of reference simulation parameters, which we refer to as reference tissue parameters. Table 3.1 shows the values in simulation units. Figure 2.7 displays the dependence of the bulk growth rate k^* on the imposed pressure P^* . The pressure response coefficient κ^* is obtained by a linear fit to the data. In principle, the homeostatic pressure P_H^* could be obtained from extrapolation to the point where the growth rate vanishes. However, we choose to measure it independently via the virial stress in a simulation box with full periodic boundary conditions, without rescaling the volume periodically. Both procedures yield similar values. Figure 2.8 shows the dependence of κ^* on the model parameters. While κ^* decreases with increasing growth-force strength G^\dagger , it is basically independent of the cell-cell adhesion coefficient f_1^\dagger . Figure 2.9 shows the dependence of the average pressure P^* measured in simulations with mirror boundary conditions on the simulation box length L_z^* . The interface growth coefficients $a\Delta k_s^{0*}$ and $a\Delta k_s^{1*}$ are obtained by a fit of equation (2.4.5) to the simulation data. Figure 2.10 displays the dependence of $a\Delta k_s^{0*}$ and $a\Delta k_s^{1*}$ on simulation parameters. $a\Delta k_s^{0*}$ grows slowly with increasing growth-force strength G^\dagger and more strongly with growing cell-cell interaction coefficient f_1^\dagger , as can be seen by the slope and the shift of the linear regressions. On the other hand, $a\Delta k_s^{1*}$ does not show a clear dependence on model parameters within the errors of the linear regressions parameters. In the main text, we fixed two different tissues. Table 2.2 shows their simulation parameters and measured tissue properties.

Table 2.1: Simulation parameters of the reference tissue

Parameter	Symbol	Value
Time step	Δt	10^{-3}
Pair potential interaction range	R_{pp}	1
Cellular expansion pressure constant	r_0	1
Cell division distance threshold	r_{ct}	0.8
New cell particle initial distance	r_{d}	0.00001
Growth force strength	G	40
Mass	m	1
Intracell dissipation coefficient	γ_{c}	100
Intercell dissipation coefficient	γ_{t}	50
Background dissipation coefficient	γ_{b}	0.1
Apoptosis rate	k_{a}	0.01
Noise intensity	$k_{\text{B}}T$	0.1
Repulsive cell-cell potential coefficient	f_0	2.39566
Attractive cell-cell potential coefficient	f_1	6.0
Isothermal compressibility	β_{T}	1
Relaxation time constant	t_{p}	1

Table 2.2: Simulation parameters and measured properties of the two fixed tissues discussed in the main text. Errors of κ^* , $a\Delta k_{\text{s}}^{0*}$ and $a\Delta k_{\text{s}}^{1*}$ are fit uncertainties determined by scipy. Errors of P_{H}^* are determined by block averaging method.

Parameter	Fixed tissue 1	Fixed tissue 2
G^\dagger	1	1.125
f_1^\dagger	1	1.166
P_{H}^*	0.1321 ± 0.0005	-0.0830 ± 0.0028
κ^*	2.676 ± 0.080	2.632 ± 0.088
$a\Delta k_{\text{s}}^{0*}$	2.43 ± 0.13	3.44 ± 0.19
$a\Delta k_{\text{s}}^{1*}$	6.24 ± 0.88	6.56 ± 0.88

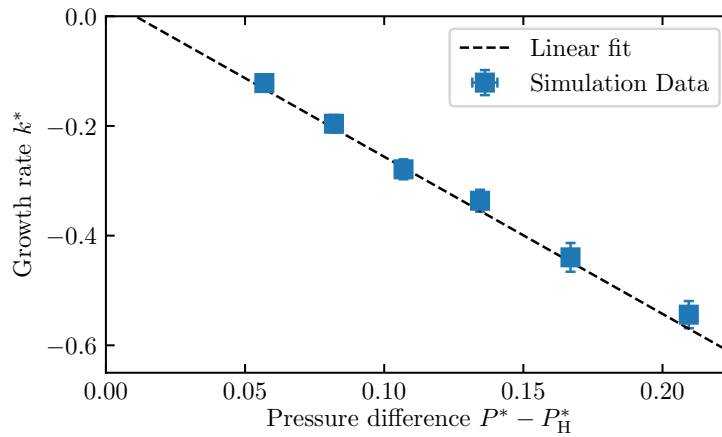


Figure 2.7: Growth rate $k^* = k/k_a$ as a function of the pressure $P^* = PR_{PP}^4/G_0$, shifted by the homeostatic pressure P_H , for one exemplary tissue ($G^\dagger = 1.125$, $f_1^\dagger = 1.166$). Blue squares display simulation results and the dashed line a fit of equation (2.2.1) to them. The errors bars are determined by block averaging method.

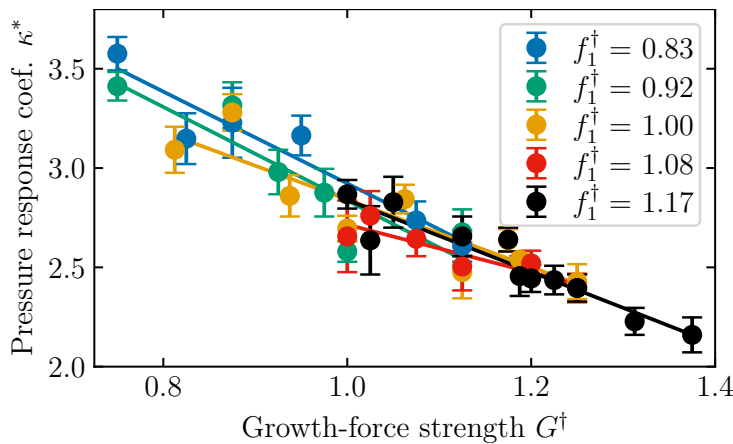


Figure 2.8: Pressure response coefficient $\kappa^* = \kappa G_0/(k_a R_{PP}^4)$ dependence on growth-force strength G^\dagger for various cell-cell adhesion coefficients f_1^\dagger . Error bars are fit uncertainties determined by scipy. The solid lines are linear regressions, taking the errors into account.

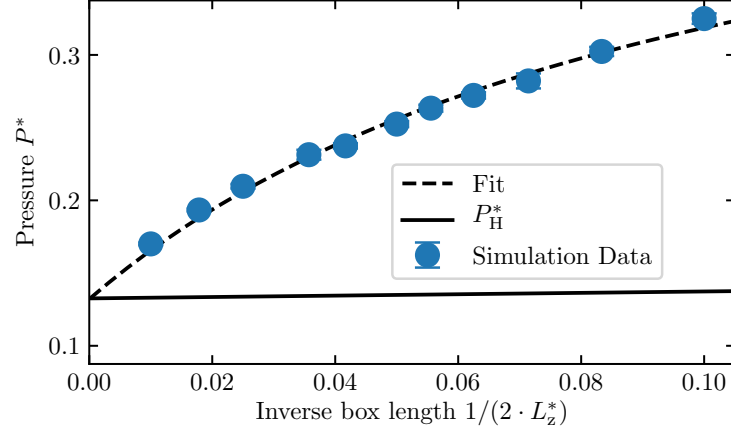


Figure 2.9: Average pressure in simulations with mirror boundary conditions as a function of the simulation box length L_z for the reference tissue. The dashed line shows a fit of equation (2.4.5) and the solid line the homeostatic pressure of the tissue. Error bars are obtained by block averaging method.

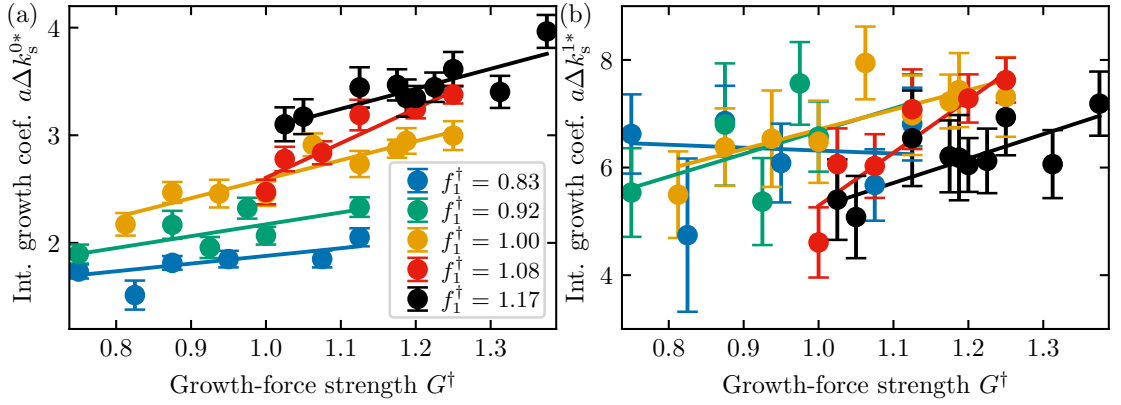


Figure 2.10: (a) Dependence of the interface growth coefficient $a\Delta k_s^{0*} = a\Delta k_s^0/k_a$ on growth-force strength G^\dagger for various cell-cell adhesion coefficients f_1^\dagger . (b) Same as in (a), but for $a\Delta k_s^{1*} = a\Delta k_s^1 G_0/(k_a R_{PP}^4)$. Error bars are fit uncertainties determined by scipy. The solid lines are linear regressions, taking the errors into account

3 Tissue evolution: mechanical interplay of adhesion, pressure, and heterogeneity

3.1 Abstract

The evolution of various competing cell types in tissues, and the resulting persistent tissue population, is studied numerically and analytically in a particle-based model of active tissues. Mutations change the properties of cells in various ways, including their mechanical properties. Each mutation results in an advantage or disadvantage to grow in the competition between different cell types. While changes in signaling processes and biochemistry play an important role, we focus on changes in the mechanical properties by studying the result of variation of growth force and adhesive cross-interactions between cell types. For independent mutations of growth force and adhesion strength, the tissue evolves towards cell types with high growth force and low internal adhesion strength, as both increase the homeostatic pressure. Motivated by biological evidence, we postulate a coupling between both parameters, such that an increased growth force comes at the cost of a higher internal adhesion strength or vice versa. This tradeoff controls the evolution of the tissue, ranging from unidirectional evolution to very heterogeneous and dynamic populations. The special case of two competing cell types reveals three distinct parameter regimes: two in which one cell type outcompetes the other, and one in which both cell types coexist in a highly mixed state. Interestingly, a single mutated cell alone suffices to reach the mixed state, while a finite mutation rate affects the results only weakly. Finally, the coupling between changes in growth force and adhesion strength reveals a mechanical explanation for the evolution towards intra-tumor heterogeneity, in which multiple species coexist even under a constant evolutionary pressure.

3.2 Introduction

Mutations change the cell fitness and thus its chance to survive and proliferate [1]. Advantageous mutations are more likely to persist due to natural selection, which drives the evolution of a tissue towards fitter cells [2]. Cancer represents an example of evolu-

tion on a short time scale [3]. Furthermore, cancer is a multistep process, i.e. several mutations are needed for a tumor in order to develop and become malignant [4]. Hence, tumorigenesis might be expected to happen in a serial manner, i.e. a cell acquiring a "beneficial" mutation and taking over the whole tissue. After some time, a daughter cell acquires another mutation and again takes over. Interestingly, however, tumors do not consist of a single cell type, but instead several subpopulations coexist within the same tumor. This is called intra-tumor heterogeneity [5].

Each mutation changes certain biochemical properties of a cell. This ranges from misfunction in the error correction machinery during DNA replication and disruptions in signaling pathways to epigenetic changes in the expression level of certain proteins [1, 6, 7]. All these changes can also affect the mechanical properties of the mutated cell, e.g. mutated cells which express less adhesion proteins might be able to detach from the primary tumor more easily [8], a necessary step for the formation of metastases. However, the metastatic process seems to be more complex, as adhesion proteins such as E-cadherin are still found in metastatic cells, while a recent study points out that E-cadherin might even be necessary in order to form metastases [9]. On the other hand, mechanics feeds back onto growth in several ways, e.g. increased apoptosis rate due to mechanical stresses [10, 11] or dependence of the growth of tissue spheroids on the properties of the surrounding medium [12, 13, 14].

It is the mechanical contribution to tissue development that we want to focus on in this work. For mechanically regulated growth, homeostatic pressure plays an important role [15]. In the homeostatic state, when apoptosis and division balance each other, a tissue exerts a certain pressure onto its surrounding, the homeostatic pressure P_H . The tissue is able to grow as long as the external pressure P is smaller than P_H . For the competition between different tissues for space, it has been suggested that the tissue with the higher homeostatic pressure grows at the expense of the weaker tissue. Several theoretical studies employ this concept in order to describe interface propagation between two competing tissues [16, 17, 18]. A metastasis would need to reach a critical size, below which the additional Laplace pressure due to surface tension would cause the metastasis to shrink and disappear [15]. However, reduced adhesion between tissues, which increases surface tension, leads to an enhanced growth rate at the interface between them, stabilizing coexistence even for differing homeostatic pressures [19].

The evolutionary aspect of tumor development has been studied extensively under the viewpoint of resistance to chemotherapy [20]. Heterogeneities can contribute to the evolution of resistance to certain drug treatments not only in the cancer cell phenotypes but also in the tumor microenvironment[21]. A main research focus is the design of

treatment strategies which take already existing resistances and the development of new resistances into account [21, 22]. Resistance may come at the cost of a fitness disadvantage in the absence of therapy. This lead to the proposal of adaptive therapy, in which a stable, non-resistant population is maintained by low-dose treatment, which then suppresses proliferation of resistant phenotypes [23, 24].

A related system of clusters and swarms of growing and dividing cells with a significant mutation rate are bacterial colonies and biofilms [25, 26]. These are interesting model systems, because they can easily be cultured and studied in vitro experimentally. For example, the gene expression in various cell types can be detected by fluorescent fusion proteins [27]. Therefore, detailed studies of bacterial colonies can help to understand how properties of microscopic cellular components determine macroscopic, multicellular biological function.

In this work, we study the influence of mutations that change the mechanical properties of cells on the competition dynamics, especially the interplay between changes in the adhesive properties and the strength with which a cell pushes onto its surrounding. Particularly interesting is the case where loss of adhesion comes at the cost of lower growth strength. This is motivated by the observed down-regulation of E-cadherin, an adhesion protein in epithelia, in many types of cancer [28]. Interestingly, E-cadherin is also involved in signaling processes connected to cell growth [29]. We find that in this case several cell types with different mechanical properties can coexist and that the cell type with the highest homeostatic pressure does not necessarily dominate the competition.

3.3 Simulation model

Several models have been developed previously in order to study tissue growth [30], in combination with different simulation techniques, including vertex [31, 32] and particle-based [33, 34] models as well as Cellular Potts models [35, 36]. We employ the two particle growth (2PG) model of [19, 37, 38]. A cell is described by two particles which repel each other via a growth force

$$\mathbf{F}_{ij}^G = \frac{G}{(r_{ij} + r_0)^2} \hat{\mathbf{r}}_{ij}, \quad (3.3.1)$$

with strength G , unit vector $\hat{\mathbf{r}}_{ij}$, distance r_{ij} between the two particles and a constant r_0 . Different cells interact via a soft repulsive force \mathbf{F}_{ij}^V on short distances, maintaining an excluded volume, and a constant attractive force \mathbf{F}_{ij}^A on intermediate distances, modeling

cell-cell adhesion, with

$$\left. \begin{aligned} \mathbf{F}_{ij}^V &= f_0 \left(\frac{R_{PP}^5}{r_{ij}^5} - 1 \right) \hat{\mathbf{r}}_{ij} \\ \mathbf{F}_{ij}^A &= -f_1 \hat{\mathbf{r}}_{ij} \end{aligned} \right\} \text{for } r_{ij} < R_{PP}, \quad (3.3.2)$$

with exclusion coefficient f_0 , adhesion strength coefficient f_1 , and cut-off length R_{PP} . A cell divides when the distance between its two particles reaches a size threshold r_{ct} . A new particle is then placed close (randomly within a short distance r_d) to each of the two particles of the divided cell. Each of these pairs then constitutes a new cell. Apoptosis is modeled by removing cells randomly at a constant rate k_a .

In real cells, the cell cycle and the cell division process are correlated with mechanical forces, but not fully determined by it [39]. Hence, in order to study the influence of the details of the division mechanism, we also employ a division mechanism, where cells divide with a finite rate k_{div} after reaching a smaller size threshold $r'_{ct} < r_{ct}$. The growth force equation 4.3.1 is set to zero when the distance between the two particles exceeds r_{ct} . This mechanism leads to a broader distribution of cell sizes at division and an additional source of randomness [40, 41]. Unless otherwise mentioned, the sharp threshold division mechanism is employed.

We employ a dissipative particle dynamics-type thermostat, with an effective temperature T , to account for energy dissipation and random fluctuations. We choose the value of T such that cells can escape local minima, but other thermal effects are negligible. Note that all parameters can be set individually for each cell type as well as between different cell types for inter-cell interactions. We only vary the growth-force strength G^α and adhesion strength $f_1^{\alpha\beta}$ between cells of the same ($\alpha = \beta$) and different ($\alpha \neq \beta$) cell types, respectively, where α and β are cell-type numbers. We report simulation parameters relative to a standard host cell type (see SI for numerical values), denoted with a dagger, e.g. $G^\dagger = G/G^0$. Time is measured in terms of the inverse apoptosis rate k_a , distance in units of the pair potential cut-off length R_{PP} and stresses in units of G^0/R_{PP}^4 . Quantities reported in these units are denoted by an asterisk *. All simulations are performed in a cubic box with edge length $L = 12 \cdot R_{PP}$ and periodic boundary conditions in all directions, unless stated otherwise.

Tumor cells even within the same tumor are not all identical, but vary in terms of all kind of attributes, e.g. expression levels of different proteins [42] or their reaction to certain treatments [43]. Hence, there is not only a competition between the tumor and the host, but also between cell-subpopulations of the tumor. Different models exist to describe tumor heterogeneity, e.g. cancer stem cells [44] or clonal evolution [45]. In the

latter case, a tumor originates from a single mutated cell, which can acquire additional mutations over time, yielding additional subpopulations. We model this behavior by defining a fixed number n of different "genotypes", each having a different growth-force strength G^α and adhesion strength $f_1^{\alpha\alpha}$. Mutations are implemented by offering each daughter cell after a division event the chance to change its genotype with a certain probability. Cancer cells typically have much higher mutation rates than healthy cells, e.g. due to malfunction of the error correction machinery during DNA replication [6, 46, 47]. Even for a moderate mutation rate a cell can acquire many mutations over several generations [48]. However, how many of these mutations actually lead to phenotypic variations and changes of the mechanical properties of a cell remains an open question. We therefore study the influence of the mutation rate on our results systematically.

In tissues, several adhesion mechanisms exist, serving a variety of different functions to maintain tissue integrity. Between epithelial cells, the strength of cell-cell adhesion is to a large degree regulated by anchoring junctions, e.g. adherens junctions, which connect the actin cytoskeletons of neighbouring cells. Adherens junctions are mediated by cadherins, which form homophilic bonds between cells. Thus, the strength of adhesion between cells is limited by the cell expressing less cadherin, or, in terms of our simulation model $f_1^{\alpha\beta} = \min(f_1^{\alpha\alpha}, f_1^{\beta\beta})$. A reduced adhesion strength yields a higher homeostatic pressure [38], which is otherwise dominated by the growth-force strength G .

Naturally such a minimalistic model can not cover the full complexity of real tumor development. How random are mutations? How likely do these mutations alter the mechanical properties of a cell? What is the role of the biochemical microenvironment? Instead our model focuses on generic aspects of mechanics alone. The two key aspects underlying this work, the evolutionary nature of cancer and the observed mechanical alterations of cancer cells, are well established in the literature [1, 2, 49, 50]. Our aim is to study the combined action of these two aspects of cancer, while the complexity of real tumors will have to be integrated stepwise in future studies.

3.4 Results

For free parameter evolution, the tissue evolves to a strong-growing and low-adhesive genotype (see figure 3.1), as predicted by the homeostatic pressure approach [15]. However, E-cadherin also plays a role in signaling processes connected to cell growth, and thus a reduced expression might come at the cost of a lower growth-force strength G , which in turn yields a lower homeostatic pressure. We thus turn our attention to the case where an increase in growth-force strength G^α comes at the cost of a higher

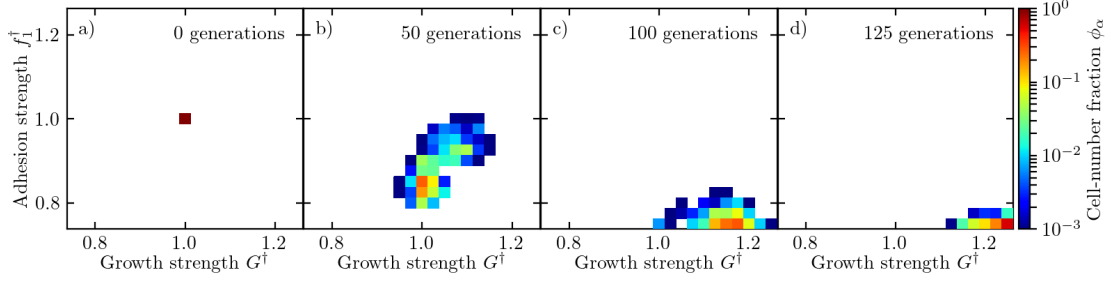


Figure 3.1: Evolution of a tissue with mutations altering growth-force strength G^\dagger and adhesion strength f_1^\dagger independently. Heatmaps displaying cell-number fractions after (a) zero generations (initial condition), (b) 50 generations, (c) 100 generations and (d) 125 generations. See Video S1 for a movie of the time evolution of the heatmap.

self-adhesion strength $f_1^{\alpha\alpha}$. We assume the relations as

$$G^\alpha = (1 + D^\alpha)G^0 \quad (3.4.1)$$

$$f_1^{\alpha\alpha} = (1 + D^\alpha \cdot \tau)f_1^0, \quad (3.4.2)$$

with genotype number α in the range $[-(n-1)/2, (n-1)/2]$, evolutionary distance $D^\alpha = d \cdot \alpha$, distance d between neighbouring genotypes and tradeoff parameter τ (with $G^\alpha, f_1^{\alpha\alpha} > 0 \forall \alpha$). After a division event, each daughter cell might mutate into a new genotype with probability p_m . If the cell mutates, its genotype number is changed to $\alpha_{\text{mother}} \pm 1$ randomly. This yields a mutation rate $k_m = 2p_mk_a$.

Figure 3.2 displays results of such simulations for four different cases: only variation of growth-force strength ($\tau = 0$), balanced tradeoff ($\tau = 1$), adhesion strength varied twice as much as growth-force strength ($\tau = 2$) and only variation of adhesion strength ($\tau \rightarrow \infty$). Without tradeoff (figure 3.2(a)), the tissue evolves towards the strongest growing genotype or, equivalently, the one with the highest homeostatic pressure. Similarly, for $\tau \rightarrow \infty$ (figure 3.2(d)), the system evolves towards the lowest adhesive genotype (again, the one with the highest P_H). We find the most dynamic evolution for a balanced tradeoff (figures 3.3 and 3.2(b)). At first, the system evolves to stronger growing and more adhesive genotypes. Over time a noticeable fraction of cells evolves also towards weak-growing, less adhesive genotypes. The genotype number fractions $\phi_\alpha = N_\alpha/N$ (with individual and total number of cells, N_α and N), show large fluctuations (see figures 3.3(b) and (c)), with individual genotypes not being populated at all for certain time periods. Besides this highly dynamic temporal evolution, after an initial time period the system is dominated by genotypes with increased growth force and adhesion strength at all times, with the one at the upper boundary having the highest number

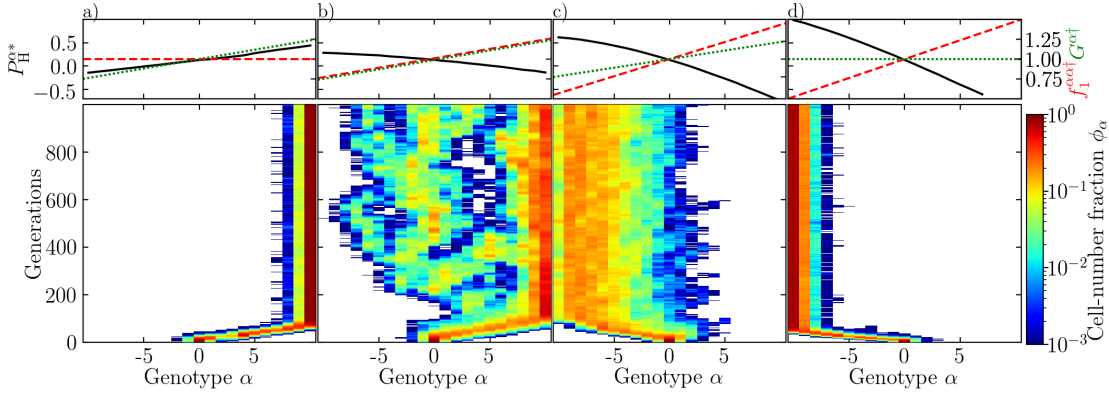


Figure 3.2: Time evolution of the genotype number fractions ϕ_α for tradeoff parameter (a) $\tau = 0$, (b) $\tau = 1$, (c) $\tau = 2$ and (d) $\tau \rightarrow \infty$, $d \rightarrow 0$. Simulations start from a host (standard) tissue at homeostasis, with $n = 21$ genotypes, $p_m = 0.01$ in all and $d = 0.025$ in (a)-(c). White space corresponds to times where no cells of the genotype exist. Color is coded on a logarithmic scale. Curves above display homeostatic pressure $P_H^{\alpha*}$ (black solid), growth-force strength $G^{\alpha\dagger}$ (red dashed) and self adhesion strength $f_1^{\alpha\dagger}$ (green dotted) of the corresponding genotype number α . See Video S2 for a visualization of the temporal evolution of a tissue with $\tau = 1.25$.

fraction for most of the time (see figure 3.3(a)). This result comes at a surprise, as this is also the genotype with the lowest homeostatic pressure, while the one at the lower boundary, which is basically never populated, has the highest P_H . For a higher tradeoff (figure 3.2(c)), we still find a broad distribution of genotypes, with less adhesive genotypes dominating over the stronger growing ones, i.e. the loss in growth-force strength is overcompensated by a lower adhesion strength. Interestingly, these results are not altered qualitatively by additional randomness in the division mechanism or a reduced mutation probability (see SI).

In order to gain insight into the underlying mechanism of this dynamic evolution, we study the competition between two genotypes and no mutations ($p_m = 0$). Simulations are started from a single mutated cell (with increased/decreased growth force and adhesion strength) in a host tissue at the homeostatic state (we label the mutant with M and the host (wild type) with W). Even in this simplified case, we find one parameter regime in which the mutant is not able to grow, one regime with stable coexistence in a highly mixed state and another regime in which the mutant outcompetes the host. Figure 3.4 shows the averaged number fractions of the mutant at the steady state. For reduced growth force and adhesion strength (figure 3.4(a)), the mutant can only grow against the host if its adhesion strength is reduced below a critical f_1^{crit} . In terms of

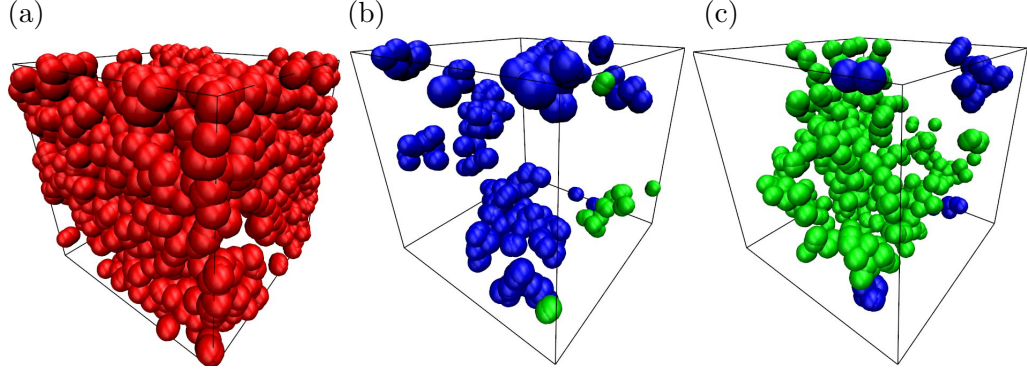


Figure 3.3: Simulation snapshots obtained from the simulation shown in figure 3.2(b). (a) The dominating genotype ($\phi_{10} = 0.283$) after 1000 generations. (b) Genotype $\alpha = -6$ (blue) and $\alpha = 6$ (green) after 485 generations ($\phi_{-6} = 0.027$, $\phi_6 = 0.002$). (c) Same as (b), but after 910 generations ($\phi_{-6} = 0.003$, $\phi_6 = 0.045$).

equation (3.4.2), the value of f_1^{crit} roughly corresponds to a balanced tradeoff ($\tau \approx 1$). Already for $f_1^{\text{MM}} > f_1^{\text{crit}}$, the homeostatic pressure of the mutant exceeds the one of the host, i.e. a parameter regime exists in which the mutant is not able to grow, despite of the higher P_H . The reverse happens when growth force and adhesion strength are increased. The mutant completely takes over the compartment, although its homeostatic pressure is smaller than that of the host. Again, coexistence is only found when the adhesion strength is increased above f_1^{crit} . In the coexistence regime, the mutant number fraction scales as $\phi^{\text{M}} \propto 1/(f_1^{\text{MM}} - f_1^{\text{WW}})$.

Altogether, the competition between two genotypes alone yields the same qualitative results as the more complex multi-genotype case discussed before. Still, the question remains how a genotype with a lower homeostatic pressure can outcompete a genotype with a higher homeostatic pressure. The answer can only lie in the adhesion strength $f_1^{\text{MW}} = \min(f_1^{\text{MM}}, f_1^{\text{WW}})$ between mutant and host cells. This choice of cross-adhesion strength breaks symmetry, as the stronger adhering genotype has more free space at the interface, which favors divisions [19].

To address this question, we develop a phenomenological model which incorporates pressure-dependent growth as well as interfacial effects, in order to obtain a qualitative explanation of the simulation results.

We start with the expansion of the bulk growth rate k_b around the homeostatic pressure,

$$k_b = \kappa(P - P_H), \quad (3.4.3)$$

with the pressure response coefficient κ . Due to the high degree of mixing, the number

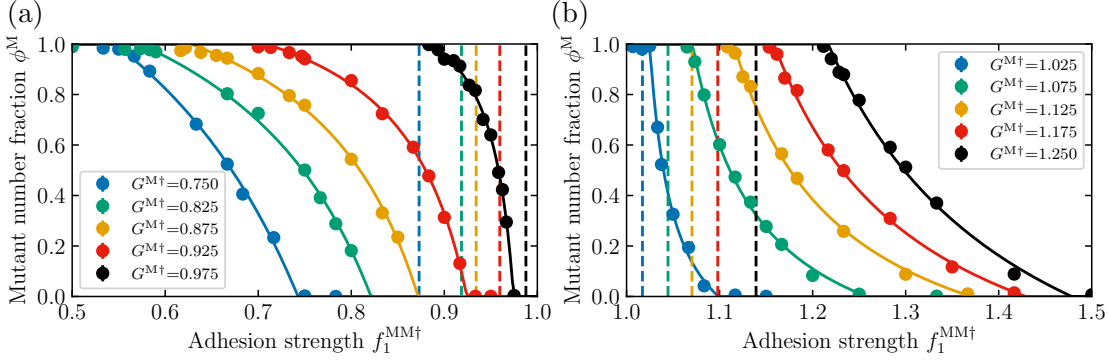


Figure 3.4: (a) Average number fraction ϕ^M of the mutant in terms of its adhesion strength $f_1^{MM†}$ for various (reduced) growth-force strengths $G^{M†}$. Error bars are obtained via block-averaging method (hidden behind markers) [51]. Dashed vertical lines indicate the points below which the mutant has a higher homeostatic pressure, solid lines are fits to equation (3.4.8). (b) Same as in (a) but for increased growth force and adhesion strengths of the mutant.

fractions $\phi^{M/W}$ and hence the strength of interfacial effects vary locally. In a mean-field approximation, we take the interfacial effects to be proportional to $\phi^M(1 - \phi^M)$, with individual prefactors $\Delta k_s^{M/W}$ for each genotype. The time evolution is then given by

$$\partial_t \phi^M = \kappa(P_H^M - P)\phi^M + \Delta k_s^M \phi^M(1 - \phi^M) \quad (3.4.4)$$

$$\begin{aligned} \partial_t(1 - \phi^M) &= \kappa(P_H^M + \Delta P_H - P)(1 - \phi) \\ &\quad + \Delta k_s^W \phi^M(1 - \phi^M), \end{aligned} \quad (3.4.5)$$

with the difference in homeostatic pressure $\Delta P_H = P_H^W - P_H^M$. Addition of equations (3.4.4) and (3.4.5) yields the pressure

$$P = P_H^W - \Delta P_H \phi^M + \frac{\Delta k_s^M + \Delta k_s^W}{\kappa} \phi^M(1 - \phi^M). \quad (3.4.6)$$

Thus, the pressure is given by the homeostatic pressures of the two genotypes weighted by their number fraction plus an interfacial term. A figure displaying the pressure measured during the simulations shown in figure 3.4 can be found in the SI. Insertion of equation (3.4.6) into equation (3.4.4) yields a differential equation for the number fraction with three fixed points ($\partial_t \phi^M = 0$), $\phi_1^M = 0$, $\phi_2^M = 1$, and

$$\phi_3^M = \frac{-\kappa \Delta P_H + \Delta k_s^M}{\Delta k_s^M + \Delta k_s^W}. \quad (3.4.7)$$

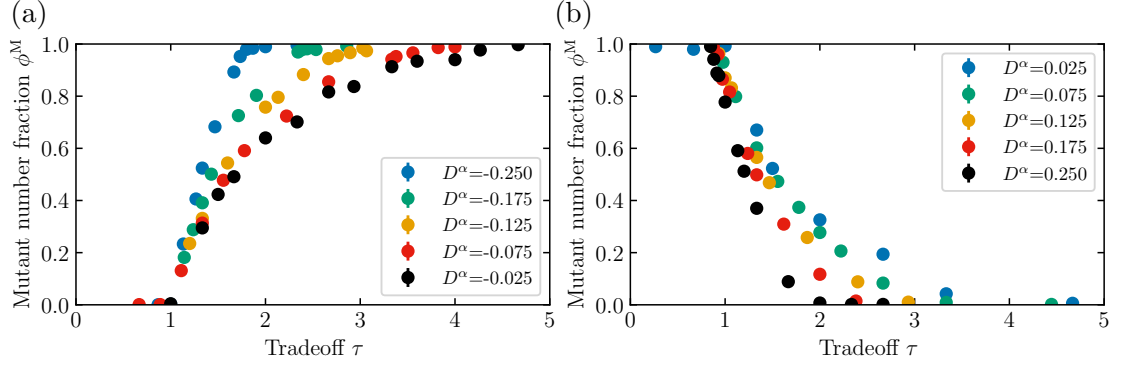


Figure 3.5: (a) Average number fractions of the mutant (same simulations as shown in figure 3.4(a)) as a function of the tradeoff τ of equation (3.4.2) for different evolutionary distances D^α . (b) Same as in (a) but with results from figure 3.4(b). Error bars are obtained via block-averaging method (hidden behind markers).

We discuss this result for the case of reduced growth force and adhesion strength of the mutant. Δk_s^M might be expected to vanish, as $f_1^{MM} = f_1^{MW}$ and mutant cells thus would not feel whether neighbouring cells are mutant or host cells. However, in order to grow, a cell needs to impose a strain on its surrounding. Host cells adhere more strongly to each other, thus it is harder for a mutant cell to impose a strain when surrounded by host cells. Hence, Δk_s^M is actually negative and the homeostatic pressure of the mutant needs to exceed the host pressure by $-\Delta k_s^M/\kappa$ in order to be able to grow against the host. At this point, ϕ_3^M becomes positive, as long as $\Delta k_s^M + \Delta k_s^W > 0$. Host cells can impose a strain more easily when surrounded by mutant cells and, additionally, have more free space than when surrounded by other host cells. Hence, $|\Delta k_s^M| < \Delta k_s^W$ and the above mentioned condition is fulfilled. Similarly, coexistence can be found for increased growth force and adhesion strength when $\Delta P_H > -\Delta k_s^W/\kappa$. The above mentioned scaling of the mutant number fraction can be obtained by an expansion of ΔP_H and $\Delta k_s^{M/W}$ to linear order in terms of $\epsilon := (f_1^{MM} - f_1^{WW})/f_1^{WW}$ in equation (3.4.7),

$$\phi_3^M = \frac{-\kappa \Delta P_H^0}{(\Delta k_s^{M1} + \Delta k_s^{W1})\epsilon} + \frac{-\kappa \Delta P_H^1 + \Delta k_s^{M1}}{\Delta k_s^{M1} + \Delta k_s^{W1}}. \quad (3.4.8)$$

The zeroth order terms of $\Delta k_s^{M/W}$ vanish as there are no interfacial effects when the adhesion strength between host and mutant cells is equal to their self-adhesion strength, while ΔP_H^0 can be non-zero due to a changed growth-force strength. Indeed, equation (3.4.8) reproduces the simulation data reasonably well (see figure 3.4). A discussion of the numerical values of the fitted parameters and additional results can be found in the SI.

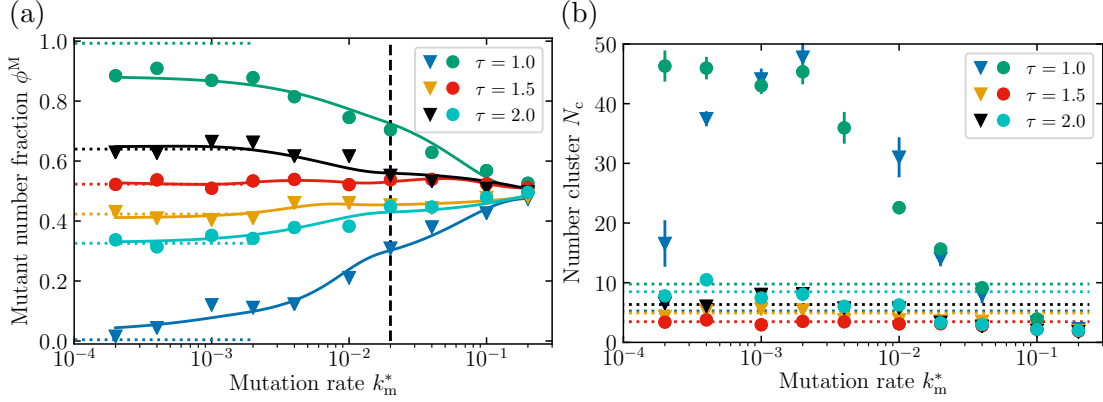


Figure 3.6: (a) Average number fraction ϕ^M of the mutant as a function of the mutation rate k_m^* for different values of the tradeoff τ , for evolutionary distances $D^\alpha = 0.025$ (circles) and $D^\alpha = -0.025$ (triangles). Horizontal dotted lines display results for a single mutation event. Vertical black dashed line indicates standard mutation rate. Solid lines are a guide to the eye. (b) Average number of clusters of the weaker genotype N_c measured in the same competitions in (a). Horizontal dotted lines display results for a single mutation event. Error bars are obtained via block-averaging method.

Figure 3.5 displays similar results as shown in figure 3.4, but now as a function of the tradeoff τ in equation (3.4.2). For $\tau < 1$ the genotype with higher growth-force strength outcompetes the weaker genotype, for $1 < \tau < 2$ a transition towards the less adhesive genotype occurs, while for even higher values of the tradeoff $\tau > 2$ the less adhesive genotype outcompetes the second genotype. This transition from strongly growing, adhesive to weakly growing, less adhesive genotypes is found in the same range of τ as in the competition between many genotypes. Hence, the simplified case of two competing genotypes captures the essential physics to explain the coexistence between many competing genotypes and, additionally, provides a quantitative description.

Next, we turn our attention to the effect of a finite mutation rate on the evolution of the system. Figure 3.6(a) shows the number fraction of the mutant as a function of k_m for different combinations of evolutionary distance D^α and tradeoff τ , in comparison to the number fraction reached for a single mutation event. As expected, the number fraction converges towards $1/2$ with increasing k_m for all combinations. For moderate mutation rates, however, the number fraction largely fluctuates around the same average as of a single mutation event. The single mutation leads to a stable coexistence of the two genotypes - additional mutations quickly relax back to this state. Significant deviations occur only if in the steady state of the single mutation event the number fraction of one genotype is close to zero (in the following termed the weaker genotype, while, vice versa,

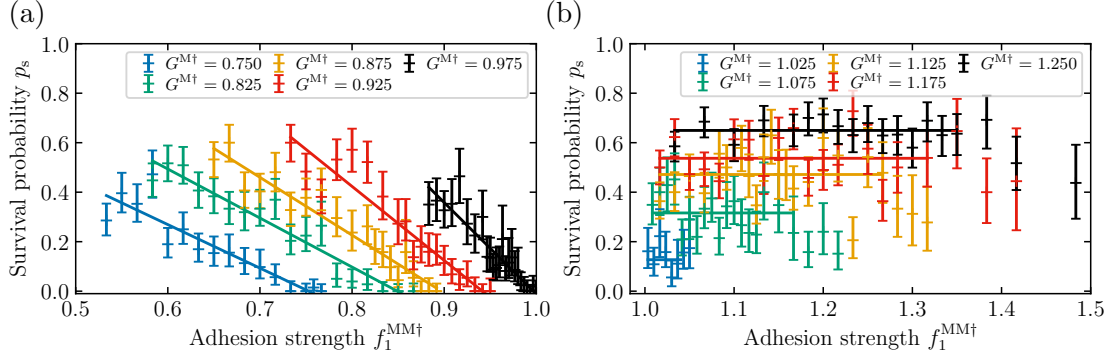


Figure 3.7: (a) Probability p_s of a single mutated cell to grow to macroscopic size as a function of its (reduced) adhesion strength $f_1^{MM†}$ for several values of the (reduced) growth-force strength $G^{M†}$. Error bars are a 1σ binomial confidence interval obtained by Clopper-Pearson. Solid lines are linear fits. (b) Same as in (a), but with a constant fitted in the plateau regime and increased growth force and adhesion strength. Box size $L^* = 8$.

the genotype with number fraction close to one is termed the stronger genotype). In that case, the weaker genotype consists only of one or very few small cohesive clusters of cells, because cells of the weaker genotype need to detach from the primary cluster in order to form new clusters, but are likely to die when they do so, as they are only surrounded by cells of the stronger genotype. Hence, the distribution of cells is highly non-homogeneous. Compared to the single mutation event, even a small mutation rate leads to the formation of multiple small cluster all over the system, thus increasing the number fraction of the weaker genotype (see figure 3.6(b) for comparison in terms of number of clusters and SI for further discussion). This result explains why at least two genotypes, in addition to the dominating genotype, are populated as well in the cases shown in figures 3.2 (a) and (d). When the number fractions of both genotypes are sufficiently large (for $1 \leq \tau \leq 2$), deviations from the average of a single mutation are still small for the standard mutation probability. Additionally, in the competitions between many genotypes, mutations change the genotype to $\alpha \pm 1$ randomly and not in a preferred direction. Hence, we conclude that the precise value of the mutation probability does not play an important role in the regime where we find a heterogeneous distribution of genotypes, as long as it is reasonably small ($k_m \ll k_a$).

Given that a single mutated cell can grow to tissue of macroscopic size in a certain parameter regime for $f_1^{MW} = \min(f_1^{MM}, f_1^{WW})$, the question arises how likely it is to actually reach this state. In order to study this probability, we mutate again a single cell in a host tissue at its homeostatic state. A mutation that reaches a certain threshold

$N_t = 20$ of cells counts as a survival event (the chance to die after reaching this threshold becomes extremely small), apoptosis of the last mutant cell as a death event. Figure 3.7 shows the averages of many such simulations. For reduced growth force and adhesion strength, the survival probability p_s is only non-zero below the critical adhesion strength f_1^{crit} . For $f_1^{\text{MM}} < f_1^{\text{crit}}$, p_s increases linearly with further decreasing adhesion strength. On the other hand, when growth force and adhesion strength are increased, the survival probability first shows a plateau, whose value increases with increasing growth force strength, from which it will probably drop to zero with further increase. Simulations in this regime are difficult, because a mutated cell can easily grow to a few cells, but will hardly reach the number threshold nor completely vanish again. Due to the high self-adhesion strength on the one hand, it becomes hard to detach from the other cells, but on the other hand easy to grow against the host when only few or no other mutant cells are around. This explains the larger error bars at the highest values of the adhesion strength, where the sample size is small.

3.5 Discussion

We have shown how intra-tumor heterogeneity, the existence of multiple subpopulations within the same tumor, can arise due to mechanical interactions alone, while most studies on evolutionary dynamics in tumors focused on the adaptation to chemotherapy and development of resistance to certain drugs [20, 21]. The simultaneous change of the adhesion and growth-force strength stabilizes the coexistence of multiple subpopulations, in a highly dynamic state. A higher growth-force strength alone, as well as a lower adhesion strength, favor proliferation of a single subpopulation and the evolution of the system to cell types with the highest growth-force strength, or lowest adhesion strength, respectively. A tradeoff between the two, however, yields coexistence between multiple subpopulations of different cell types. Interestingly, the expression of the adhesion protein E-cadherin, which also affects cell growth, has been found to be down-regulated in many real tumors [28].

The simulations also reveal that the homeostatic pressure of a cell type is not necessarily the only quantity that determines the result of a competition. Interactions between different cell types, in our model determined by the adhesion between them, can lead to a completely reverse outcome, i.e. a cell type with a lower homeostatic pressure can outcompete a cell type with a higher homeostatic pressure completely. A phenomenological model explains the results on a qualitative level. The evolution of each cell type is governed by mechanically-regulated growth, while mutation rates only play a minor

role in the dynamics.

We have focused here on tissue evolution driven by mechanics alone, neglecting other possible selection forces which determine the overall fitness of a subpopulation in a real tumor, which consequently affects its evolution. Possible examples are spatially varying distributions of growth-limiting resources or presence of chemotherapeutic drugs. This could be included into our simulation model by making certain model parameters, e.g. growth-force strength or apoptosis rate, dependent on the local concentration of these substances [52]. An interesting future aspect for competition regulated purely by mechanics is the influence of open boundaries. A tissue with a negative homeostatic pressure then naturally grows to a spheroid of finite size, with an enhanced rate of division at the surface [38]. For competing cell types, this would lead to an interplay between surface and interfacial effects.

3.6 Acknowledgements

The authors gratefully acknowledge the computing time granted through JARA-HPC on the supercomputer JURECA [53] at Forschungszentrum Jülich. Parts of the simulations were performed with computing resources granted by RWTH Aachen University under project rwth0475.

Bibliography chapter 3

- [1] R. A. Weinberg (2007), *The biology of cancer*. New York: Garland Science.
- [2] M. Greaves and C. C. Maley (2012), “Clonal evolution in cancer”, *Nature*, **481**(7381), 306.
- [3] I. Bozic, et al. (2013), “Evolutionary dynamics of cancer in response to targeted combination therapy”, *eLife*, **2**, e00747.
- [4] B. Vogelstein and K. W. Kinzler (1993), “The multistep nature of cancer”, *Trends Genet.*, **9**(4), 138–141.
- [5] G. H. Heppner (1984), “Tumor heterogeneity”, *Cancer Res.*, **44**(6), 2259–2265.
- [6] B. D. Preston, T. M. Albertson, and A. J. Herr (2010), “DNA replication fidelity and cancer”, *Semin. Cancer Biol.*, **20**(5), 281–293.
- [7] M. Schnekenburger and M. Diederich (2012), “Epigenetics offer new horizons for colorectal cancer prevention”, *Curr. Colorectal Cancer Rep.*, **8**(1), 66–81.
- [8] Y. I. Petrova, L. Schecterson, and B. M. Gumbiner (2016), “Roles for E-cadherin cell surface regulation in cancer”, *Mol. Biol. Cell*, **27**(21), 3233–3244.
- [9] V. Padmanaban, et al. (2019), “E-cadherin is required for metastasis in multiple models of breast cancer”, *Nature*, **573**(7774), 439–444.
- [10] F. Wernig and Q. Xu (2002), “Mechanical stress-induced apoptosis in the cardiovascular system”, *Prog. Biophys. Mol. Bio.*, **78**(2), 105 – 137.
- [11] G. Cheng, J. Tse, R. K. Jain, and L. L. Munn (2009), “Micro-environmental mechanical stress controls tumor spheroid size and morphology by suppressing proliferation and inducing apoptosis in cancer cells”, *PLoS ONE*, **4**(2), e4632.
- [12] F. Montel, et al. (2011), “Stress clamp experiments on multicellular tumor spheroids”, *Phys. Rev. Lett.*, **107**(18), 188102.
- [13] K. Alessandri, et al. (2013), “Cellular capsules as a tool for multicellular spheroid production and for investigating the mechanics of tumor progression in vitro”, *Proc. Natl. Acad. Sci. U.S.A.*, **110**(37), 14843–14848.
- [14] G. Helmlinger, P. A. Netti, H. C. Lichtenbeld, R. J. Melder, and R. K. Jain (1997), “Solid stress inhibits the growth of multicellular tumor spheroids”, *Nat. Biotechnol.*, **15**(8), 778–783.

- [15] M. Basan, T. Risler, J.-F. Joanny, X. Sastre-Garau, and J. Prost (2009), “Homeostatic competition drives tumor growth and metastasis nucleation”, *HFSP J.*, **3**(4), 265–272.
- [16] J. J. Williamson and G. Salbreux (2018), “Stability and roughness of interfaces in mechanically regulated tissues”, *Phys. Rev. Lett.*, **121**(23), 238102.
- [17] J. Ranft, M. Aliee, J. Prost, F. Jülicher, and J.-F. Joanny (2014), “Mechanically driven interface propagation in biological tissues”, *New J. Phys.*, **16**(3), 035002.
- [18] N. Podewitz, F. Jülicher, G. Gompper, and J. Elgeti (2016), “Interface dynamics of competing tissues”, *New J. Phys.*, **18**(8), 083020.
- [19] N. Ganai, T. Büscher, G. Gompper, and J. Elgeti (2019), “Mechanics of tissue competition: interfaces stabilize coexistence”, *New J. Phys.*, **21**(6), 063017.
- [20] R. A. Burrell and C. Swanton (2014), “Tumour heterogeneity and the evolution of polyclonal drug resistance”, *Mol. Oncol.*, **8**(6), 1095–1111.
- [21] J. J. Cunningham, R. A. Gatenby, and J. S. Brown (2011), “Evolutionary dynamics in cancer therapy”, *Mol. Pharm.*, **8**(6), 2094–2100.
- [22] J. A. Gallaher, P. M. Enriquez-Navas, K. A. Luddy, R. A. Gatenby, and A. R. Anderson (2018), “Spatial heterogeneity and evolutionary dynamics modulate time to recurrence in continuous and adaptive cancer therapies”, *Cancer Res.*, **78**(8), 2127–2139.
- [23] R. A. Gatenby, A. S. Silva, R. J. Gillies, and B. R. Frieden (2009), “Adaptive therapy”, *Cancer Res.*, **69**(11), 4894–4903.
- [24] A. S. Silva, et al. (2012), “Evolutionary approaches to prolong progression-free survival in breast cancer”, *Cancer Res.*, **72**(24), 6362–6370.
- [25] P. Ghosh, J. Mondal, E. Ben-Jacob, and H. Levine (2015), “Mechanically-driven phase separation in a growing bacterial colony”, *Proc. Natl. Acad. Sci. U.S.A.*, **112**(17), E2166–E2173.
- [26] F. D. Farrell, M. Gralka, O. Hallatschek, and B. Waclaw (2017), “Mechanical interactions in bacterial colonies and the surfing probability of beneficial mutations”, *J. R. Soc. Interface*, **14**(131), 20170073.
- [27] H. Jeckel, et al. (2019), “Learning the space-time phase diagram of bacterial swarm expansion”, *Proc. Natl. Acad. Sci. U.S.A.*, **116**(5), 1489–1494.

- [28] I. Beavon (2000), “The E-cadherin–catenin complex in tumour metastasis: structure, function and regulation”, *Eur. J. Cancer*, **36**(13), 1607–1620.
- [29] S. Pece and J. S. Gutkind (2000), “Signaling from E-cadherins to the MAPK Pathway by the recruitment and activation of epidermal growth factor receptors upon cell-cell contact formation”, *J. Biol. Chem.*, **275**(52), 41227–41233.
- [30] P. Van Liedekerke, M. M. Palm, N. Jagiella, and D. Drasdo (2015), “Simulating tissue mechanics with agent-based models: concepts, perspectives and some novel results”, *Comp. Part. Mech.*, **2**(4), 401–444.
- [31] R. Farhadifar, J.-C. Röper, B. Aigouy, S. Eaton, and F. Jülicher (2007), “The influence of cell mechanics, cell-cell interactions, and proliferation on epithelial packing”, *Curr. Biol.*, **17**(24), 2095–2104.
- [32] S. Alt, P. Ganguly, and G. Salbreux (2017), “Vertex models: From cell mechanics to tissue morphogenesis”, *Phil. Trans. R. Soc. B*, **372**(1720), 20150520.
- [33] D. Drasdo and S. Höhme (2005), “A single-cell-based model of tumor growth in vitro: monolayers and spheroids”, *Phys. Biol.*, **2**(3), 133–147.
- [34] G. Schaller and M. Meyer-Hermann (2005), “Multicellular tumor spheroid in an off-lattice voronoi-delaunay cell model”, *Phys. Rev. E*, **71**(5), 051910.
- [35] F. Graner and J. A. Glazier (1992), “Simulation of biological cell sorting using a two-dimensional extended Potts model”, *Phys. Rev. Lett.*, **69**(13), 2031–2034.
- [36] A. Szabó and R. M. Merks (2013), “Cellular Potts modeling of tumor growth, tumor invasion, and tumor evolution”, *Front. Oncol.*, **3**, 87.
- [37] M. Basan, J. Prost, J.-F. Joanny, and J. Elgeti (2011), “Dissipative particle dynamics simulations for biological tissues: rheology and competition”, *Phys. Biol.*, **8**(2), 026014.
- [38] N. Podewitz, M. Delarue, and J. Elgeti (2015), “Tissue homeostasis: A tensile state”, *Europhys. Lett.*, **109**(5), 58005.
- [39] M. Uroz, et al. (2018), “Regulation of cell cycle progression by cell–cell and cell–matrix forces”, *Nat. Cell Biol.*, **20**(6), 646.
- [40] M. Basan, J. Elgeti, E. Hannezo, W.-J. Rappel, and H. Levine (2013), “Alignment of cellular motility forces with tissue flow as a mechanism for efficient wound healing”, *Proc. Natl. Acad. Sci. U.S.A.*, **110**(7), 2452–2459.

- [41] A.-K. Marel, N. Podewitz, M. Zorn, J. O. Rädler, and J. Elgeti (2014), “Alignment of cell division axes in directed epithelial cell migration”, *New J. Phys.*, **16**(11), 115005.
- [42] A. Marusyk, V. Almendro, and K. Polyak (2012), “Intra-tumour heterogeneity: a looking glass for cancer?”, *Nat. Rev. Cancer*, **12**(5), 323–334.
- [43] A. Marusyk and K. Polyak (2010), “Tumor heterogeneity: causes and consequences”, *Biochim. Biophys. Acta*, **1805**(1), 105 – 117.
- [44] M. Shackleton, E. Quintana, E. R. Fearon, and S. J. Morrison (2009), “Heterogeneity in cancer: Cancer stem cells versus clonal evolution”, *Cell*, **138**(5), 822–829.
- [45] P. Nowell (1976), “The clonal evolution of tumor cell populations”, *Science*, **194**(4260), 23–28.
- [46] D. Hao, L. Wang, and L.-j. Di (2016), “Distinct mutation accumulation rates among tissues determine the variation in cancer risk”, *Sci. Rep.*, **6**(1), 19458.
- [47] J. H. Bielas, K. R. Loeb, B. P. Rubin, L. D. True, and L. A. Loeb (2006), “Human cancers express a mutator phenotype”, *Proc. Natl. Acad. Sci. U.S.A.*, **103**(48), 18238–18242.
- [48] I. P. Tomlinson, M. Novelli, and W. Bodmer (1996), “The mutation rate and cancer”, *Proc. Natl. Acad. Sci. U.S.A.*, **93**(25), 14800–14803.
- [49] P. Katira, R. T. Bonneau, and M. H. Zaman (2013), “Modeling the mechanics of cancer: effect of changes in cellular and extra-cellular mechanical properties”, *Front. Oncol.*, **3**, 145.
- [50] T. W. Remmerbach, et al. (2009), “Oral cancer diagnosis by mechanical phenotyping”, *Cancer Res.*, **69**(5), 1728–1732.
- [51] M. P. Allen and D. J. Tildesley (1989), *Computer simulation of liquids*. Oxford: Clarendon Press.
- [52] R. Hornung, et al. (2018), “Quantitative modelling of nutrient-limited growth of bacterial colonies in microfluidic cultivation”, *J. R. Soc. Interface*, **15**(139), 20170713.
- [53] Jülich Supercomputing Centre (2018), “JURECA: Modular supercomputer at Jülich Supercomputing Centre”, *J. Large-Scale Res. Facil.*, **4**(A132).

3.7 Supplementary Informations: Tissue evolution: mechanical interplay of adhesion, pressure, and heterogeneity

3.7.1 Standard (host) tissue and simulation parameters

We define a set of reference simulation parameters, which we refer to as host parameters. Table 3.1 shows the values in simulation units. In simulations we keep the host W fixed and vary the parameters of the mutant M around the values of the host.

Table 3.1: Simulation parameters and measured properties of the standard (host) tissue.

Parameter	Symbol	Value
Time Step	Δt	10^{-3}
Pair potential interaction range	R_{PP}	1
Cellular expansion pressure constant	r_0	1
Cell division distance threshold	r_{ct}	0.8
Reduced cell division distance threshold	r'_{ct}	0.4
New cell particle initial distance	r_d	0.00001
Growth-force strength	G	40
Mass	m	1
Intracell dissipation coefficient	γ_c	100
Intercell dissipation coefficient	γ_t	50
Background dissipation coefficient	γ_b	0.1
Apoptosis rate	k_a	0.01
Division rate	k_{div}	0.1
Mutation probability	p_m	0.01
Noise intensity	$k_B T$	0.1
Repulsive cell-cell potential coefficient	f_0	2.39566
Attractive cell-cell potential coefficient	f_1	6.0
Isothermal compressibility	β_T	1
Relaxation time constant	t_P	1
Homeostatic pressure	P_H^*	0.1321 ± 0.0005
Pressure response coefficient	κ^*	2.676 ± 0.080

3.7.2 Additional Results

Additional randomness in division mechanism

Figure 3.8 displays results of simulations similar to figure 3.2, but with the altered division mechanism, in which cells only divide with a pre-defined rate once exceeding the size threshold. Both division mechanisms yield qualitatively identical results, especially the heterogeneous coexistence between many subpopulations does not depend on the

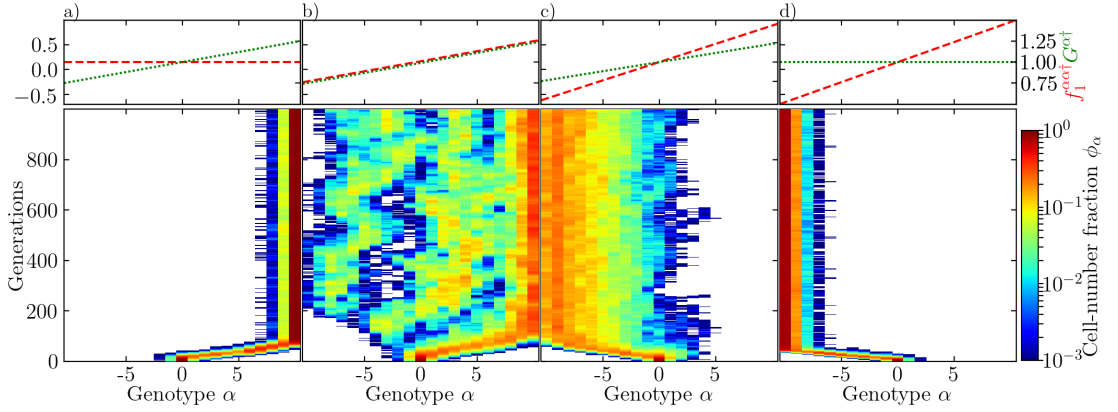


Figure 3.8: Time evolution of the genotype number fractions ϕ_α with altered division mechanism and otherwise identical parameter as in figure 3.2. White space corresponds to times where no cells of the genotype exist. Color is coded on a logarithmic scale. Curves above display growth-force strength $G^{\alpha\dagger}$ (red dashed) and self adhesion strength $f_1^{\alpha\alpha\dagger}$ (green dotted) of the corresponding genotype number α .

details of the division mechanism. In order to test whether both mechanisms also show quantitative agreement, we also performed pair competitions between two genotypes. The steady state number fraction of the mutant is similar for both mechanisms (see figure 3.9, compare also figure 3.4 of the main text).

Reduced mutation rate

In order to test the dependence on the mutation rate for the case of many genotypes, we performed evolution simulations with tradeoff, with a tenfold reduced mutation rate (see figure 3.10, compare figure 3.2 of the main text). While the dynamics are somewhat slowed down, as expected, the steady state heterogeneity after many generations is unaltered.

Pressure

Figure 3.11 displays the average pressure P at the steady state. The pressure converges towards the homeostatic pressure of the host when the number fraction of the mutant becomes small.

Numerical values model

According to equation (3.4.8), the values for $\Delta k_s^{M/W}$ when fitted to the simulation results displayed in figure 3.4 should be similar for all curves. Looking at the actual values

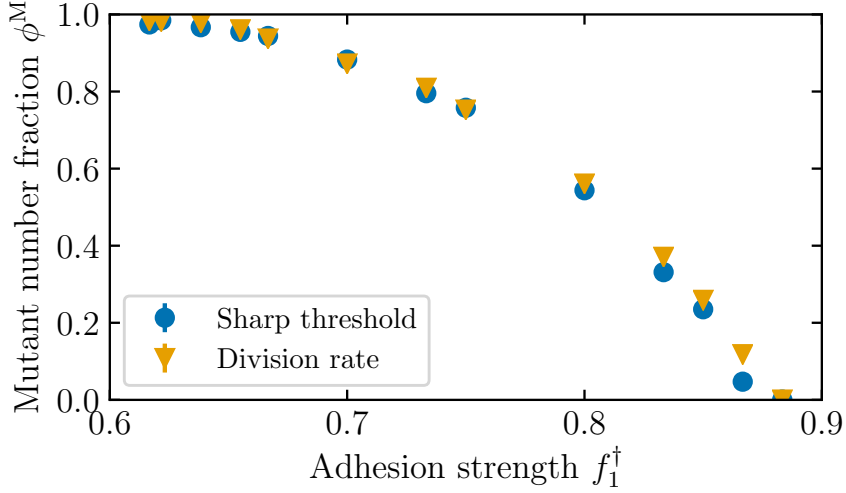


Figure 3.9: Average number fraction ϕ^M of the mutant in terms of its adhesion strength $f_1^{MM\dagger}$ for $G^{M\dagger} = 0.875$, for the sharp threshold division mechanism (blue circles) and the constant division rate mechanism (yellow triangles). Error bars are obtained via block-averaging method (hidden behind markers).

displayed in tables 3.2 and 3.3, this is not perfectly true. For increased growth force and adhesion strength, the values for Δk_s^{M1} are indeed very similar and for Δk_s^{W1} only the value for $G^\dagger = 1.025$ deviates noticeably. For reduced growth force and adhesion strength, however, both, Δk_s^{M1} and Δk_s^{W1} decrease with decreasing G^\dagger .

Table 3.2: Values obtained for Δk_s^{M1} and Δk_s^{W1} by fitting the simulation results displayed in figure 3.4(a) to equation (3.4.8) for reduced growth force and adhesion strength of the mutant.

$G^{M\dagger}$	Δk_s^{M1}	Δk_s^{W1}
0.750	-1.709 ± 0.010	2.432 ± 0.006
0.825	-2.106 ± 0.013	3.132 ± 0.008
0.875	-2.130 ± 0.015	3.588 ± 0.010
0.925	-2.241 ± 0.015	4.138 ± 0.008
0.975	-2.647 ± 0.028	4.549 ± 0.013

We can only speculate what the reason for this is. One thing we did not consider in the derivation of equation (3.4.8) is a varying degree of mixing. As genotypes have different adhesion strengths, they segregate to a certain degree due to an interfacial tension. A way to measure the degree of mixing is to look at the number of neighbouring (within interaction range) mutant and host cells for each cell. If the genotypes were perfectly

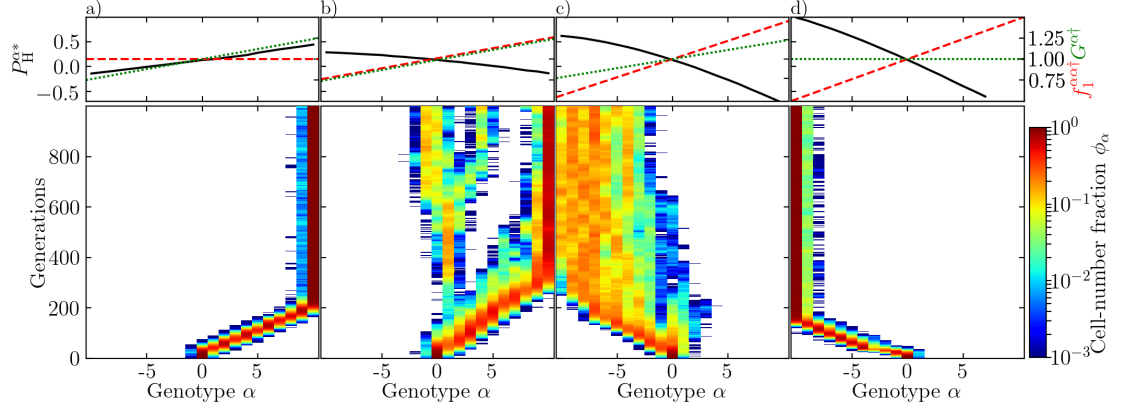


Figure 3.10: Time evolution of the genotype number fractions ϕ_α for tenfold reduced mutation probability $p_m = 0.001$ and otherwise identical parameter as in figure 3.2. White space corresponds to times where no cells of the genotype exist. Color is coded on a logarithmic scale. Curves above display homeostatic pressure P_H^* (black solid), growth-force strength $G^{\alpha\dagger}$ (red dashed) and self adhesion strength $f_1^{\alpha\dagger}$ (green dotted) of the corresponding genotype number α .

Table 3.3: Values obtained for Δk_s^{M1} and Δk_s^{W1} by fitting the simulation results displayed in figure 3.4(b) to equation (3.4.8) for increased growth force and adhesion strength of the mutant.

$G^{M\dagger}$	Δk_s^{M1}	Δk_s^{W1}
1.025	4.798 ± 0.040	-1.809 ± 0.045
1.075	4.865 ± 0.022	-2.178 ± 0.028
1.125	4.808 ± 0.028	-2.313 ± 0.027
1.175	4.712 ± 0.029	-2.328 ± 0.027
1.250	4.641 ± 0.041	-2.340 ± 0.027

mixed, one would expect

$$\bar{N}_{MW}^{\text{exp}} = \phi^W \bar{N}_M^{\text{tot}},$$

with the expected number of neighbouring host cells for mutant cells $\bar{N}_{MW}^{\text{exp}}$ and the total number of neighbours \bar{N}_M^{tot} of mutant cells, with the average taken over all mutant cells. However, the measured value $\bar{N}_{MW}^{\text{sim}}$ is substantially smaller. Hence, we define the mixedness degree $c = \bar{N}_{MW}^{\text{sim}} / \bar{N}_{MW}^{\text{exp}}$ and expand $\Delta k_s^{M/W} = \Delta k_s^{M/W1} c \epsilon$ in equation (3.4.7). Fitting again with the measured values of c yields the values for Δk_s^{M1} and Δk_s^{W1} for reduced growth force and adhesion strength shown in table 3.4. They are nearly identical for Δk_s^{W1} and vary only by about 25% for Δk_s^{M1} . Hence, taking into account the

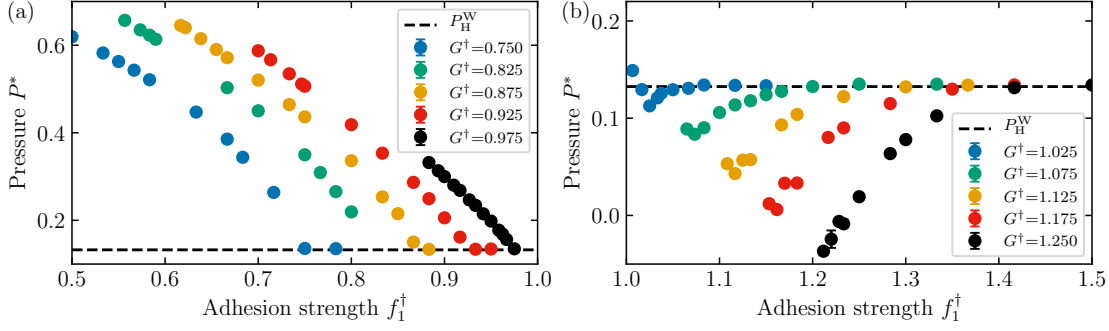


Figure 3.11: (a) Average pressure P^* measured at the steady state in the competitions displayed in figure 3.4 for reduced growth force and adhesion strength of the mutant. Error bars are obtained via block-averaging method (hidden behind markers). Dashed horizontal line displays the homeostatic pressure of the host. (b) Same as in (a) but for increased growth force and adhesion strength of the mutant.

Table 3.4: Values obtained for Δk_s^{M1} and Δk_s^{W1} by taking into account the degree of mixedness c for decreased growth force and adhesion strength of the mutant.

$G^{M\dagger}$	Δk_s^{M1}	Δk_s^{W1}
0.750	-2.729 ± 0.170	5.588 ± 0.080
0.825	-2.918 ± 0.060	5.517 ± 0.033
0.875	-2.832 ± 0.054	5.499 ± 0.033
0.925	-2.700 ± 0.036	5.638 ± 0.020
0.975	-3.247 ± 0.080	5.684 ± 0.035

degree of mixing seems to explain the deviation to a large degree. However, the hereby obtained values for increased growth force and adhesion strength differ more than the ones displayed in table 3.3.

Stability analysis

The right hand side of the differential equation from which we obtained the fixed point equation (3.4.7) is given by (dropping the index of ϕ^M)

$$\begin{aligned} \mathcal{F}(\phi) = & \phi^3(\Delta k_s^M + \Delta k_s^W) + \phi^2(-2\Delta k_s^M - \Delta k_s^W \\ & + \kappa\Delta P_H) + \phi(\Delta k_s^M - \kappa\Delta P_H). \end{aligned} \quad (3.7.1)$$

A fixed point ϕ_i of an autonomous differential equation is stable if $\mathcal{F}'(\phi_i) < 0$. Insertion of the three fixed points into $\mathcal{F}'(\phi)$ yields

$$\mathcal{F}'(\phi_1 = 0) = \Delta k_s^M - \kappa \Delta P_H \quad (3.7.2)$$

$$\mathcal{F}'(\phi_2 = 1) = \Delta k_s^W + \kappa \Delta P_H \quad (3.7.3)$$

$$\mathcal{F}'(\phi_3) = -(\Delta k_s^W + \kappa \Delta P_H) \phi_3. \quad (3.7.4)$$

With the arguments discussed in the main text for the case $f_1^{\text{MW}} = \min(f_1^{\text{MM}}, f_1^{\text{WW}})$, the regime of ΔP_H in which $\mathcal{F}'(\phi_{1/2}) > 0$ and $\mathcal{F}'(\phi_3) < 0$ is the same as the one in which $0 < \phi_3 < 1$. Hence, ϕ_3 is a stable fixed point there.

We test our phenomenological model by looking at the case $f_1^{\text{MW}} = \max(f_1^{\text{MM}}, f_1^{\text{WW}})$. For increased growth force and adhesion strength, host cells have less space when surrounded by mutant cells, while mutant cells do not feel a difference in that regard. Hence, the advantage of mutant cells at the interface is smaller than for $f_1^{\text{MW}} = \min(f_1^{\text{MM}}, f_1^{\text{WW}})$, while the disadvantage of host cells is bigger. Thus, the condition $\Delta k_s^M + \Delta k_s^W > 0$ is not fulfilled anymore. The difference in homeostatic pressure needs to be bigger than $\Delta k_s^W / \kappa$, such that ϕ_3 becomes bigger than zero. Contrary to the case $f_1^{\text{MW}} = \min(f_1^{\text{MM}}, f_1^{\text{WW}})$, in the regime of ΔP_H where $0 < \phi_3 < 1$, ϕ_1 and ϕ_2 are stable and ϕ_3 is an unstable fixed point. Hence, we should not find stable coexistence and a single mutated cell should take over the whole compartment as long as $\phi_3 > 0$ and not be able to grow otherwise. Furthermore, when starting the simulation from an initial number fraction ϕ_{init}^M of mutant cells, the mutant should only win when $\phi_{\text{init}}^M > \phi_3$ and vanish when started below. Figure 3.12 shows results of such competitions for different initial number fractions, with random initial mutation of cells. For each parameter combination, five independent competitions were performed. The initial number fraction needed such that the mutant wins in all cases increases with growing adhesion strength, as expected. Most of the time we find a finite regime in which both genotypes can win the competition instead of a sharp transition, which is mainly due to the random initial conditions.

Cluster analysis

As explained in the main text, a constant rate of mutation leads to an enhanced formation of clusters when the weaker genotype is barely able to grow against the stronger genotype and consists of only one or few clusters for a single mutation event. We define a cluster as all cells of the same genotype that are in interaction range to at least one other member of the cluster (DBSCAN clustering algorithm with number of minimal points equal to one). Figure 3.6(b) displays the number of clusters of the weaker genotype

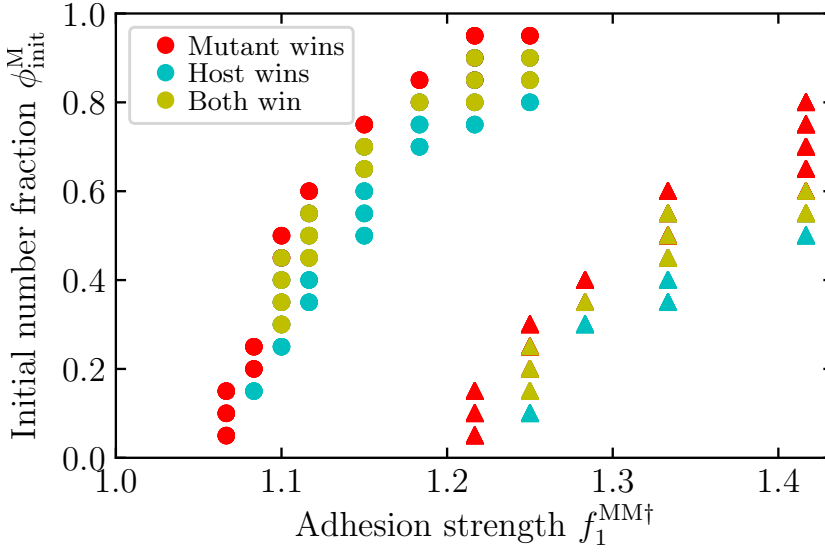


Figure 3.12: Result of competitions with adhesion strength $f_1^{MW} = \max(f_1^{MM}, f_1^{WW})$ between host and mutant cells for $G^{M\dagger} = 1.075$ (circles) and $G^{M\dagger} = 1.25$ (triangles) for different initial number fractions ϕ_{init}^M of the mutant in terms of its adhesion strength $f_1^{MM\dagger}$. For each combination five simulations were performed. Colors show whether all competitions are won by the mutant (red), the host (cyan) or both win at least one competition (yellow).

in the competitions displayed in figure 3.6(a), in comparison to the result of a single mutation event. Indeed, when the number fraction of the weaker genotype is small for a the single mutation event ($\tau = 1$), we find significant deviations even for small mutation rates. In this case, the number of clusters first strongly increases with mutation rate, with roughly a tenfold increase at the peak. For even higher mutation probability, the number of clusters decreases again, due to merging of clusters, finally leading to percolation.

3.7.3 Additional material

S1 Video. Free evolution. Time evolution of a tissue for the free evolution case displayed in Fig 3.1. Mutations can alter growth-force strength G^\dagger and adhesion strength f_1^\dagger independently.

S2 Video. Heterogeneity. Time evolution of a tissue with tradeoff $\tau = 1.25$ between mutations of growth-force strength G^\dagger and adhesion strength f_1^\dagger . Visualizations of the trajectory and of the individual cell-number fractions ϕ_α are displayed.

4 Instability and fingering of interfaces in growing tissue

4.1 Abstract

Interfaces in tissues are ubiquitous, both between tissue and environment as well as between populations of different cell types. The propagation of an interface can be driven mechanically. Computer simulations of growing tissues are employed to study the stability of the interface between two tissues on a substrate. From a mechanical perspective, the dynamics and stability of this system is controlled mainly by four parameters of the respective tissues: (i) the homeostatic stress (ii) cell motility (iii) tissue viscosity and (iv) substrate friction. For propagation driven by a difference in homeostatic stress, the interface is stable for tissues which differ in their substrate friction even for very large differences of homeostatic stress; however, it becomes unstable above a critical stress difference when the tissue with the larger homeostatic stress has a higher viscosity. A small difference in directed bulk motility between the two tissues suffices to result in propagation with a stable interface, even for otherwise identical tissues. Larger differences in motility force, however, result in a finite-wavelength instability of the interface. Interestingly, the instability is apparently bound by nonlinear effects and the amplitude of the interface undulations only grows to a finite value in time.

4.2 Introduction

Interfaces of tissues, their propagation as well as their stability, play an important role in various biological contexts, ranging from tissue development [1] to wound healing [2, 3] and cancer [4]. In many of these processes, the interface propagates, driven by cell proliferation and/or motility. This leads to the question how the tissue maintains a stable interface, as this is crucial e.g. in development in order to arrive at the desired distinct cell populations, while interface instabilities can have severe consequences, as in cancer metastasis. Several mechanisms act simultaneously in this problem, where each of them can either have a stabilizing or destabilizing effect on the interface. Interfacial tension,

e.g. caused by differential adhesion between cell populations [5], stabilizes an interface, as it penalizes increase of interface area. On the other hand, increase of interfacial area can be further amplified, e.g. due to enhanced growth rates in the protruding region, where cells have more free space and access to nutrients, as commonly observed during wound healing [2, 6, 7].

Interface instabilities in systems far from equilibrium are well known in solid-state physics, where several instability mechanisms have been found and studied [8]. Examples are the Saffman-Taylor instability (also known as viscous fingering), which occurs during the injection of a low-viscosity fluid into one of a larger viscosity, the Mullins-Sekerka instability in unidirectional solidification, which arises from the unstable diffusive transport of the latent heat of solidification, and leads to dendritic growth at later stages, and the Rayleigh-Taylor instability between two immiscible fluids when the fluid with higher density is placed on top of the lighter one. Also, in vapor deposition flat interfaces are unstable to roughening, in which the interface width initially grows slowly, but monotonically with time and saturates at a finite value at late times. For tissues, or bacterial colonies as a related example, growth and division of cells can give rise to new instability mechanisms. For example, an undulation instability of an incompressible epithelium adjacent to a viscoelastic stroma has been found, where the instability is driven by enhanced growth in the protruding region, which creates a shear flow that builds up pressure at the bottom of the protrusion [9]. Coupling cell growth to nutrient diffusion leads to an additional instability, as cells in the protruding region have access to more nutrients, reminiscent of the Mullins-Sekerka instability [10]. In growing bacterial colonies of *E. coli* inside a microfluidic device, a streaming instability has been observed due to steric interactions between large, slow-moving and small, fast-moving cells [11]. During growth of bacterial colonies on a petri dish, instabilities of the advancing front arise, displaying different levels of complexity, which range from a small number of fingers to densely-branched, dendritic structures [12, 13, 14, 15].

Mechanically-regulated propagation of tissues has been studied by employing the concept of homeostatic stress [16, 17, 18]. The homeostatic stress is defined as the stress a tissue exerts onto its surrounding at the state when apoptosis and division balance each other. It has been proposed that in a competition for space between two tissues, the tissue with the lower homeostatic stress (higher homeostatic pressure) grows at the expense of the other [19]. Furthermore, motility forces generated by cells migrating on a substrate can generate stresses on neighboring tissues and affect the competition [18]. This has recently been studied by in vitro experiments. Two different confluent cell-layers were initially separated by a fixed gap. Upon release, the two tis-

sues migrate towards each other and collide "head on". Interestingly, Ras-transformed Madin-Darby Canine Kidney (MDCK) cells were pushed back by the corresponding wild type cells [20], while conversely Ras-transformed Human Embryonic Kidney (HEK) cells outcompeted the corresponding wild type. The cell population which generates larger collective stresses displaces the other population and drives the propagation of the interface between them [21].

The stability of a propagating interface, driven by homeostatic stress and/or bulk motility differences, between two competing tissues on a substrate has recently been studied theoretically by a linear stability analysis [18]. Three instability criteria are obtained, where two yield a critical homeostatic stress difference and one a critical difference in motility-force strength above which the interface becomes unstable.

Using a particle-based model of growing tissues [17], we study the mechanically-regulated competition of two tissues and explore the stability of the interface. Our simulations suggest that nonlinearities provide a strong stabilizing effect on the interface. Contrary to linear-stability analysis, we find a stable interface when the two tissues differ in their respective substrate friction, even for large homeostatic stress differences. On the other hand, for different viscosities of the two tissues, an instability arises above a critical difference in homeostatic stress. However, the instability does not grow forever; instead, a finger-like protrusion of the weaker tissue is left behind in the stronger tissue, which otherwise advances with a broad front. For a difference in motility-force strength, we find that a small motility has a stabilizing effect onto the interface, causing a decrease of the interface saturation width with growing difference in motility force, while large motility forces cause an unstable interface above a critical point. Beyond the instability, distinct modes grow strongly in amplitude, but saturate at finite values depending on the strength of motile forces. Hence, the instability due to motility forces seems to be bound by nonlinearities.

Our results demonstrate that the structure of the interface between two competing tissues may serve as a key observable in characterizing mechanical properties of the competing tissues. Indeed, it is often the interfacial properties that reveal malignancy in tumor biology [22, 23].

4.3 Simulation model

Several models have been developed in order to study mechanical properties and growth of cell monolayer in general and interfaces between different cell types in particular [24, 25, 26]. For example, vertex-based models are commonly employed, e.g. to study

physical properties such as shear and compression modulus, or jamming transitions [27, 28, 29, 30]. We employ the well-established particle-based growth model of [17, 31], which has been mapped onto various systems of growing cell sheets, such as wound healing assays or growth of bacterial colonies in microfluidic devices [2, 32]. A cell is represented by two particles which repel each other via an active growth force

$$\mathbf{F}_{ij}^G = \frac{G}{(r_{ij} + r_0)^2} \hat{\mathbf{r}}_{ij}, \quad (4.3.1)$$

with growth-force strength G , unit vector $\hat{\mathbf{r}}_{ij}$ and distance r_{ij} between the two particles and a constant r_0 . When the distance between the particles exceeds a threshold r_{ct} the cell divides. A new particle is then placed in close vicinity of each particle of the mother cell. These pairs constitute the two daughter cells. Particles between different cells interact via a soft repulsive force \mathbf{F}_{ij}^V on short distances and a constant attractive force \mathbf{F}_{ij}^A on intermediate distances, where

$$\left. \begin{aligned} \mathbf{F}_{ij}^V &= f_0 \left(\frac{R_{PP}^5}{r_{ij}^5} - 1 \right) \hat{\mathbf{r}}_{ij} \\ \mathbf{F}_{ij}^A &= -f_1 \hat{\mathbf{r}}_{ij} \end{aligned} \right\} \text{for } r_{ij} < R_{PP}, 0 \text{ otherwise}, \quad (4.3.2)$$

with volume exclusion coefficient f_0 , adhesion strength f_1 and cut-off length R_{PP} . These forces and the corresponding interaction potentials are shown in Fig. 3.1(a) and (b). The discontinuity of the adhesion force \mathbf{F}_{ij}^A at $r = R_{PP}$ reflects the contact interaction of cellular adhesion molecules such as E-cadherin. We model apoptosis by removing cells randomly at a constant rate k_a . Interactions with the underlying substrate are given by a friction force

$$\mathbf{F}_i^B = -\gamma_b \mathbf{v}_i, \quad (4.3.3)$$

with velocity \mathbf{v}_i . Forces in migrating cell monolayers do not solely arise at the front, but collectively over the whole monolayer [21, 33]. In a simplified picture, this is modeled by a homogeneous bulk motility force [18], given by a constant force perpendicular to the interface

$$\mathbf{F}_i^M = f_m \cdot \hat{\mathbf{e}}_x, \quad (4.3.4)$$

with motility-force strength f_m and direction $\hat{\mathbf{e}}_x$ perpendicular to the interface. This choice of motility model further facilitates comparison of results with [18]. Other choices for the motility model are possible, for instance by orienting the motility force towards the local interface. Such an orientation could be important once protrusions start to form. For simplicity and consistency with [18], we restrict the analysis to the simple

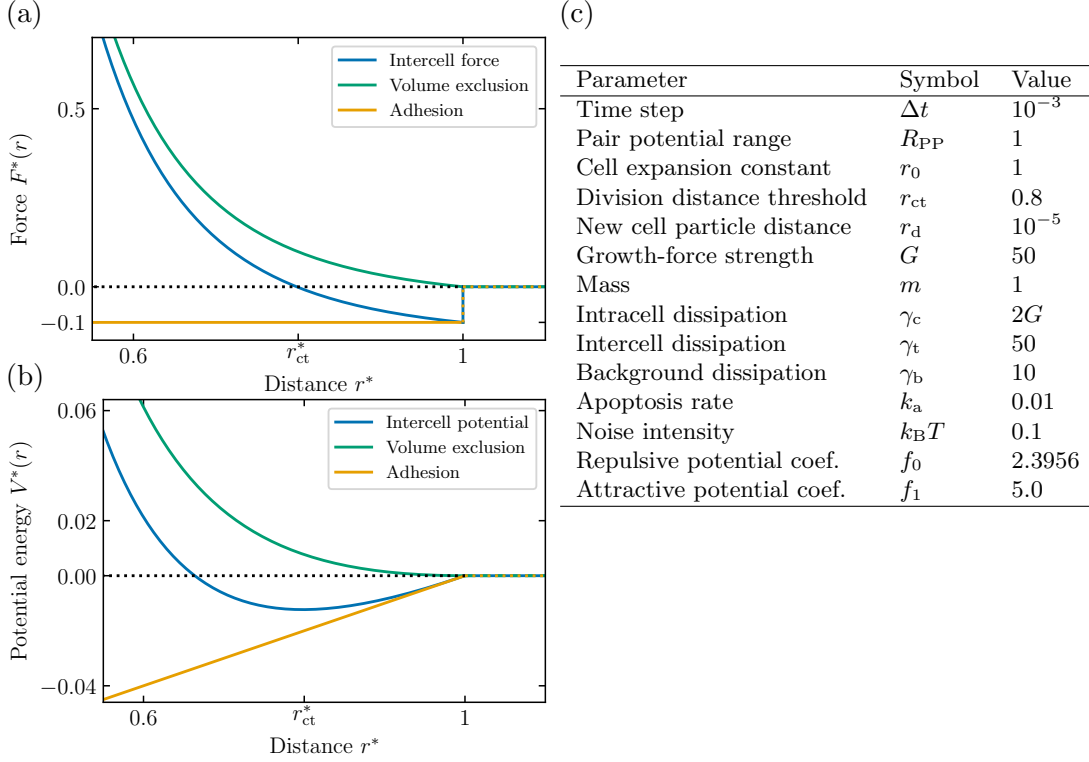


Figure 4.1: (a) Sketch of the cell-cell interaction force. (b) Corresponding potential to the force displayed in (a). (c) Simulation parameters of the reference tissue.

motility model of equation (4.3.4). A dissipative particle dynamics thermostat is employed in order to account for energy dissipation and random fluctuation, satisfying the fluctuation-dissipation theorem. It consists of a dissipative force

$$\mathbf{F}_{ij}^D = -\gamma \omega^D(r_{ij})(\hat{\mathbf{r}}_{ij} \cdot \mathbf{v}_{ij})\hat{\mathbf{r}}_{ij}, \quad (4.3.5)$$

with the strength γ (which can be chosen independently for intra- and intercell as well as background dissipation) and the relative velocity $\mathbf{v}_{ij} = \mathbf{v}_j - \mathbf{v}_i$ as well as a random force

$$\mathbf{F}_{ij}^R = \sigma \omega^R(r_{ij})\xi_{ij}\hat{\mathbf{r}}_{ij}, \quad (4.3.6)$$

with strength $\sigma^2 = 2k_B T \gamma$, a Gaussian random variable ξ_{ij} with zero mean and unit variance. The weight functions $\omega^D(r_{ij})$ and $\omega^R(r_{ij})$ are related to each other via $\omega^D(r_{ij}) = \omega^R(r_{ij})^2$ to fulfill the fluctuation-dissipation theorem. For intracell dissipation, we use uniform weighting with cutoff $\omega^D(r_{ij}) = \Theta(r_{ij} - R_{PP})$, with the Heavyside step func-

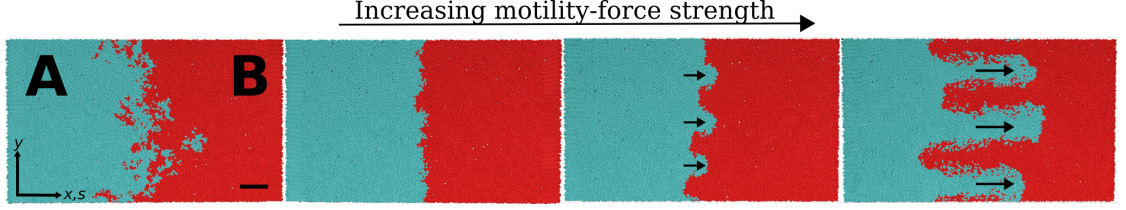


Figure 4.2: Simulation snapshots in competitions with different motility-force strengths $f_m^{A\dagger}$ of tissue A. The tissues are otherwise identical. The interface moves towards tissue B. From left to right: $f_m^{A\dagger} = [0, 0.002, 0.045, 0.08]$. The length of the arrows corresponds to the distance the interface moves over one generation (too small for $f_m^{A\dagger} = 0.002$). System size $L_y^* = 80$ and time $t^* = 80$ in all. The scale bar is 10 cell sizes. Note that for $f_m^{A\dagger} \geq 0.002$ the snapshots are representative of the steady state and the undulations do not grow further.

tion $\Theta(r)$. For intercell dissipation, we employ $\omega^D(r_{ij}) = \omega^R(r_{ij})^2 = (1 - r_{ij}/R_{PP})^2$. Each parameter can be set independently for each cell type and between cell types for inter-cell interactions. The dynamics of particle i is then determined by

$$m_i \ddot{\mathbf{r}}_i = \mathbf{F}_{ik}^G + \mathbf{F}_{ik}^D + \mathbf{F}_{ik}^R + \sum_{j \neq i, k} (\mathbf{F}_{ij}^A + \mathbf{F}_{ij}^V + \mathbf{F}_{ij}^D + \mathbf{F}_{ij}^R) + \mathbf{F}_i^B + \mathbf{F}_i^M, \quad (4.3.7)$$

with mass m_i of particle i and particle k which forms a cell with particle i . We integrate the equations of motion with a self-consistent velocity-Verlet algorithm.

We define a set of standard-tissue parameters and report simulation parameter relative to these standard values, denoted with a dagger, e.g. $G^\dagger = G/G_0$ (see table 4.1 for numerical values). The choice of parameters is motivated by some basic requirements and considerations. After division, the two daughter cells should be in contact with each other ($r_{ct} < R_{PP}$), roughly at the minimum of the cell-cell interaction potential ($r_{ct} \approx \sqrt[5]{f_0/(f_0 + f_1)}$) in order to minimize the sudden stress created after division. The tissue as a whole should be expansive ($\sigma_H < 0$). The homeostatic stress increases linearly with the adhesion coefficient f_1 and decreases linearly with the growth-force strength G [34]. As we keep f_1 fixed, this sets a lower bound on G above which the tissue is expansive. We choose a value larger than this lower bound for the reference tissue, in order to be able to study positive and negative homeostatic stress differences. For both tissues to have the same free growth rate, the intercell dissipation coefficient is scaled accordingly ($\gamma_c = 2G$). This choice further ensures that the free growth rate (i.e.

without neighbour cells)

$$k_g^{\text{free}} \approx \frac{G}{\gamma_c + \gamma_b} \int_{r_d}^{r_{ct}} (r_0 + r) dr \quad (4.3.8)$$

is significantly larger than the apoptosis rate ($k_g^{\text{free}} \gg k_a$), such that the tissues can easily replenish. The temperature T is chosen low enough that cells can escape local minima, but other thermal effects are small. Time is measured in terms of the inverse apoptosis rate k_a of the standard tissue, distance in terms of the cut-off length R_{PP} and force in units of G_0/R_{PP}^2 . Thus, the length unit corresponds to the cell size, while time is measured in generations. After one time unit, all cells have divided once on average. Quantities reported in these units are denoted with an asterisk *. We vary the growth-force strength G , the apoptosis rate k_a , background friction γ_b , and motility-force strength f_m . The cross-adhesion strength between the two tissues is the same as the adhesion strength within one tissue. Thus, no passive interfacial tension is present in our simulations. A reduced cross-adhesion causes enhanced interfacial growth [35, 36]. This interfacial growth promotes a fingering instability [9], while the increased interfacial tension favors a flattening of the interface, i.e. the two effects compete with each other. To keep the model simple, we restrict the analysis to the case of vanishing passive interfacial tension in this work.

We use the "treadmilling simulation setup" introduced in [17] in order to obtain steady-state interface progression, by keeping the interface position at the center of the simulation box. All cells are shifted accordingly every 1000 timesteps; excess cells at one end of the simulation box are removed while the weaker tissue replenishes on the other end. In this way, both tissues reach their homeostatic state sufficiently far away from the interface (with system size $L_x^* = 140$ in all simulations), thus the interface properties can be studied on long time scales in a computationally efficient way. We measure all quantities in a comoving reference system $s = x - x_0$, with interface position x_0 .

4.4 Results

It was shown in [17] that the competition between two tissues differing only in homeostatic stress results in a steady-state interface propagation, where the stronger tissue invades the weaker one with a constant velocity. While only stable interfaces were observed in [17], [18] proposes three different routes to instability for an interface between two competing tissues: (A) For propagation driven by bulk motility, the interface becomes unstable above a critical difference in motility-force strength. For propagation

driven by homeostatic stress, the interface is only unstable under the condition that the two tissues either differ (B) in substrate friction or (C) viscosity. For both cases, (B) and (C), the interface becomes unstable above a case-specific critical difference in homeostatic stress. For a combination of both, bulk motility force $f_m^{A/B}$ and homeostatic stress difference $\Delta\sigma_H = \sigma_H^B - \sigma_H^A$, the interface velocity

$$v_{\text{int}} = \frac{\Delta\sigma_H + l_A \hat{f}_m^A + l_B \hat{f}_m^B}{\xi_A l_A + \xi_B l_B} \quad (4.4.1)$$

is predicted, with substrate friction $\xi = 2\gamma_b\rho$, cell density ρ , motility-force density $\hat{f}_m^{A/B} = 2\rho f_m^{A/B}$, and stress decay length $l = \sqrt{\chi\tau/\xi}$. Here, χ is the elastic modulus, τ the time scale at which the tissue loses its elastic character due to cell division and apoptosis, and the product $\chi\tau$ is an effective viscosity. The growth rate k is expanded to linear order around the homeostatic stress as $k = \kappa(\sigma - \sigma_H)$, with stress-response coefficient κ . The viscosity is connected to the stress-response coefficient via $\kappa = 1/\chi\tau$. For our simulations, these coarse-grained tissue parameters are either direct input parameters, or can be measured in independent single tissue simulations.

Figure 4.3(a) displays a comparison between equation (4.4.1), with parameters fixed by independent simulations (see [17, 34] for details), and the measured interface velocity, which shows very good agreement. In the following, we focus on the proposed instabilities and study each of them individually.

4.4.1 Bulk motility force

We study first the effect of bulk motility without additional difference in homeostatic stress, i.e. the two tissues are identical except that tissue A has a motility force $f_m^A > 0$ while tissue B is non-motile ($f_m^B = 0$). As predicted in [18], a prescribed motility force can drive interface propagation and the motile tissue invades the non-motile one at constant velocity. An instability is predicted for

$$\Delta v_f > \frac{2\Gamma(l_A\xi_A + l_B\xi_B)}{l_A l_B \xi_A \xi_B (l_A + l_B)}, \quad (4.4.2)$$

with difference in bulk velocity $\Delta v_f = f_m^A/\xi_A - f_m^B/\xi_B$ and interfacial tension Γ [18].

Figure 4.2 displays simulation snapshots for increasing motility-force strength of tissue A. For vanishing motility force, the two competing tissues are identical, including the interaction between cells of different tissues, and thus the interface width $w(t) = \sqrt{\langle h^2 \rangle - \langle h \rangle^2}$ (with height field $h(y,t)$, see [17] for more details) diverges as a function of time (see snapshots in figure 4.2 and blue line in figure 4.3(b), as well as video S1 in the

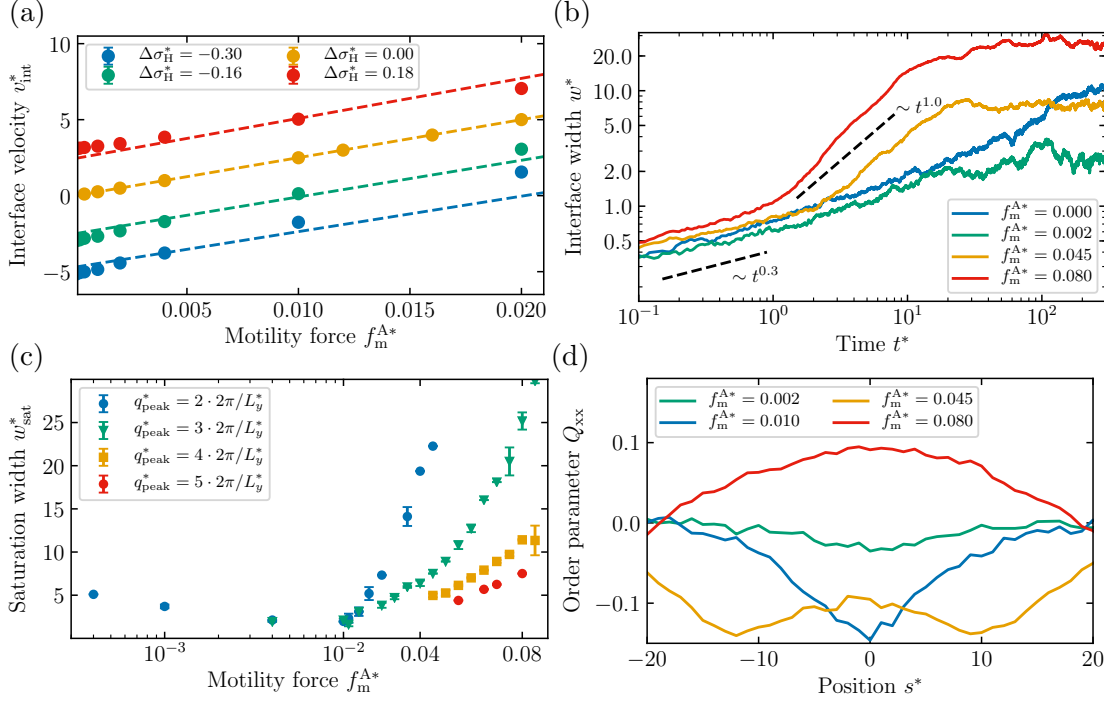


Figure 4.3: Interface velocity, interface (saturation) width, and order parameter dependence on motility-force strength of tissue A in competitions with a non-motile tissue. System size $L_y^* = 80$ in all, $\Delta\sigma_H^* = 0$ in (b)-(d). (a) Interface velocity v_{int} as a function of the motility-force strength f_m^{A*} of tissue A for various homeostatic stress differences $\Delta\sigma_H^*$. Dashed lines represent theoretical predictions according to equation (4.4.1), with parameters fixed by independent simulations. Error bars display standard deviations (hidden behind markers). (b) Interface width w^* as a function of time t^* for different values of motility-force strength f_m^{A*} of tissue A. Note the logarithmic time scale, the interface width for non-vanishing motility is almost constant for 80% of the time. (c) Saturation width w_{sat}^* as a function of motility-force strength f_m^{A*} of tissue A for different peak wave vectors q_{peak}^* . Note the logarithmic scale for $f_m^{A*} < 0.01$. Error bars represent standard deviations. (d) Nematic order parameter Q_{xx} as a function of the position s^* for various motility-force strengths f_m^{A*} of tissue A. Peak wave vector $q_{\text{peak}}^* = 3 \cdot 2\pi/L_y^*$ for all curves.

SI). However, a rather small motility-force strength of tissue A ($f_m^A \approx 5 \cdot 10^{-4} G_0 / R_{PP}^2$) suffices to arrive at a finite interface saturation width w_{sat} , i.e. small motility forces have a stabilizing effect on the interface (see snapshots in figure 4.2 and green line in figure 4.3(b), as well as video S2 in the SI). For larger motility-force strengths, protrusions of the motile into the non-motile tissue form at one particular finite wavelength. Over the time course of the first cell generation the interface width grows slowly with time ($w \sim t^{0.3}$). After the unstable wave mode has been selected, the interface width increases linear with time ($w \sim t^{1.0}$). However, the mode amplitude does not grow indefinitely, but saturates at a motility-force dependent plateau due to nonlinear effects after about ten cell generations (see snapshots in figure 4.2 and orange and red line in figure 4.3(b), as well as videos S3 and S4 in the SI).

The resulting wave pattern is remarkably stable over time once the steady state has been reached. Figure 4.3(c) displays the saturation width w_{sat} as a function of the motility-force strength. The saturation width first decreases with increasing motility-force strength, with w_{sat} of the order of one or two cell layers at the minimum, i.e. an almost flat interface. For higher motility-force strength, the saturation width starts to increase and the aforementioned protrusions form, which we interpret as the onset of instability. Interestingly, independent simulations for identical parameter yield different wavelengths at the steady state. While the saturation width decreases with increasing q_{peak} for identical f_m^A , the smallest motility-force strength at which a particular wave mode is found increases with q_{peak} . This matches the predicted evolution of the most unstable wave mode in [18]. In order to study the observed interface patterns quantitatively, we calculate the time-averaged structure factor

$$S(q) = \langle \tilde{h}(q, t) \tilde{h}(-q, t) \rangle, \quad (4.4.3)$$

at the steady state, where $\tilde{h}(q, t)$ denotes the spatial Fourier transform of the height field $h(y, t)$ (see [17] for further details). For self-affine surface growth the structure factor displays a power-law decay at the steady state [26, 37]. Figure 4.4(a) shows the structure factor for the same values of motility-force strength as in figures 4.2 and 4.3(b). $S(q)$ displays deviations from a power-law decay by a peak at a certain wave vector larger than the system-spanning one (in figure 4.4(a) $q_{\text{peak}} = 3 \cdot 2\pi/L$), which gets more pronounced for increasing motility-force strength and corresponds to the wavelength of the protrusions in figure 4.2. As mentioned above, for the same value of f_m^A , different wave vectors can become the dominating mode at the steady state in independent simulations. Figure 4.4(b) displays the structure factor for three different peak modes for identical motility-force strength. The maximum decreases with increasing peak wave vectors,

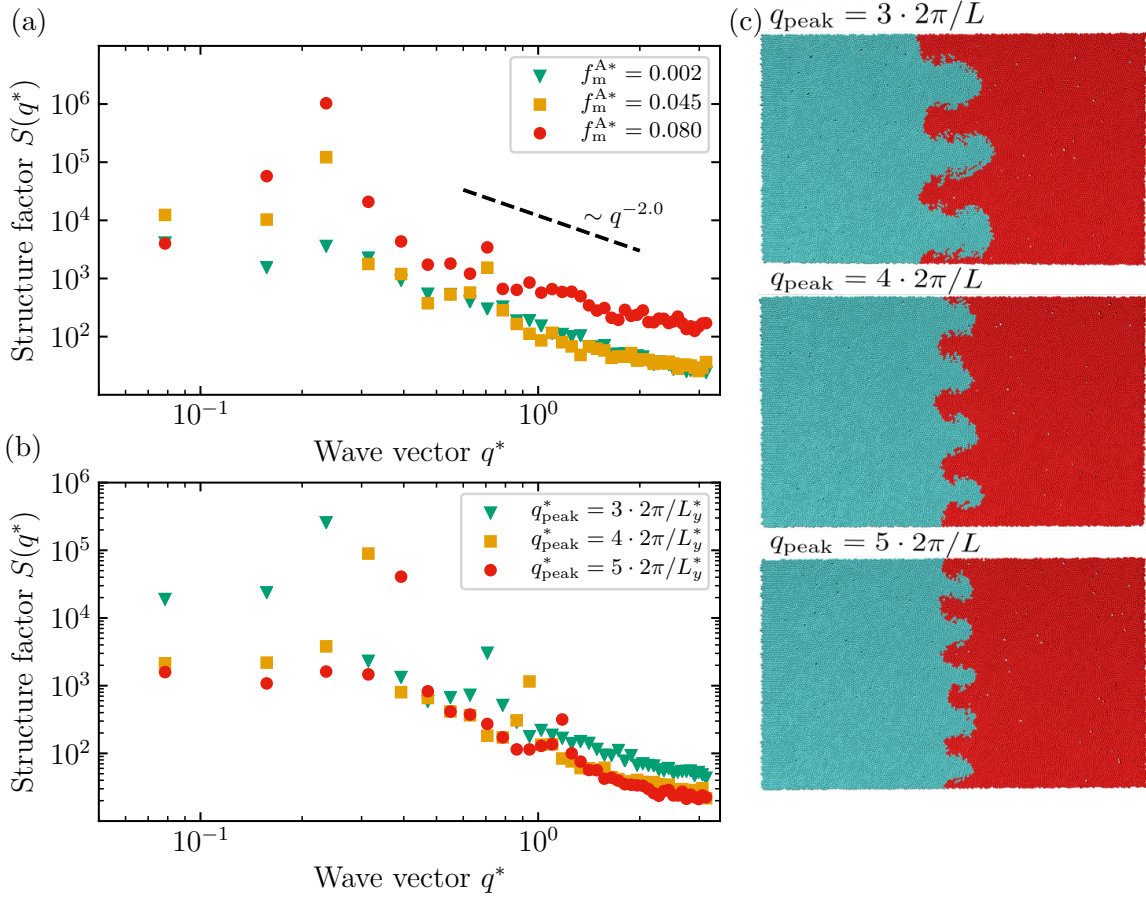


Figure 4.4: (a) Structure factor $S(q^*)$ at the steady state for different values of the motility-force strength f_m^{A*} of tissue A for $\Delta\sigma_H = 0$ and $q_{peak}^* = 3 \cdot 2\pi/L^*$. The dashed line is a guide to the eye. (b) Same as (a), but for fixed motility-force strength $f_m^{A*} = 0.55$ and different peak wave vectors q_{peak}^* . (c) Snapshots obtained in the simulations of (b) at the steady state at $t^* = 80$. Note that the different stable peak wave vectors arise by chance from an initially flat interface. System size $L_y^* = 80$ in all.

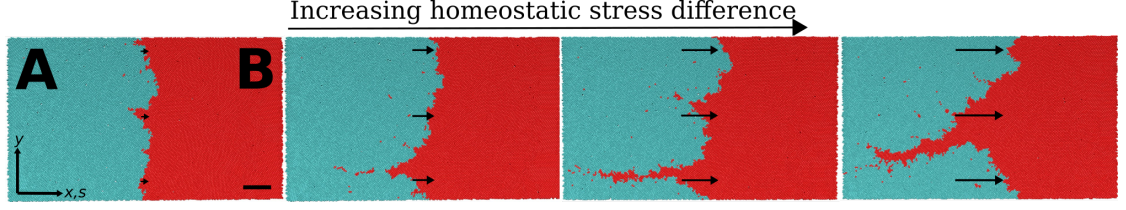


Figure 4.5: Simulation snapshots in competitions with different homeostatic stress differences $\Delta\sigma_H^*$ and reduced apoptosis rate $k_a^{B\dagger} = 0.2$ of tissue B. The interface moves towards tissue B. From left to right: $\Delta\sigma_H^* = [0.18, 0.36, 0.56, 0.78]$. The length of the arrows corresponds to the distance the interface moves over five generations. System size $L_y^* = 80$ and time $t^* = 80$ in all. The scale bar is 10 cell sizes. The snapshots are not representative of a steady state, as fingers detach, disappear and reform over time.

consistent with the higher saturation width for smaller q_{peak} (see figure 4.3(c)).

The stabilizing effect is accompanied by a preferred alignment of cells perpendicular to the interface, quantified by the nematic order parameter $Q_{xx} = 2p_x p_x - 1$, with p_x the x -component of the unit vector between the two cell particles. This leads to an active interfacial tension $\Gamma = \int_{-\infty}^{\infty} (\sigma_{yy}(s) - \sigma_{xx}(s)) ds$, due to cell growth [17]. Figure 4.3(d) displays the order parameter for different motility-force strengths. The overall alignment along the y -direction (i.e. negative Q_{xx}) first increases with growing f_m^A , with a maximum at the interface position. In the regime where protrusions start to form, the maximum splits into two maxima located to the left and the right of the interface, where the position of the maxima corresponds to the width of the protrusions. For even higher motility-force strength, when the saturation width becomes large, we find an overall alignment along the x -direction.

4.4.2 Homeostatic stress difference

As shown in [17, 18], interface propagation can be driven by homeostatic stress alone. For two tissues that only differ by their homeostatic stress, a stable interface propagating at constant velocity is found in the simulations [17]. Two instability conditions for competition driven by a difference in homeostatic stress $\Delta\sigma_H$ have been proposed in [18], given by

$$\Delta\sigma_H > \frac{27}{4} \Gamma \frac{(\xi_A l_B - \xi_B l_A)^2 (\xi_A l_A + \xi_B l_B)}{l_A^2 l_B^2 (\xi_B - \xi_A)^3}, \quad \xi_B > \xi_A \quad (4.4.4)$$

$$\Delta\sigma_H > 2\Gamma \frac{(\xi_A l_A + \xi_B l_B)}{\kappa_B^{-1} - \kappa_A^{-1}}, \quad \kappa_B^{-1} > \kappa_A^{-1} \quad (4.4.5)$$

While substrate friction ξ can be changed as an input parameter, the stress-response

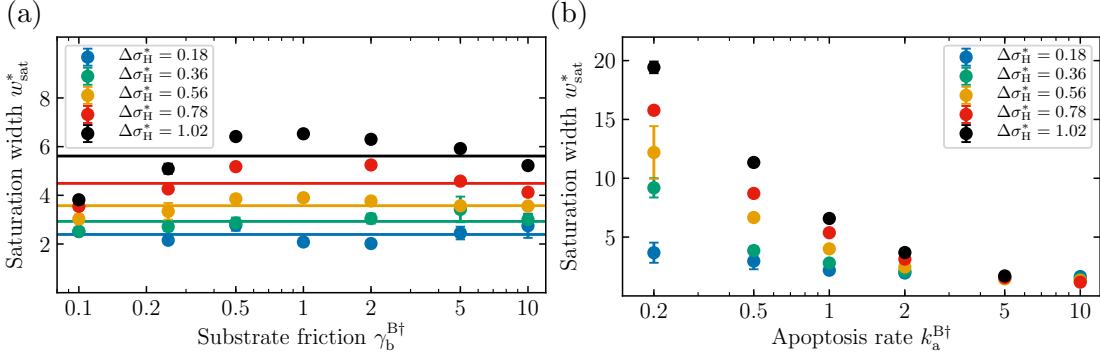


Figure 4.6: (a) Saturation width w_{sat}^* as a function of substrate friction $\gamma_b^{A\dagger}$ of tissue A for various homeostatic stress differences $\Delta\sigma_H^*$. (b) Same as (a) but as a function of the apoptosis rate $k_a^{B\dagger}$ of tissue B. System size $L_y^* = 80$ in both. Error bars represent standard deviations. Note the different scales on the y -axis between (a) and (b).

coefficient κ is a tissue property, which needs to be determined in simulations and can not be controlled directly. In order to measure κ , we use a constant-stress ensemble and measure the growth rate as a function of the applied stress. κ is then obtained by a linear fit [17, 34]. Since $\kappa = 1/\chi\tau$, with the characteristic time τ for cell turnover, κ can be changed by varying the apoptosis rate k_a . Reduction of k_a yields a lower stress-response coefficient and thus a higher viscosity.

For different substrate frictions, we do not observe any instabilities, even for large differences in homeostatic stress. While the overall saturation width increases with growing homeostatic stress difference, w_{sat} does not show systematic variations with substrate friction (see figure 4.6(a)).

According to equation (4.4.5), instabilities should only be obtained if the weaker tissue (the tissue with the higher homeostatic stress, here tissue B) has a larger viscosity, i.e. a lower apoptosis rate than the stronger tissue. Figure 4.5 displays simulation snapshots for different homeostatic stress differences. With increasing difference, a finger of the weaker tissue is found to develop into the stronger one. In contrast to the motility-driven case, no steady state is reached. The finger occasionally detaches, leaving a large island behind in the stronger tissue, moves along the interface and forms again (see video S5 in the SI). However, we still find a mostly stable saturation width of the interface. Figure 4.6(b) displays w_{sat} as a function of the apoptosis rate k_a^B of tissue B for various different values of $\Delta\sigma_H$. We find that w_{sat} increases for a reduced apoptosis rate (compared to $k_a^B = k_a^A$) above a critical homeostatic stress difference ($\Delta\sigma_H^* \approx 0.4 - 0.5$), while the saturation width decreases for increased k_a^B , i.e. an enhanced apoptosis rate of the weaker tissue has a stabilizing effect.

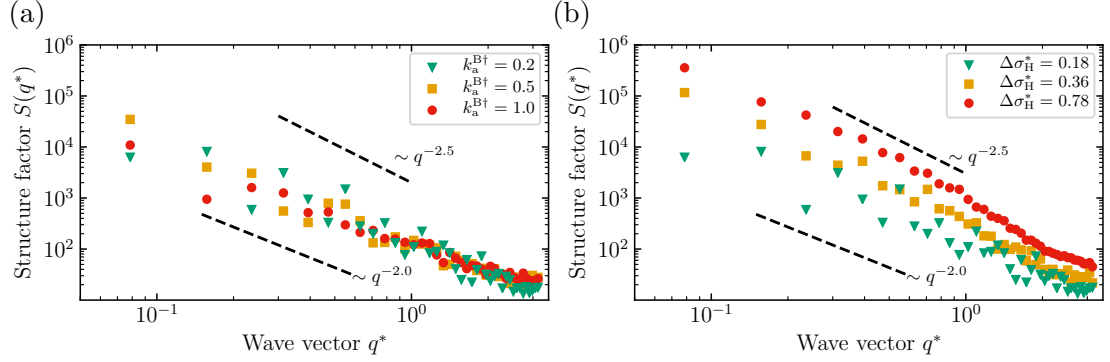


Figure 4.7: (a) Structure factor $S(q^*)$ at the steady state for different values of the apoptosis rate $k_a^{B\dagger}$ of tissue B for $\Delta\sigma_H^* = 0.18$ (below the critical stress difference). The dashed lines are guides to the eye. (b) Same as (a), but for different values of $\Delta\sigma_H^*$ and fixed $k_a^{B\dagger} = 0.2$. System size $L_y^* = 80$ in all.

The structure factor reflects the increase in saturation width with growing homeostatic stress difference (see figure 4.7). Below the critical stress difference, the structure factor for reduced apoptosis rate does not deviate significantly from the case of identical apoptosis rates of the competing tissues (see figure 4.7(a)). However, for a fixed (reduced) apoptosis rate of tissue B, the amplitude of all wave modes increases with growing $\Delta\sigma_H$ (see figure 4.7(b)), which matches the increase of the interface saturation width.

4.4.3 Bulk motility force & homeostatic stress difference

Finally, we take a closer look at a combination of differences in motility and homeostatic stress, with substrate friction and apoptosis rate identical for both tissues. For small motility forces, the results of [17] are not altered, the interface is stable and propagates at a constant velocity. In the regime where we find protrusions of the motile tissue into the non-motile tissue for vanishing homeostatic stress difference, the interface saturation width likewise starts to increase (see figure 4.8(a)). However, we do not observe protrusions at a particular wave length as for $\Delta\sigma_H^* = 0$, but a highly dynamic shape of the interface (see snapshots in figure 4.8(b) for a comparison and video S6 in the SI).

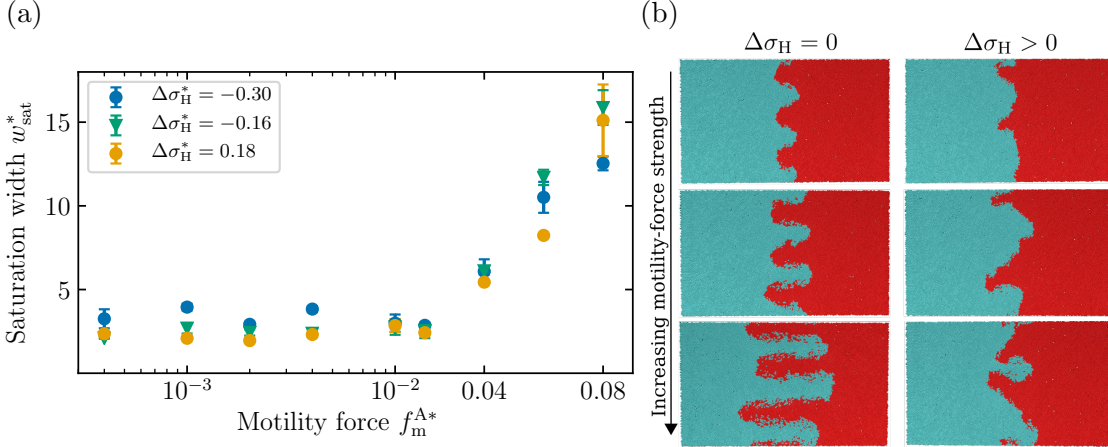


Figure 4.8: (a) Saturation width w_{sat}^* as a function of the motility-force strength f_m^{A*} of tissue A for various homeostatic stress differences $\Delta\sigma_H^*$ in competitions with the standard tissue with $f_m^{B*} = 0$ and system size $L^* = 80$. Note the logarithmic scale for $f_m^{A*} < 0.01$. Error bars represent standard deviations. (b) Simulation snapshots for different motility-force strengths f_m^{A*} of tissue A, without (left) and with a homeostatic stress difference $\Delta\sigma_H^* = 0.18$ (right). From top to bottom: $f_m^{A*} = [0.04, 0.06, 0.08]$. The interface moves to the right. The tissues are otherwise identical. System size $L_y^* = 80$ and time $t^* = 80$ in all. Note that the snapshots with a homeostatic stress difference are not representative of the steady state, as the interface shape is highly dynamic.

4.5 Discussion

We have investigated the stability of a propagating interface between two competing tissues over a broad parameter range in simulations of a particle-based model.

While the width of an interface between two tissues with identical properties diverges as a function of time, we find that already a very small directed bulk motility force of one tissue suffices to stabilize the interface at a finite width, similar to a homeostatic stress difference [17]. Above a critical motility-force strength, a single mode with wave length less than the system size becomes unstable. However, the amplitude of this mode does not diverge, as expected by linear-stability analysis, but nonlinear effects limit its growth, resulting in remarkably stable steady-state undulations of the interface. Cells align preferentially parallel to the interface for small motility forces, which transits into perpendicular alignment with growing motility-force strength. This parallel alignment results in an active interfacial tension due to cell growth [17], which could explain the stabilizing effect of small motility forces.

For interface propagation driven by a difference in homeostatic stress, an enhanced viscosity of the weaker tissue results in an unstable interface above a critical homeostatic

stress difference, reminiscent of a Saffman-Taylor instability (viscous fingering), where a low-viscosity fluid is injected into a high-viscosity fluid. Contrary to the classical case, viscosity here is the bulk viscosity due to cell turnover [18] rather than shear viscosity, and is accordingly varied by changing the apoptosis rates of the competing tissues. Displacement of the more viscous fluid does not take place by injection of the less viscous fluid, but occurs naturally as the less viscous tissue grows at the expense of the more viscous tissue. The resulting pattern in the homeostatic-stress-driven case is much more dynamic than in the motility-driven case. A finger of the weaker tissue remains within the propagating front. This finger constantly reforms, moves and disappears.

These two instabilities have recently been predicted by linear-stability analysis [18]. For both instabilities, our results match the predicted evolution of the most unstable wave mode qualitatively. However, a quantitative comparison remains elusive, since we do not consider interfacial tension due to differential adhesion, as this would cause interfacial growth due to more free space for cells at the interface [35].

However, we do not observe the predicted instability for a difference in substrate friction of the competing tissues, even for large differences in the homeostatic stress between the competing tissues.

Our results suggest that interfacial patterns of competing tissues provide information about the underlying mechanical properties of the competing tissues. For example, a relatively regular — almost sinusoidal — undulation pattern would suggest a motility-driven invasion, whereas a "remaining finger" of the host in the invading tissue would indicate a lower viscosity of the invader. However, experimental evidence of this kind of structures and instabilities will be needed before definite conclusions can be drawn. From a theoretical perspective, possible future research directions on the stability of interfaces could be to account for anisotropic cell growth or enhanced interfacial growth rates [35].

4.6 Acknowledgements

The authors gratefully acknowledge the computing time granted by the JARA Verbundprogramm and provided on the JARA Partition part of the supercomputer JURECA at Forschungszentrum Jülich and of the supercomputer CLAIX at RWTH Aachen University.

Bibliography chapter 4

- [1] E. Batlle and D. G. Wilkinson (2012), “Molecular mechanisms of cell segregation and boundary formation in development and tumorigenesis”, *Cold Spring Harbor Perspectives in Biology*, **4**(1), a008227.
- [2] M. Basan, J. Elgeti, E. Hannezo, W.-J. Rappel, and H. Levine (2013), “Alignment of cellular motility forces with tissue flow as a mechanism for efficient wound healing”, *Proc. Natl. Acad. Sci. U.S.A.*, **110**(7), 2452–2459.
- [3] A. Ravasio, et al. (2015), “Gap geometry dictates epithelial closure efficiency”, *Nat. Commun.*, **6**(1), 7683.
- [4] A. Brú, S. Albertos, J. L. Subiza, J. L. García-Asenjo, and I. Brú (2003), “The universal dynamics of tumor growth.”, *Biophys. J.*, **85**(5), 2948–2961.
- [5] R. A. Foty and M. S. Steinberg (2005), “The differential adhesion hypothesis: a direct evaluation”, *Dev. Biol.*, **278**(1), 255–263.
- [6] V. Cristini, et al. (2005), “Morphologic instability and cancer invasion”, *Clin. Cancer Res.*, **11**(19), 6772–6779.
- [7] M. Poujade, et al. (2007), “Collective migration of an epithelial monolayer in response to a model wound”, *Proc. Natl. Acad. Sci. U.S.A.*, **104**(41), 15988–15993.
- [8] F. Gallaire and P.-T. Brun (2017), “Fluid dynamic instabilities: theory and application to pattern forming in complex media”, *Philos. Trans. A Math. Phys. Eng. Sci.*, **375**(2093), 20160155.
- [9] M. Basan, J.-F. Joanny, J. Prost, and T. Risler (2011), “Undulation instability of epithelial tissues”, *Phys. Rev. Lett.*, **106**(15), 158101.
- [10] T. Risler and M. Basan (2013), “Morphological instabilities of stratified epithelia: a mechanical instability in tumour formation”, *New J. Phys.*, **15**(6), 065011.
- [11] W. Mather, O. Mondragón-Palomino, T. Danino, J. Hasty, and L. S. Tsimring (2010), “Streaming instability in growing cell populations”, *Phys. Rev. Lett.*, **104**(20), 208101.
- [12] S. N. Santalla, et al. (2018), “Nonuniversality of front fluctuations for compact colonies of nonmotile bacteria”, *Phys. Rev. E*, **98**(1), 012407.

- [13] C. Giverso, M. Verani, and P. Ciarletta (2015), “Branching instability in expanding bacterial colonies”, *J. R. Soc. Interface*, **12**(104), 20141290.
- [14] K. Kawasaki, A. Mochizuki, M. Matsushita, T. Umeda, and N. Shigesada (1997), “Modeling spatio-temporal patterns generated by *Bacillus subtilis*”, *J. Theor. Biol.*, **188**(2), 177–185.
- [15] M. Matsushita and H. Fujikawa (1990), “Diffusion-limited growth in bacterial colony formation”, *Physica A*, **168**(1), 498–506.
- [16] J. Ranft, M. Aliee, J. Prost, F. Jülicher, and J.-F. Joanny (2014), “Mechanically driven interface propagation in biological tissues”, *New J. Phys.*, **16**(3), 035002.
- [17] N. Podewitz, F. Jülicher, G. Gompper, and J. Elgeti (2016), “Interface dynamics of competing tissues”, *New J. Phys.*, **18**(8), 083020.
- [18] J. J. Williamson and G. Salbreux (2018), “Stability and roughness of interfaces in mechanically regulated tissues”, *Phys. Rev. Lett.*, **121**(23), 238102.
- [19] M. Basan, T. Risler, J.-F. Joanny, X. Sastre-Garau, and J. Prost (2009), “Homeostatic competition drives tumor growth and metastasis nucleation”, *HFSP J.*, **3**(4), 265–272.
- [20] S. Porazinski, et al. (2016), “Epha2 drives the segregation of ras-transformed epithelial cells from normal neighbors”, *Current Biology*, **26**(23), 3220–3229.
- [21] S. Moitrier, et al. (2019), “Collective stresses drive competition between monolayers of normal and Ras-transformed cells”, *Soft matter*, **15**(4), 537–545.
- [22] M.-T. Tsai, et al. (2008), “Effective indicators for diagnosis of oral cancer using optical coherence tomography”, *Opt. Express*, **16**(20), 15847–15862.
- [23] Z. Hamdoon, et al. (2012), “Structural validation of oral mucosal tissue using optical coherence tomography”, *Head Neck Oncol.*, **4**(1), 29.
- [24] H. Byrne and D. Drasdo (2009), “Individual-based and continuum models of growing cell populations: a comparison”, *J. Math. Biol.*, **58**(4-5), 657–687.
- [25] P. Van Liedekerke, M. M. Palm, N. Jagiella, and D. Drasdo (2015), “Simulating tissue mechanics with agent-based models: concepts, perspectives and some novel results”, *Comp. Part. Mech.*, **2**(4), 401–444.

- [26] M. Block, E. Schöll, and D. Drasdo (2007), “Classifying the expansion kinetics and critical surface dynamics of growing cell populations”, *Phys. Rev. Lett.*, **99**(24), 248101.
- [27] S. Alt, P. Ganguly, and G. Salbreux (2017), “Vertex models: From cell mechanics to tissue morphogenesis”, *Phil. Trans. R. Soc. B*, **372**(1720), 20150520.
- [28] D. B. Staple, et al. (2010), “Mechanics and remodelling of cell packings in epithelia”, *Eur. Phys. J. E*, **33**(2), 117–127.
- [29] N. Murisic, V. Hakim, I. G. Kevrekidis, S. Y. Shvartsman, and B. Audoly (2015), “From discrete to continuum models of three-dimensional deformations in epithelial sheets”, *Biophys. J.*, **109**(1), 154–163.
- [30] D. Bi, J. H. Lopez, J. M. Schwarz, and M. L. Manning (2015), “A density-independent rigidity transition in biological tissues”, *Nat. Phys.*, **11**(12), 1074–1079.
- [31] A.-K. Marel, N. Podewitz, M. Zorn, J. O. Rädler, and J. Elgeti (2014), “Alignment of cell division axes in directed epithelial cell migration”, *New J. Phys.*, **16**(11), 115005.
- [32] R. Hornung, et al. (2018), “Quantitative modelling of nutrient-limited growth of bacterial colonies in microfluidic cultivation”, *J. R. Soc. Interface*, **15**(139), 20170713.
- [33] X. Treppe, et al. (2009), “Physical forces during collective cell migration”, *Nat. Phys.*, **5**(6), 426–430.
- [34] N. Podewitz, M. Delarue, and J. Elgeti (2015), “Tissue homeostasis: A tensile state”, *Europhys. Lett.*, **109**(5), 58005.
- [35] N. Ganai, T. Büscher, G. Gompper, and J. Elgeti (2019), “Mechanics of tissue competition: interfaces stabilize coexistence”, *New J. Phys.*, **21**(6), 063017.
- [36] T. Büscher, N. Ganai, G. Gompper, and J. Elgeti (2020), “Tissue evolution: Mechanical interplay of adhesion, pressure, and heterogeneity”, *New Journal of Physics*, **22**(3), 033048.
- [37] J. Krug (1997), “Origins of scale invariance in growth processes”, *Adv. Phys.*, **46**(2), 139–282.

4.7 Supplementary Informations: Instability and fingering of interfaces in growing tissue

4.7.1 Additional material

S1 Video. Two identical tissues. Interface dynamics between two identical tissues without motility force over 270 generations, starting from an initially flat interface. The interface position does not move besides fluctuations. The two tissues mix and thus the interface width (purple bar) increases with time.

S2 Video. Small motility force. Interface dynamics between a motile ($f_m^A = 0.1$, blue) and a non-motile ($f_m^B = 0.0$, red) tissue over 120 generations. The tissues are otherwise identical. The interface position moves towards the right, as indicated by the moving checkerboard pattern in the background. Note that the interface is stable and the interface width saturates at a value between one and two cell layers.

S3 Video. Medium motility force. Interface dynamics between a motile ($f_m^A = 0.4$, blue) and a non-motile ($f_m^B = 0.0$, red) tissue over 150 generations. The interface is unstable and protrusions of the motile into the non-motile tissue form. The amplitude of these protrusions saturates at a finite value and the pattern is stable afterwards.

S4 Video. Large motility force. Interface dynamics between a motile ($f_m^A = 0.8$, blue) and a non-motile ($f_m^B = 0.0$, red) tissue over 150 generations. Protrusions with large amplitude of the motile into the non-motile tissue form.

S5 Video. Fingering instability. Interface dynamics between two tissue with homeostatic stress difference $\Delta\sigma_H = 0.78$ over 200 generations. The weaker tissue (red) has a lower apoptosis rate and thus a higher viscosity than the stronger tissue (blue). A finger of the weaker tissue is left behind in the stronger one. No steady state is reached, as the finger moves, detaches, and reforms.

S6 Video. Motility force and homeostatic stress difference. Interface dynamics between two tissue with homeostatic stress difference $\Delta\sigma_H = 0.18$ and motility force of the stronger tissue (blue) $f_m^A = 0.4$ over 80 generations. The interface pattern is highly dynamic and no well-defined wave mode emerges.

5 Summary and outlook

5.1 Summary

The competition between different tissues or cell populations is heavily affected by biochemistry. For example, better access to limited resources necessary for growth, such as nutrients or growth factors, or resistance to certain chemotherapeutic drugs, provide an advantage for a certain cell population. This advantage may result in a higher growth rate or reduced apoptosis rate of that population compared to others. The population thus grows in size and increases its occupied volume. Hence, for densely packed tissues, such as epithelia, and limited compartment size, the competition can be regarded as a competition for space. Thermodynamic arguments suggest that such a competition can be affected by mechanics. The conjugate force to volume is pressure, which the growing cell population needs to exert onto its surrounding. From this, it is easy to see why tissue growth, with and without competition, is affected by the mechanical properties of the tissue environment. It is simply force balance which tells us that a tissue can only grow as long as the pressure acting on it is smaller than the pressure it is able to exert. It has thus been argued that the tissue which exerts the larger pressure dominates the competition, which has been formulated in the concept of homeostatic pressure [1].

Such mechanically-regulated competitions for space between different tissues have been the central theme of this thesis. However, we have seen that the outcome of the competition can not be predicted by individual tissue properties such as the homeostatic pressure alone, but that the cross-interactions between different tissues and the resulting interfacial effects can be of similar importance. As competition between different populations is a central aspect of evolution, the interfacial effects consequently affect the evolutionary dynamics. Phrased in terms of this perspective: the fitness of a cell population is not a single scalar variable, but a complex function of the interactions with the other cell populations against which it competes. The strength of the interfacial effects is naturally affected by the shape of the interface itself. Throughout this thesis, we have encountered a rich set of interfacial structures. This ranges from sharp interfaces in different geometrical arrangements, such as spherical and cylindrical inclusions, over a mixed, sponge-like state to an instability similar to Saffman-Taylor viscous fingering.

In this thesis, we focused on cell-cell adhesion as key interaction parameter. We have started with the extreme case of vanishing cross-adhesion strength f_c in chapter 2, in which we studied bulk competition between two different tissues in three dimensions. Reduced cross-adhesion, relative to the internal adhesion strengths of the competing tissues, increases the interfacial tension. The two tissues thus segregate into two distinct compartments in order to reduce the interfacial area or, equivalently, minimize the free adhesion energy. This results in a well-defined and sharp interface between them. At both sides of the interface, in a region of one or two cell layers, the division rate is enhanced and several times larger than the apoptosis rate, i.e. both tissues proliferate at the interface. This raises the pressure in the system, which reduces the division rate in the bulk of each tissue, where the growth rate is actually negative. The excess of cells from the interface creates a flux of cells towards the bulk. This mechanism suffices to stabilize coexistence between the competing tissues, even when they differ in homeostatic pressure. The tissue with the larger homeostatic pressure does not overwhelm the weaker one completely, contrary to the prediction made for competitions regulated by homeostatic pressure [1]. Instead, the tissue with the lower homeostatic pressure decreases in size, thereby reducing its apoptotic volume, until the excess of cells generated at the interface matches the loss of cells in the bulk. The interface plays a similar role as the free surface during in vitro experiments of growing tissue spheroids, in which an apoptotic core is sustained by proliferation at the surface [2, 3].

An analytic two-rate growth model, with a linear expansion of the growth rates around the homeostatic state, matches the simulation results quite well, with model parameters measured in independent simulations. This model accounts for the temporal evolution of the cell number fractions as well as the system pressure at the steady state, which is always larger than the two individual homeostatic pressures.

Due to the periodic boundary conditions, different structures can become stable, depending on the initial conditions from which the competitions are started. Examples are spherical and cylindrical inclusions, flat interfaces, and a bicontinuous structure. When f_c is increased towards the internal adhesion strength, all of these structures break apart at roughly the same cross-adhesion strength. At this point, cells can overcome the forces resulting from interfacial tension by their active growth and the two tissues start to mix, ending up in a sponge-like state when the cross-adhesion strength matches the internal adhesion strengths of the competing tissues.

Our results provide a mechanical explanation of how small, symptom-free lesions or occult tumors (tumors unnoticed by the host) can exist. For instance, occult tumors are commonly found in the prostate [4]. Our findings furthermore elucidate the role that

adhesion molecules, which are often down-regulated in cancer cells, may play during tumorigenesis [5]. Down-regulation of the expression of a protein or loss of its function occur via epigenetic changes and mutations. Each mutation yields a new cell population with distinct properties, including the mechanical ones as the example of adhesion molecules such as E-cadherin shows. The new cell population may be fitter than the surrounding populations and thus grows in size or be less fit and may vanish accordingly. Hence, mutations make tumorigenesis an example of Darwinian evolution, in which the fittest cell populations are automatically selected as a result of the competition between them. However, our results of chapter 2 suggest that loss of adhesion can also lead to stable coexistence between two populations - at least for vanishing cross-adhesion. We thus turned our attention to a more cancer-evolutionary perspective and shifted our attention from the steady state to evolutionary dynamics in chapter 3. Motivated by the homophilic binding between cadherins of different cells (which puts a limit on the adhesion strength by the cell expressing less cadherin), the cross-adhesion strength between cells of different populations has been set to the lower of the two internal adhesion strengths. Besides its function in mediating adhesive interactions between cells, E-cadherin is further involved in various signaling processes, some of which are connected to cell growth [6]. This motivates a coupling between changes in adhesion and growth strength. In this chapter, we thus introduced mutations changing the two parameters connected to adhesion and growth, namely the growth-force strength G and the adhesion strength f_1 .

For unconstrained evolution, the tissue quickly evolves towards a state dominated by cells with a high growth-force strength and low adhesion strength. Both, increased growth force and reduced adhesion, increase the homeostatic pressure of a cell population [7], i.e. the evolution of the tissue follows the predictions made by the homeostatic pressure concept [1]. As E-cadherin is involved in both, mediating inter-cell adhesion and regulation of cell growth, we introduced a tradeoff τ , which couples changes in growth force and adhesion strength, i.e. reduced adhesion comes at the cost of a lower growth-force strength and vice versa. For the two extreme cases, vanishing and infinite tradeoff, the tissue again evolves either to populations with strong growth force (vanishing tradeoff) or weak adhesion strength (infinite tradeoff). However, between the extremes, a parameter regime exists in which the evolution of the tissue shows a highly dynamic behavior. The most interesting case is a diverging evolution. While the majority of cells evolves into a preferred direction (either increase or decrease of both, adhesion and growth-force strength), a substantial fraction of cells also evolves into the opposite direction. The cell number fractions of individual cell populations show large

fluctuations, while the overall coexistence between populations with very different mechanical properties is remarkably stable. Interestingly, this state of coexistence is not dominated by the cell population with the largest homeostatic pressure. In fact, for a balanced tradeoff, the cell population with the lowest homeostatic pressure occupies the largest fraction of the available space. The underlying reason lies in the cross-adhesion between different cell populations. The interfacial tension is small and the competing tissues mix. Although no well-defined interface exists anymore, interfacial effects are still present. Cells of a population with large internal adhesion strength have a growth advantage when surrounded by less adhesive cells: it is then easier to create the necessary strain needed to divide than when surrounded by cells with large internal adhesion. The opposite effect occurs for cells of a low-adhesive population.

During tumorigenesis, the evolutionary nature of cancer leads to so-called intra-tumor heterogeneity, the observation that cells of the same tumor are not all identical, but several subpopulations coexist. Tumor heterogeneity is a major obstacle for cancer treatment, for example by chemotherapy, as one subpopulation might have developed a resistance to a specific drug. Our results show how tumor heterogeneity can arise by mechanics alone and that the coexistence between many different cell populations may, from an evolutionary point of view, be the most stable fixed point of the competition. The fitness of a cell population, given by the chance of a cell to divide, depends strongly on the interactions with the cell populations against which it competes, and the outcome of the competition is not determined by individual tissue properties, such as the homeostatic pressure, alone.

In chapters 2 and 3 we have studied competitions in three dimensions. However, most cancers originate from epithelial tissues, which are often effectively two-dimensional [5]. Furthermore, three-dimensional competitions are difficult to study experimentally. Two dimensional cell cultures are readily available, and indeed, competitions in two dimensions have recently been realized: two monolayers, initially separated by a gap, migrated into the empty space between them. After collision, the competition was driven by the monolayer generating larger collective stresses [8]. In chapter 4 we have thus studied competitions on a two-dimensional substrate, which may facilitate comparison with experiments. Competitions on a substrate have already been studied for a difference in homeostatic pressure between otherwise identical tissues [9], which results in a propagation of the interface at constant velocity. Starting from a flat interface, the interface initially roughens, but saturates at longer times at a width of a few cell layers.

The structure of the interface between tumor and host has been shown to provide information about a tumors malignancy [10]. This can thus be used for cancer diagno-

sis, for example in the oral cavity [11]. An unstable interface is often associated with increased malignancy, as detachment of cells from the primary tumor is a necessary requirement for the formation of metastases [12]. Given the importance of the interfacial structure, the question arises which physical mechanisms determine the stability of the interface between tissues. We have addressed this question for several mechanical properties of the competing tissues in chapter 4. We have studied two different mechanisms which drive the competition, namely a difference in homeostatic pressure and collective motility of one tissue directed towards the other.

The interface between two *identical* tissues is unstable, as cell death and division give rise to a diffusive motion of cells [13, 14]. The interface width thus increases with time, while the interface position itself does not move. A motility force f_m of one tissue directed towards the other leads to propagation of the interface at constant velocity in direction of the non-motile tissue. Interestingly, already for a small motility-force strength the interface width does not grow indefinitely anymore, but saturates at a finite value. With increasing f_m the saturation width w_{sat} further decreases, i.e. moderate motility forces stabilize the interface between two tissues during propagation. Above a critical motility-force strength, however, the interfaces becomes unstable and protrusions of the motile into the non-motile tissue form at a well-defined wavelength smaller than the system size. The amplitude of these protrusions is bound by nonlinearities and the interface width still saturates at a motility-force dependent value. In independent competitions for identical f_m , different wave modes can become unstable, with different saturation widths at the steady state. The resulting interface pattern is very stable in time and does not change over hundreds of cell generations.

For interface propagation driven by a difference in homeostatic pressure it has been shown in [9] that the interface is stable when the tissues are otherwise identical. We have studied the case in which the competing tissues additionally differ in their respective substrate friction and viscosity. Here, viscosity denotes an effective viscosity due to cell turnover and can be changed by varying the apoptosis rate k_a , where a lower apoptosis rate yields a higher viscosity. The interface becomes unstable when the tissue with the lower homeostatic pressure has the larger viscosity. This instability is characterized by a finger of the weaker tissue which is left behind in the stronger tissue during propagation and is reminiscent of Saffman-Taylor viscous fingering during injection of a low viscosity fluid into one of larger viscosity. Contrary to the motility-driven case, no steady interface pattern emerges: the finger moves along the interface and occasionally detaches from the weaker tissue, leaving a large island behind, which shrinks in size over time as proliferation of these cells is suppressed by the surrounding stronger tissue.

Different mechanisms can drive the instability of a tumor interface, for instance oxygen and nutrient limitations [12]. Mechanics alone suffices to drive a fingering instability between epithelium and stroma, which gets further amplified when cells inside the finger have access to more nutrients [15, 16]. Our results reveal that the pattern of the interface can also yield information about the mechanical properties of the competing tissues and the mechanism by which interface propagation is driven. They further show that no interfacial tension due to differential adhesion is needed in order to arrive at a stable interface during the competition. However, further comprehensive research will be needed to explore how these different causes of structural patterning interact.

Overall, consideration of interfacial effects and the cross-interactions between different tissues in mechanically-regulated competition for space reveal that such competitions bear a richer and more complex behavior than expected. Interfacial growth acts to stabilize coexistence between different tissues or cell populations, in a steady state fashion with a well-defined interface as well as in a dynamic scenario in a mixed state of many cell populations under the influence of evolutionary forces. Growth and motility forces affect structure and shape of the interface, which is thus subject to mechanical instabilities.

5.2 Outlook

In chapter 2, we have found that the mechanism which stabilizes the coexistence between two tissues is similar to the one acting in the growth of tissue spheroids. In both, proliferation at the surface, or interface respectively, sustains an apoptotic bulk. The next natural step would thus be to study the combined action of the two effects, surface and interface growth. A necessary requirement would be a negative homeostatic pressure of the competing tissues. A tissue with negative homeostatic pressure naturally grows to a spheroid of finite size in open boundary conditions [17]. A promising question to study would be the importance of the position where a mutation happens. Clearly, a mutated cell would have a higher chance to grow at the surface than in the bulk. However, due to the flux of cells from the surface towards the bulk, the mutated cell might be advected away from the surface before it actually grows to a substantial size. In that case, the outcome would probably be the same as if the mutation had initially occurred in the apoptotic core. For mutations in the bulk region, we expect interfacial effects to play a crucial role. A mutated cell with a larger homeostatic pressure, but cross-interactions not affected, may not be able to grow at all inside the core. However, interfacial growth could stabilize a small spheroid of the mutant inside the bigger host spheroid. Interestingly, this would result in a larger overall spheroid size, as the apoptotic region is reduced.

Another interesting scenario is based on the DAH. According to the DAH, when two spheroids come in contact with each other, cells of the less adhesive tissue will start to spread over the other spheroid, eventually enveloping it completely. During this process the surface area of the less adhesive tissue gradually increases and, vice versa, decreases for the strongly adhesive one. Accordingly, the enveloped spheroid may decrease in size or vanish completely, even when the other tissue is weaker in growth.

On a broader perspective, a promising direction could be to extend our model by coupling the mechanical interactions to concentration fields of nutrients, growth factors, or chemotherapeutic drugs. The dynamics of the concentration fields would be given by PDE, e.g. by a reaction-diffusion model. Such an approach has already been successfully applied to study the growth of bacterial colonies in microfluidic devices [18]. This would allow to address a variety of interesting questions with connections to a broad range of fields, as it makes a step towards a more biological model. One example could be to study the response to chemotherapy and the role of resistance of a certain cell population to it. Such a resistance may come at the cost of reduced fitness of that cell population compared to others in the absence of treatment [19], which could be modeled by a reduced growth-force strength of that population.

Our results further provide input for future theoretical studies. For mechanically-regulated tissue competition, interactions between the competing tissues have so far only been taken into account as passive interfacial tension [1, 20, 21]. Consideration of interfacial growth might alter the speed at which the interface propagates or its profile. Regarding the stability of the interface, our mechanism of interfacial growth could further introduce a fascinating competition between two opposing factors. While the resulting interfacial tension favors minimization of the interfacial area, enhanced growth at the interface could lead to a feedback loop which promotes further growth of an undulation. It would be interesting to see in which parameter regime such an instability, if existent, could be expected and how it depends on individual tissue properties such as viscosity or substrate friction.

The diverging evolution of a tissue towards coexistence between cell populations with very different mechanical properties could potentially be of interest for evolutionary studies of cancer. Interaction terms in the fitness function could account for the interfacial effects studied here. However, these effects act only locally within a range of one or two cell layers. This might make the evolution dependent on how much cells actually move throughout their lifetime. So far, we have studied cells subject to diffusive motion due to random cell death alone. Active motility of cells could thus have a surprising effect on the evolution of a tissue.

Bibliography chapter 5

- [1] M. Basan, T. Risler, J.-F. Joanny, X. Sastre-Garau, and J. Prost (2009), “Homeostatic competition drives tumor growth and metastasis nucleation”, *HFSP J.*, **3**(4), 265–272.
- [2] F. Montel, et al. (2011), “Stress clamp experiments on multicellular tumor spheroids”, *Phys. Rev. Lett.*, **107**(18), 188102.
- [3] M. Delarue, et al. (2013), “Mechanical control of cell flow in multicellular spheroids”, *Phys. Rev. Lett.*, **110**(13), 138103.
- [4] M. J. Bissell and W. C. Hines (2011), “Why don’t we get more cancer? A proposed role of the microenvironment in restraining cancer progression”, *Nat. Med.*, **17**(3), 320–329.
- [5] R. A. Weinberg (2007), *The biology of cancer*. New York: Garland Science.
- [6] S. Pece and J. S. Gutkind (2000), “Signaling from E-cadherins to the MAPK Pathway by the recruitment and activation of epidermal growth factor receptors upon cell-cell contact formation”, *J. Biol. Chem.*, **275**(52), 41227–41233.
- [7] N. Podewitz, M. Delarue, and J. Elgeti (2015), “Tissue homeostasis: A tensile state”, *Europhys. Lett.*, **109**(5), 58005.
- [8] S. Moitrier, et al. (2019), “Collective stresses drive competition between monolayers of normal and Ras-transformed cells”, *Soft matter*, **15**(4), 537–545.
- [9] N. Podewitz, F. Jülicher, G. Gompper, and J. Elgeti (2016), “Interface dynamics of competing tissues”, *New J. Phys.*, **18**(8), 083020.
- [10] Z. Hamdoon, et al. (2012), “Structural validation of oral mucosal tissue using optical coherence tomography”, *Head Neck Oncol.*, **4**(1), 29.
- [11] M.-T. Tsai, et al. (2008), “Effective indicators for diagnosis of oral cancer using optical coherence tomography”, *Opt. Express*, **16**(20), 15847–15862.
- [12] V. Cristini, et al. (2005), “Morphologic instability and cancer invasion”, *Clin. Cancer Res.*, **11**(19), 6772–6779.
- [13] J. Ranft, et al. (2010), “Fluidization of tissues by cell division and apoptosis”, *Proc. Natl. Acad. Sci. U.S.A.*, **107**(49), 20863–20868.

- [14] M. Basan, J. Prost, J.-F. Joanny, and J. Elgeti (2011), “Dissipative particle dynamics simulations for biological tissues: rheology and competition”, *Phys. Biol.*, **8**(2), 026014.
- [15] M. Basan, J.-F. Joanny, J. Prost, and T. Risler (2011), “Undulation instability of epithelial tissues”, *Phys. Rev. Lett.*, **106**(15), 158101.
- [16] T. Risler and M. Basan (2013), “Morphological instabilities of stratified epithelia: a mechanical instability in tumour formation”, *New J. Phys.*, **15**(6), 065011.
- [17] N. Podewitz, M. Delarue, and J. Elgeti (2015), “Tissue homeostasis: A tensile state”, *Europhys. Lett.*, **109**(5), 58005.
- [18] R. Hornung, et al. (2018), “Quantitative modelling of nutrient-limited growth of bacterial colonies in microfluidic cultivation”, *J. R. Soc. Interface*, **15**(139), 20170713.
- [19] R. A. Gatenby, A. S. Silva, R. J. Gillies, and B. R. Frieden (2009), “Adaptive therapy”, *Cancer Res.*, **69**(11), 4894–4903.
- [20] J. J. Williamson and G. Salbreux (2018), “Stability and roughness of interfaces in mechanically regulated tissues”, *Phys. Rev. Lett.*, **121**(23), 238102.
- [21] J. Ranft, M. Aliee, J. Prost, F. Jülicher, and J.-F. Joanny (2014), “Mechanically driven interface propagation in biological tissues”, *New J. Phys.*, **16**(3), 035002.

List of figures

1.1	Cryosection and two-rate growth model sketch.	10
1.2	Growth dependence on pressure.	11
1.3	Gedankenexperiment homeostatic pressure and tissue competition.	12
1.4	Evolutionary adaptation in cellular automaton model.	14
1.5	Cellular Potts Model with angiogenesis.	16
1.6	Tumor invasion in center-based model.	17
1.7	Growth mechanism of the simulation model used in this thesis.	19
2.1	Snapshots of various structures of tissue coexistence.	34
2.2	Snapshot flat interface and division profile.	35
2.3	Pressure dependence on box length and time evolution number fractions.	37
2.4	Number fraction and pressure dependence on homeostatic pressure difference.	39
2.5	Number fractions for different structures.	41
2.6	Evolution of number fraction as a function of increasing cross-adhesion strength.	42
2.7	Growth rate dependence on external pressure.	51
2.8	Pressure response coefficient dependence on simulation parameters.	51
2.9	Average pressure mirror boundary conditions.	52
2.10	Interface growth coefficient dependence on simulation parameters.	52
3.1	Free evolution of a tissue.	58
3.2	Temporal evolution of a tissue with coupled mutations.	59
3.3	Simulation snapshots.	60
3.4	Number fraction dependence on mutant adhesion strength for various growth-force strengths.	61
3.5	Number fraction dependence on tradeoff for various evolutionary distances.	62
3.6	Dependence of number fraction and number of clusters on mutation rate.	63
3.7	Survival probability dependence on adhesion strength for various growth-force strengths.	64

3.8	Temporal evolution of a tissue with constant division rate for different tradeoffs.	72
3.9	Comparison between constant division rate and sharp-threshold division mechanism in terms of number fraction.	73
3.10	Temporal evolution of a tissue with reduced mutation rate.	74
3.11	Pressure dependence on mutant adhesion strength for various growth-force strengths.	75
3.12	Competition winner dependence on mutant adhesion strength and initial mutant fraction.	77
4.1	Interaction potential and force	83
4.2	Simulation snapshots motility-driven interface.	84
4.3	Interface velocity, interface (saturation) width, and order parameter dependence on motility-force strength.	87
4.4	Structure factor motility-driven interface.	89
4.5	Simulation snapshots interface driven by homeostatic stress difference for different tissue viscosity.	90
4.6	Saturation width dependence on substrate friction and apoptosis rate. . .	91
4.7	Structure factor interface driven by homeostatic stress difference.	92
4.8	Saturation width and simulation snapshots for combination of motility and homeostatic stress.	93

List of tables

2.1	Simulation parameters of the standard tissue.	50
2.2	Varied simulation parameters and measured tissue properties of fixed tissues.	50
3.1	Simulation parameters and properties of the standard tissue.	71
3.2	Interfacial growth parameters for reduced growth-force strength of the mutant.	73
3.3	Interfacial growth parameters for increased growth-force strength of the mutant.	74
3.4	Interfacial growth parameters for reduced growth-force strength of the mutant with mixedness degree.	75
4.1	Simulation parameters of the standard tissue.	99

Acknowledgements

The way to a Ph.D. thesis is usually a long one. This thesis is no exception and so I would like to thank a few people who made the journey to it quite a pleasant one, who helped me in all possible ways, and who provided advice whenever I did not know which direction to take.

First of all, I would like to thank Jens Elgeti for the opportunity to join his group, the supervision of my thesis, and taking an incredible amount of time for feedback. The fascination, enthusiasm and joy which you show for physics and science have affected me very deeply. Your positive attitude has kept me motivated in times when things did just not want to work out. Besides of all aspects regarding your supervision, I would like to thank you for all our discussion about everything else but physics and your advice on all aspects of life besides living matter.

I want to thank Gerhard Gompper for giving me the chance to do my Ph.D. in his institute and letting me present my work at various conferences. Your feedback has been of great help in all our papers and working on them together has always been quite joyful.

I thank Meike Kleinen, our institute secretary, for doing a great job and keeping the institute going in general and helping me with all kinds of problems in particular.

I want to thank the people of ICS-2 for the great atmosphere in the institute and for living a spirit of helpfulness such that one can always seek out for advice. This brings me to a few people which I would like to thank in particular. I thank Masoud Hoore, Fatemeh Alidadi Soleymani, and Özer Duman, my initial office mates, for the great help in the beginning when I needed to get used to working at FZJ and ICS-2. I thank Raphael Hornung for his help to get started with the simulation code and the physics of growing matter. I thank Nils Podewitz for developing the code in the first place. I thank Nirmalendu Ganai for the time working together during my first year. I thank Angel L. Diez for the great work he accomplished during his stay and for bearing with me as his advisor. I thank Sebastian Hillringhaus for being the only person in our institute who knew about the current football results. I thank Sebastian Rode for preventing me from becoming the senior member of Jens group. I thank Ahmet Simsek and Christian Phillips for being hungry as early as I am. I thank Lucas Campos, half for joining as an

office mate, and fully for becoming a friend with whom I would go anywhere but Berlin.

I want to thank Prof. Dr. Joachim Krug for being the second revisor of my thesis and Prof. Dr. Berenike Maier for chairing my defense.

I am at the same time sorry and grateful that I now come to the point at which I have to start skipping some names. Sorry because each person would deserve a personal thank you, grateful for the incredible amount of wonderful human beings that I had the luck to meet during my life and who make it such a beautiful experience. So, a big thanks to all the people which I summarize here as friends, for all the great moments experienced together.

I thank Lucienne, Gerd, and Pascal for making me feel at home at their place immediately.

I thank my aunt Astrid and my uncle Frank for their support throughout the years.

I thank my grandparents Heinz and Fenna for being the two wonderful persons they are, their love and their selflessness, feeling joy the most when the people around them are doing fine.

I thank my parents Holger and Gerlinde for their love, their support, for still giving me the feeling to come home even nine years after moving out. Without you two I would not be the person I am today and I am thankful for all what you have done for me.

I thank my brother Janek for becoming my best friend. No matter what, you have always been there for me. Thank you for all the times spend together and being such an amazing human being.

The last person I want to thank is Juliette. Meeting you has been the best thing that has happened to me so far in life. Your ability to make me laugh even when I am feeling down is only one of many things which I love about you and which makes the time spend together so great. You are simply a wonderful person and I want to thank you for that.

Declaration of individual contributions

Article 1

Corresponding thesis chapter: Chapter 2 **Status:** published

N. Ganai, T. Büscher, G. Gompper, and J. Elgeti (2019), "Mechanics of tissue competition: interfaces stabilize coexistence," *New J. Phys.* **21**(6) 063017

Independent contribution:

I worked on this project together with Nirmalendu Ganai with guidance from Jens Elgeti, who also conceived the project. Nirmalendu Ganai had already contributed theoretical calculations and preliminary numerical simulations when I started working on it. I have contributed further numerical simulations, data analysis and finished the theoretical calculations. I further took care of the data management. The manuscript was written by me in cooperation with Nirmalendu Ganai, Jens Elgeti, and Gerhard Gompper. The first authorship is split between Nirmalendu Ganai and me.

Article 2

Corresponding thesis chapter: Chapter 3 **Status:** published

T. Büscher, N. Ganai, G. Gompper, and J. Elgeti (2020), "Tissue evolution: mechanical interplay of adhesion, pressure, and heterogeneity," *New J. Phys.* **22**(3) 033048

Independent contribution:

The idea to this project was conceived by Jens Elgeti. Nirmalendu Ganai contributed preliminary numerical simulations. I performed all further numerical calculations and analysed the resulting data. The theoretical model was developed by me and Nirmalendu Ganai with guidance from Jens Elgeti. I took care of the data management. I prepared the manuscript in cooperation with Jens Elgeti and Gerhard Gompper.

Article 3

Corresponding thesis chapter: Chapter 4

Status: published

T. Büscher, Angel L. Diez, G. Gompper, and J. Elgeti (2020), "Instability and fingering of interfaces in growing tissue," *New J. Phys.* **22**(8) 083005

Independent contribution:

The idea for this project was designed by Jens Elgeti and me. The project was started by Angel L. Diez, who visited our lab as a summer student for three months, under my supervision. After his stay, I performed further numerical simulations on the instability of an interface between two competing tissues, which became the main emphasis of the manuscript. Overall, I performed 80% of the numerical simulations and the interpretation of the data with guidance from Jens Elgeti. Angel L. Diez contributed several analysis scripts, while the data management was done by me. I prepared the manuscript in cooperation with Jens Elgeti and Gerhard Gompper.

Erklärung der Selbstständigkeit

Ich versichere, dass ich die von mir vorgelegte Dissertation selbständig angefertigt, die benutzten Quellen und Hilfsmittel vollständig angegeben und die Stellen der Arbeit - einschließlich Tabellen, Karten und Abbildungen - , die anderen Werken im Wortlaut oder dem Sinn nach entnommen sind, in jedem Einzelfall als Entlehnung kenntlich gemacht habe; dass diese Dissertation noch keiner anderen Fakultät oder Universität zur Prüfung vorgelegen hat; dass sie - abgesehen von unten angegebenen Teilpublikationen - noch nicht veröffentlicht worden ist, sowie, dass ich eine solche Veröffentlichung vor Abschluss des Promotionsverfahrens nicht vornehmen werde. Die Bestimmungen der Promotionsordnung sind mir bekannt. Die von mir vorgelegte Dissertation ist von PD Dr. Jens Elgeti betreut worden.

[1] N. Ganai, T. Büscher, G. Gompper, and J. Elgeti (2019), "Mechanics of tissue competition: interfaces stabilize coexistence," *New J. Phys.* **21** 063017

[2] T. Büscher, N. Ganai, G. Gompper, and J. Elgeti (2020), "Tissue evolution: mechanical interplay of adhesion, pressure, and heterogeneity," *New J. Phys.* **22** 033048

[3] T. Büscher, Angel L. Diez, G. Gompper, and J. Elgeti (2020), "Instability and fingering of interfaces in growing tissue," *New J. Phys.* **22**(8) 083005

Köln, 05.10.2020

Ort, Datum

Tobias Büscher

Lebenslauf

Name:	Büscher
Vorname:	Tobias
Geburtsdatum:	14.04.1993
Geburtsort:	Nordhorn
Staatsangehörigkeit:	deutsch
Oktober 2017 - Juli 2020	Promotionsstudent Physik Universität Köln
Dezember 2016 - Juni 2020	Doktorand Physik Forschungszentrum Jülich GmbH
Oktober 2014 - September 2016	Studium Physik Technische Universität Dortmund Abschluss: Master of Science Thema: "Entanglement and Decoherence in Neutrino Oscillations"
Oktober 2011 - September 2014	Studium Physik Technische Universität Dortmund Abschluss: Bachelor of Science Thema: "Neutrinooszillationen in Materie veränderlicher Elektronendichte"
August 2004 - Juni 2011	Gymnasium Lise-Meitner Gymnasium, Neuenhaus Abschluss: Abitur